Insights into the Liquefaction Hazards in Napier and Hastings Based on the Assessment of Data from the 1931 Hawke's Bay, New Zealand Earthquake

by

Maya El Kortbawi

Thesis submitted to the faculty of the Virginia Polytechnic Institute and State University in partial fulfillment of the requirements for the degree of

Master of Science
In
Civil Engineering

Russell A. Green
Adrian Rodriguez-Marek
Nina Stark

May 8th, 2017
Blacksburg, VA

Keywords: Liquefaction, Hawke's Bay, 1931 Hawke's Bay earthquake, Groundwater Model

Insights into the Liquefaction Hazards in Napier and Hastings Based on the Assessment of Data from the 1931 Hawke's Bay, New Zealand Earthquake

Maya El Kortbawi

ABSTRACT

Hawke's Bay is situated on the east coast of the North Island of New Zealand and has experienced several earthquakes in the past during which liquefaction occurred. The 1931 Hawke's Bay earthquake is particularly interesting because it was the deadliest and one of the most damaging earthquakes in New Zealand's history. The study presented herein provides insights into the liquefaction hazards in Napier and Hastings based on the assessment of data from the 1931 Hawke's Bay event. Previous studies on the liquefaction hazard of the region have been performed, but the present work differs from those in that the liquefaction triggering and severity procedures are used to see if they can accurately predict observations from the 1931 event. Towards this end, the Cone Penetration Test (CPT)-based liquefaction triggering evaluations are used in liquefaction vulnerability assessment frameworks. It was found that liquefaction hazard in Napier is greater than Hastings. Additionally, Liquefaction Potential Index and Liquefaction Severity Number distributions across Napier and Hastings suggest that the analysis frameworks used are over-predicting the liquefaction hazard. This observation was reached through the comparison of predictions and 1931 post-earthquake observations. Possible causes for this over-prediction include the shortcomings in the analysis frameworks to account for the influence of non-liquefied layers in the profile on the severity of surficial liquefaction manifestations, shortcomings of the simplified liquefaction evaluation procedures to fully account for the depositional and compositional characteristics of the soil on liquefaction resistance, and the use of the assumption that the soils below the ground water table are fully saturated, which has been shown not to be the case at sites in Christchurch, New Zealand. The research community is still learning about earthquakes and liquefaction and this study demonstrates how historical earthquake accounts in a region can be used to assess the risk of the region from future earthquakes.

Insights into the Liquefaction Hazards in Napier and Hastings Based on the Assessment of Data from the 1931 Hawke's Bay, New Zealand Earthquake

Maya El Kortbawi

ABSTRACT FOR THE GENERAL AUDIENCE

In light of the liquefaction-induced damage in Christchurch, New Zealand, there has been an increased awareness of the potential risk of liquefaction across New Zealand. Liquefaction is a phenomenon which occurs during earthquakes and results in a loss of strength in the soil. Hawke's Bay, situated on the east coast of the North Island of New Zealand, has experienced several earthquakes in the past during which liquefaction occurred. The most common manifestations of liquefaction are the appearance of sand boils (i.e., ejecting water and mud), ground subsidence, and lateral displacements near "free" faces such as river banks. As part of this study, these observations were compiled in a database. The 1931 Hawke's Bay earthquake is particularly an interesting case study because it was the deadliest and one of the most damaging earthquakes in New Zealand's history. Thus, this study aims to provide insights into the liquefaction hazards in areas of Hawke's Bay based on the assessment of data from the 1931 event. The liquefaction analysis is performed using procedures widely used in practice. Input to the analysis comes from geotechnical site investigations, intensity of the shaking during the 1931 earthquake, and estimated groundwater elevations at the time of the earthquake. The results from the analysis are then compared to the mapped observations from the 1931 event. The research community is still learning about earthquakes and liquefaction and this study demonstrates how historical earthquake accounts in a region can be used to assess the risk of the region from future earthquakes.

Acknowledgements

This study was partially funded by the Earthquake Commission in New Zealand (EQC), the University of Auckland, New Zealand, Virginia Tech, and U.S. National Science Foundation (NSF) grants CMMI-1407428, CMMI-1435494, and CMMI-1724575. Prof. Russell Green, Dr. Liam Wotherspoon and Dr. Sjoerd van Ballegooy provided guidance and feedback throughout the work. Dr. Wotherspoon arranged travel to New Zealand and visits to Napier and Hastings. Mr. Rick Wentz helped with the logistics in Napier and Hastings. Librarians and archivists in the MTG Museum, Napier Library, and Hastings Library assisted in the collection of liquefaction observations. Historian Mr. Michael Fowler agreed to one-on-one meetings to help with the collection of liquefaction observations. Dr. van Ballegooy made the resources of Tonkin and Taylor available for this study, and Ms. Virginie Lacrosse from Tonkin and Taylor ran the liquefaction calculator based on the specified input and provided the results presented discussed herein. This support and assistance are gratefully acknowledged. However, all opinions, findings, and conclusions or recommendations expressed in this thesis are those of the author and do not necessarily reflect the views of the National Science Foundation, EQC, or the host institution of the author or the others involved in this study.

Table of Contents

CHAPTER 1 INTRODUCTION

1.1 Problem Statement

The objective of this study is to provide insights into the liquefaction hazards of Napier and Hastings from the assessment of data from the 1931 Hawke's Bay, New Zealand, earthquake. The 1931 earthquake has a significant importance because it was the deadliest and one of the most damaging earthquakes in New Zealand's history. During the earthquake, surficial manifestations of liquefaction were observed across the Hawke's Bay region. This study will be useful to parties concerned with emergency management planning to characterize the liquefaction hazard for future earthquakes. This characterization is based on a past earthquake for which consequences are known. The idea is to perform the liquefaction hazard assessment on a past earthquake and evaluate the results based on the observations from that earthquake in order to assess whether the procedures yield valid predictions for the region.

1.2 Thesis Organization

This thesis is organized into three chapters and four appendices (A-D). The second chapter is a manuscript anticipated to be submitted as a technical paper to a peer-reviewed archived journal. The third chapter presents a summary of the work, the key findings, and recommendations for future work. The back matter of this thesis consists of supplemental material to the manuscript and is organized in four appendices. It provides details on the collection of liquefaction observations from the 1931 Hawke's Bay earthquake, the characterization of 1931 ground motions, the development of a ground water model representing estimates of ground water depth at the time of the earthquake, and the parametric study performed using the liquefaction triggering assessment.

1.3 Attribution

The manuscript in Chapter 2 entitled: "Insights into the Liquefaction Hazards in Napier and Hastings Based on the Assessment of Data from the 1931 Hawke's Bay, New Zealand, Earthquake," authored by M. El Kortbawi et al., will be submitted for consideration as a journal paper. The following provides a list of the contributing co-authors and their primary role on this paper:

Russell A. Green, PhD, Department of Civil and Environmental Engineering at Virginia Tech, Blacksburg, Virginia, U.S.A.

- Research Advisor to the lead author and provided guidance, reviews, and his expertise in the subject throughout the research. Dr. Green is also credited for his major contributions in the liquefaction potential assessments following the Darfield and Christchurch, New Zealand, earthquakes.

Liam Wotherspoon, PhD, Department of Civil and Environmental Engineering at University of Auckland, Auckland, New Zealand

- Research co-Advisor to the lead author and provided guidance throughout the research. Dr. Wotherspoon assisted in the logistics of the travel to New Zealand and the site visits to Napier and Hastings. He provided the data on the ground characterization during the 1931 Hawke's Bay which are used as input to this study.

Sjoerd van Ballegooy, PhD, Technical Director at Tonkin and Taylor, Ltd, Newmarket, New Zealand

- Research co-Advisor to the lead author and provided guidance and his expertise in the subject and the area of study throughout the research. Dr. van Ballegooy made Tonkin and Taylor's resources accessible to the lead author and assisted in the liquefaction triggering assessment done using the liquefaction calculator developed by Tonkin and Taylor.

CHAPTER 2 INSIGHTS INTO THE LIQUEFACTION HAZARD IN NAPIER AND HASTINGS BASED ON THE ASSESSMENT OF DATA FROM THE 1931 HAWKE'S BAY, NEW ZEALAND, EARTHQUAKE

2.1 Abstract

Hawke's Bay is situated on the east coast of the North Island of New Zealand and has experienced several earthquakes in the past during which liquefaction occurred. The 1931 Hawke's Bay earthquake is particularly interesting because it was the deadliest and one of the most damaging earthquakes in New Zealand's history. The study presented herein provides insights into the liquefaction hazards in Napier and Hastings based on the assessment of data from the 1931 Hawke's Bay event. Previous studies on the liquefaction hazard of the region have been performed, but the present work differs from those in that the liquefaction triggering and severity procedures are used to see if they can accurately predict observations from the 1931 event. Towards this end, the Cone Penetration Test (CPT)-based liquefaction triggering evaluations are used in liquefaction vulnerability assessment frameworks. It was found that liquefaction hazard in Napier is greater than Hastings. Additionally, Liquefaction Potential Index and Liquefaction Severity Number distributions across Napier and Hastings suggest that the analysis frameworks used are over-predicting the liquefaction hazard. This observation was reached through the comparison of predictions and 1931 post-earthquake observations. Possible causes for this over-prediction include the shortcomings in the analysis frameworks to account for the influence of non-liquefied layers in the profile on the severity of surficial liquefaction manifestations, shortcomings of the simplified liquefaction evaluation procedures to fully account for the depositional and compositional characteristics of the soil on liquefaction resistance, and the use of the assumption that the soils below the ground water table are fully saturated, which has been shown not to be the case at sites in Christchurch, New Zealand. The research community is still learning about earthquakes and liquefaction and this study demonstrates how historical earthquake accounts in a region can be used to assess the risk of the region from future earthquakes.

2.2 Introduction

The objective of the study presented herein is to provide insights into the liquefaction hazard of Napier and Hastings from the assessment of data from the 1931 Hawke's Bay, New Zealand, earthquake. One impetus for this study is that much of the damage to structures and infrastructure in Christchurch, New Zealand, during 2010-2011 Canterbury Earthquake Sequence (CES) was caused by liquefaction and related phenomena (e.g., lateral spreading). Accordingly, there has been an increased awareness of the potential risk due to liquefaction and related phenomena across New Zealand. This awareness has led to numerous studies being performed in regions impacted by historical earthquakes to help identify areas prone to liquefaction, with this information ultimately being used as input into risk assessments and to guide liquefaction risk mitigation programs.

Hawke's Bay is located in the middle portion of the east coast of the North Island of New Zealand (Figure 1). The North Island is located on the Australian Plate, with the eastern portion of the island subjected to compressional stresses from the subducting Pacific Plate. As a result, the Hawke's Bay region is one of the most seismically active regions in New Zealand, with the largest historical earthquake being the 3 February 1931, surface-wave magnitude (M_s) 7.8 Hawke's Bay earthquake. The 1931 M_s7.8 event, also known as Napier earthquake, is considered to be the deadliest and one of the most damaging earthquakes in New Zealand's history. Damage from the earthquake occurred over an ~200 km stretch from Gisborne in the north to Waipukurau in the south.

Hawke's Bay is bounded to the south by Cape Kidnappers and to the northeast by the Mahia Peninsula, and is bounded by the mountain chain of the North Island to the west and the sea to the east, a distance of 50 to 65 km of gently sloping terrain and low ridges. The Tukituki, Tutaekuri, and Ngaruroro Rivers converge in southern Hawke's Bay and discharge into the sea. Through time, these rivers transported eroded material from the mountains to the west and deposited them over an extensive alluvial plain, known as the Heretaunga Plains (Lee et al. 2011). The towns of Napier and Hastings sit near the southern part of the bay, with Napier situated on the coast and Hastings, about 9.5 km inland.

Figure 1: Location of Hawke's Bay region *(modified from hpuds.co.nz)*

The combination of the depositional environment of the soils in southern Hawke's Bay and high seismicity of the region potentially result in a relatively high liquefaction hazard. Liquefaction and lateral spreading were documented to have occurred in the region following the 1863 Southern Hawke's Bay earthquake, 1904 Cape Turnagain earthquake, 1921 Central Hawke's Bay earthquake, 1931 Hawke's Bay earthquake,

and the 1932 Wairoa earthquake. Of particular interest to the study presented herein is the occurrence of liquefaction during the 1931 Hawke's Bay earthquake. Fortunately, the effects of the earthquake on land and buildings were well-documented after the event which provides valuable information for detailed studies.

Following the 1931 M_s7.8 Hawke's Bay earthquake, liquefaction was observed throughout the bay region from Wairoa in the north to Havelock North in the south. Although the entire region of Hawke's Bay was severely affected by shaking, the epicenter of the event was in the vicinity of Napier and Hastings. Consequently, these cities felt the highest shaking intensities; on the Modified Mercalli Intensity (MMI) scale Napier and Hastings had an MMI of X. In addition, Napier and Hastings had the largest populations in Hawke's Bay (Figure 2: 1931 populations: Napier 16,025; Hastings 10,850) and hence, the greatest amount of infrastructure. Note that the population in Gisborne was 28% of the population in affected areas of Hawke's Bay (1931 populations: 13,635), yet the shaking was less severe due to the large epicentral distance (Callaghan 1933).

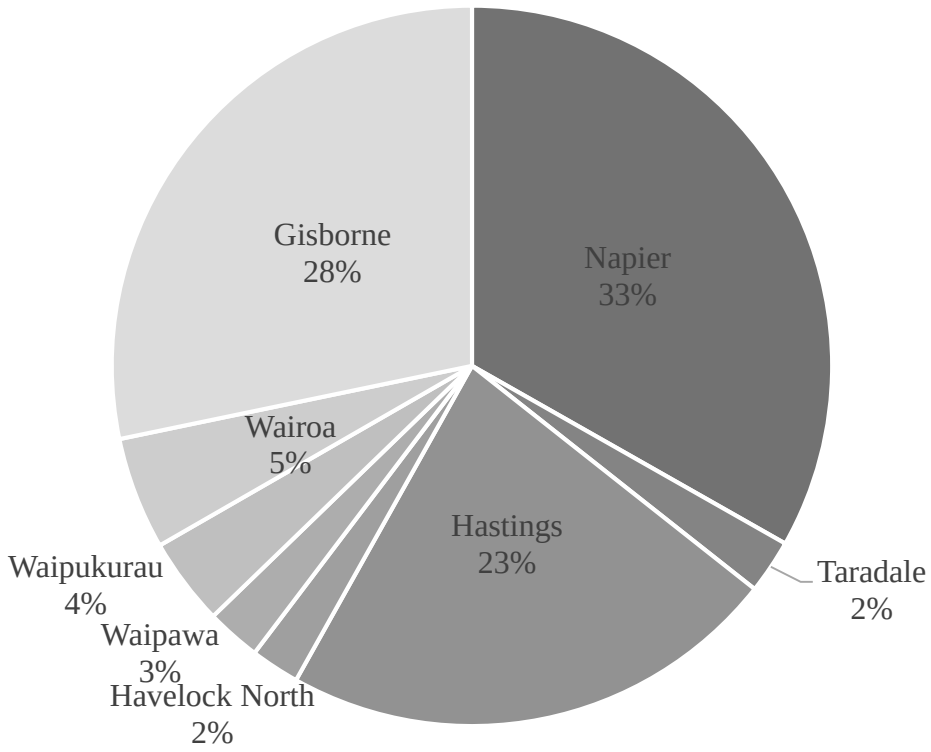

Figure 2: Percentage of the population living in affected areas in Hawke's Bay at the time of the earthquake (1931)

As stated previously, the overall objective of this study is to provide insights into the liquefaction hazard of Napier and Hastings from the assessment of data from the 1931 Hawke's Bay, New Zealand, earthquake. Towards this end, the severity of surficial liquefaction manifestations in Napier and Hastings are evaluated for the Hawke's Bay earthquake scenario using the simplified liquefaction evaluation procedure (i.e., Boulanger and Idriss 2014) within liquefaction vulnerability assessment frameworks (i.e., Liquefaction Potential Index and Liquefaction Severity Number) and the predictions compared with historical accounts. However, because many of the seismological and geotechnical parameters needed in this study are uncertain (e.g., peak ground acceleration, depth to ground water table), combinations of ranges of parameter values are considered. Regions of Napier and Hastings are identified where historical field observations fall within or outside of the prediction ranges, giving insights into where the simplified liquefaction evaluation procedure-damage index framework combinations can be expected to yield accurate predictions for future events and where the predictions are expected to be less certain.

This work follows a series of previous studies that assess liquefaction in the Hawke's Bay region (Dellow et al. 2003; Hengesh et al. 1996); results from these studies showed that the Hawke's Bay region has significant areas with high liquefaction hazard. However, the present study is distinctive from previous studies in that it uses historical accounts of the liquefaction response of soils during the 1931 M_s7.8 Hawke's Bay earthquake. As a result, this study helps identify areas prone to liquefaction, as well as to identify regions where the current evaluation procedures may yield erroneous predictions. The outcomes of this work are significant in several respects. First, the findings will upgrade or degrade the predicted liquefaction hazard in some locales, which in turn can be used to help guide the prioritization areas requiring mitigation measures. In the same vein, the study will help advise concerned parties (e.g., the Hawke's Bay Regional Council and the public) in their emergency management planning. Second, this study will contribute to the ongoing liquefaction research in New Zealand and worldwide. The research community is still learning about earthquakes and liquefaction and this study demonstrates how historical earthquake accounts in a region can be used to assess the risk of the region from future earthquakes.

This manuscript provides a full account of the work undertaken in the liquefaction potential assessment for Hawke's Bay. A literature review on the tectonic, geological, and geomorphological setting of Hawke's Bay is presented first. This is followed by a brief overview of the 1931 event. The bulk of the manuscript concentrates on the collection of the liquefaction observations made following the 1931 event and the inputs used in the liquefaction evaluations. Finally, the results of the evaluation are presented and discussed.

2.3 Background on Hawke's Bay and the 1931 Hawke's Bay Earthquake

2.3.1 *Tectonics*

New Zealand is located along the boundary between two tectonic plates: the Australian plate and the Pacific plate. The North Island lies completely on the Australian plate (Figure 3). Hawke's Bay is located on the east coast of the North Island. The plate boundary zone runs parallel to the coast. The Pacific plate subducts under the Australian plate at the Hikurangi Trough about 160 km east of Napier, and the subducting Pacific plate gets progressively deeper to the west. The Hikurangi Trough in itself is not a source of earthquakes but is a geomorphological feature indicative of the tectonic environment of the North Island.

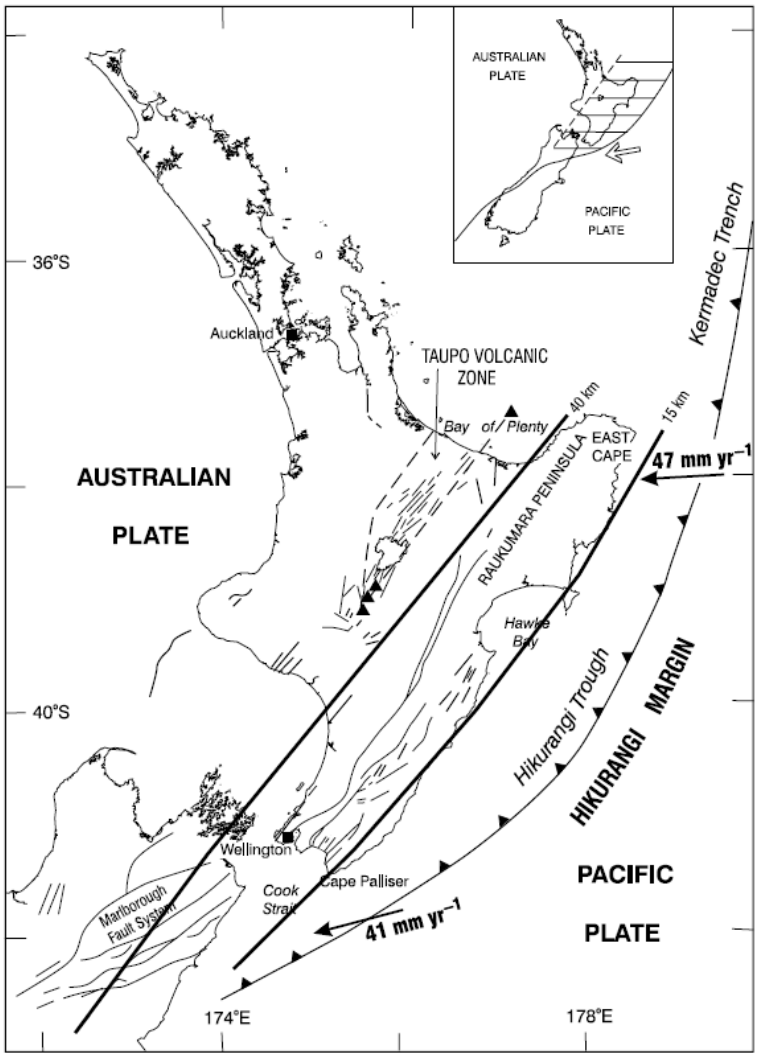

Figure 3: Tectonic setting of Hawke's Bay *(from Doser and Webb 2003)*. Bold lines indicate the depth of the Australian/Pacific plate interface. Triangles are recently active volcanoes.

The subducting Pacific plate dips gently (about 6°) immediately west of the trough but steepens beneath Hawke's Bay to about 25°. The tectonic plates are converging at an oblique angle at a rate of 47 mm/yr. The subduction process between the Australian and the Pacific plates generates oblique compressional stresses which result in a zone of great deformations. This zone is known as the East Coast Deformed Belt and extends from the trough to the axial range of the North Island (Begg et al. 1994). Hawke's Bay lies within an extensive forearc basin in eastern North Island bounded to the east by an emerged part of the accretionary wedge (which becomes submerged under the ocean to the north of Hawke's Bay) and to the west by the North Island Shear Belt (Figure 4). The geological structure of the forearc basin can be divided into four major structural domains based on styles and magnitude of deformation. These domains are, from west to east, the axial range domain which comprises the eastern North Island axial ranges, the range front contractional domain, the central forearc basin domain, and the eastern contractional domain. The major faults (Figure 5) within the axial range domain (e.g., the Wellington, Ruahine, Mohaka, and Whakatane Faults) are dominated by oblique-slip displacement. These faults are well-developed and extend linearly for up to 400 to 500 km in a NNE trend. Some degree of dip-slip occurs on these faults. The structures of the range front contractional domain comprise reverse faults. Yet, some strike-slip movement is apparent. The forearc basin on which part of Hawke's Bay sits is comparatively undeformed with minor reverse faults and folds trending NNE. West of Napier and Hastings the bedding planes dip gently to the southeast at about 2° to 20°. The eastern contractional domain includes the accretionary wedge and is characterized by reverse faulting. Some degree of strike-slip is accommodated on faults in the western part of this domain and contractional deformation is accommodated on structures in the eastern part of the domain (Bland and Kamp 2006).

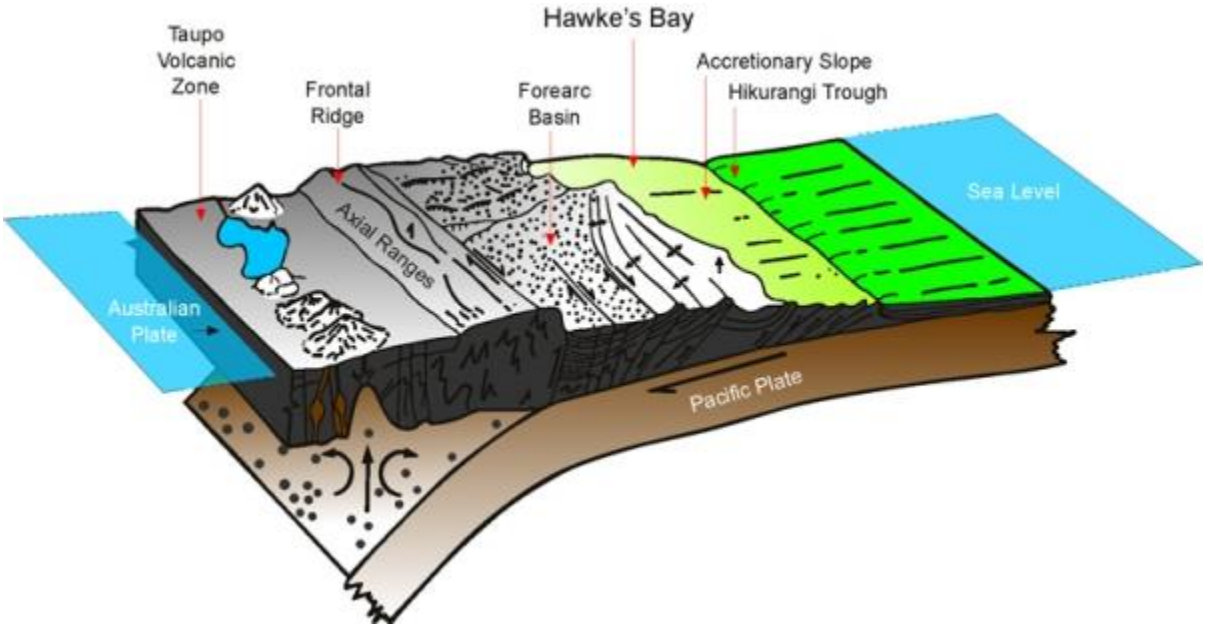

Figure 4: Idealized model of the subduction zone in Hawke's Bay *(from HBRC Emergency Management Portal n.d.)*

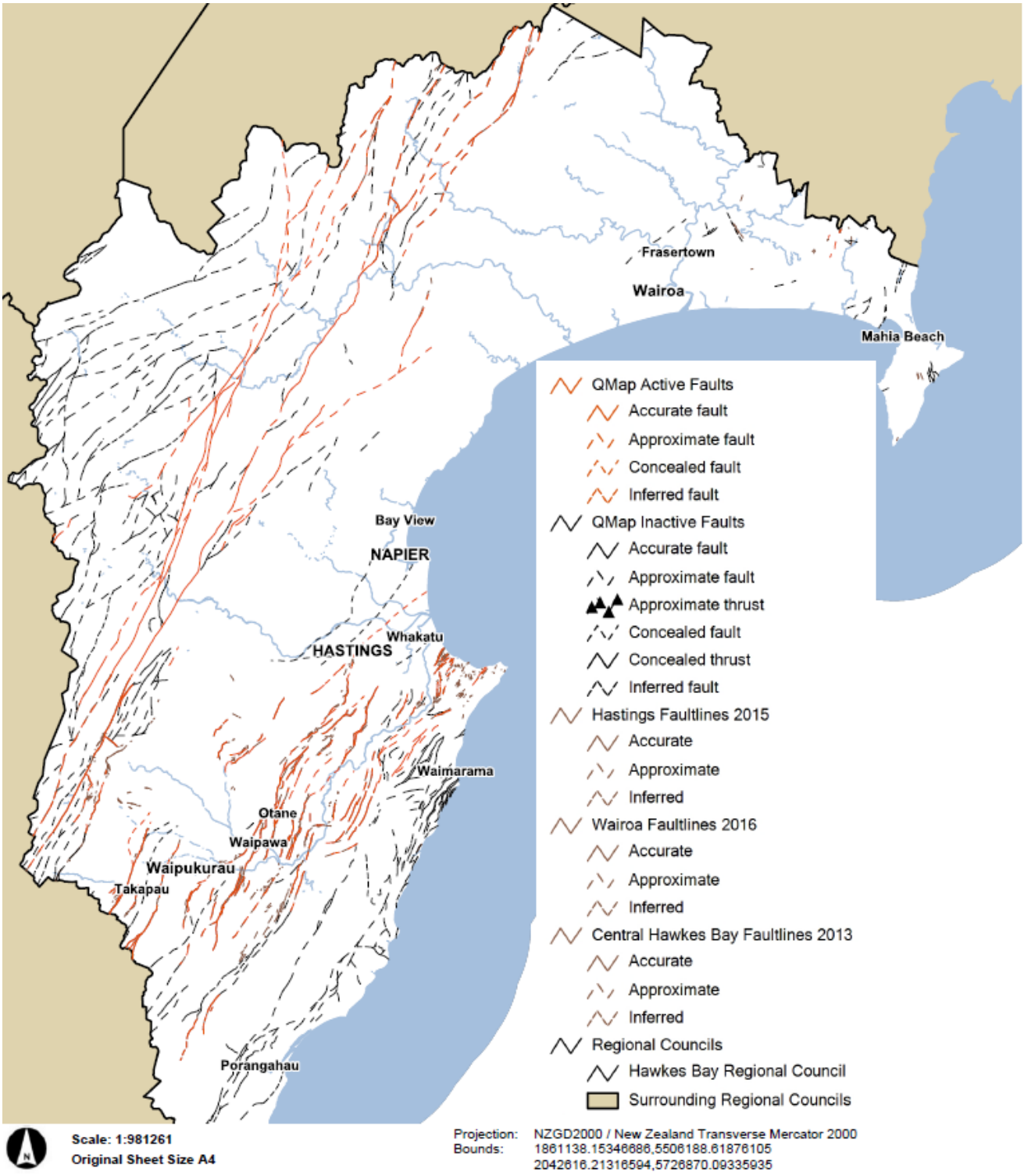

Figure 5: Active and inactive faults in Hawke's Bay *(from HBRC Emergency Management portal n.d.)*

2.3.2 *Near Surface Geology and Geomorphology*

The present geology and geomorphology of Hawke's Bay began to unveil about 2 million years ago as a result of a series of successive cold and temperate climate periods (Table 1). The Heretaunga depression is a synclinal structure in late Pliocene and early Pleistocene sediments which have undergone uplift, warping, tilting, and subsidence over the last 1 million years. Tectonic uplift and the deposition during glacial and interglacial periods resulted in the accumulation of sediments on the late Pliocene and early Pleistocene marine sediments. During the cold climate, the sea level declined to 150 m below present levels and sea beds were exposed. Rivers running through Hawke's Bay flowed eastwards and deposited gravel, sand, and silt eroded from the greywacke mountain ranges into the basin forming the Heretaunga Plains. During warm climate, sea levels rose, inundated the alluvial plain, formed coastal swamps, and lagoons, and left beach deposits over the plain. Subsidence of the Heretaunga Plains started 500,000 years ago and continues to the present day. Seismic surveys suggest that the Plain is constituted of a 900 m deep basin structure. Subsidence and preservation of interglacial marine deposits suggest a subsidence rate of about 1 m per 1000 years over the last 250,000 years. Besides the deposition of alluvial sediments from the erosion of mountain ranges, volcanic material blown by the wind (e.g., volcanic ash) or transported by the river valleys (e.g., ignimbrite, a pumice-like rock) were deposited on the plain during the Middle Pleistocene. During the last glaciation (about 23,000 years ago), erosion of the greywacke mountain ranges continued and the Ngaruroro and Tutaekuri Rivers covered the volcanic deposits with fluvial gravel deposits. About 9,000 years ago, climate warming began and sea level rose until about 6,500 years ago when it attained the present level. Consequently, marine beach estuarine and lagoonal sediments were deposited over the gravel channel deposits of the last glaciation period, forming aquifers. For the last 4,500 years, the Ahuriri Lagoon was slowly filled with sediments transported by the Ngaruroro and Tutaekuri Rivers during floods or changes of course. The lagoon was eventually reclaimed due to tectonic uplift during the 1931 earthquake (Dravid and Brown 1997).

The present Hawke's Bay geomorphology can be divided into 4 regions:

- Jurassic greywacke mountain ranges trending NE-SW forming the west boundary of Hawke's Bay
- Cretaceous hilly country (small ridges or tilted blocks exposed by folds and faults), mainly of massive mudstone, forming the east boundary
- The lowlands between the two preceding regions (the Ruataniwha Depression and the Heretaunga Plains), mainly young alluvium deposited by flooding of rivers overlying Pleistocene deposits, Ignimbrite and Holocene gravels
- North dissected plateau, mainly of limestone, siltstone, and sandstone

The Heretaunga Plains are part of the lowlands and have four distinguishable physiologic units: hills, plains, coast, and Hawke's Bay. The Napier hill is a limestone outcrop underlain by a sandy siltstone and a lower limestone. To the west and south of the Heretaunga Plains is a series of gently sloping hills ranging from 300 m above sea level in the northwest to a maximum of 200 m above sea level in the southwest. To the

west of the Heretaunga Plains, the gently sloping dissected plateau dips uniformly at 5° to 10° towards Hawke's Bay. The dissected plateau is late Pliocene and early Pleistocene limestone and mudstone overlain by fluvial gravel and silt. The Plains are bounded to the southeast by a range of limestone hills dipping westward at 26° under the Plains. These are composed of marly and sandy limestone with occasional limestone beds. A series of tilted fault blocks of limestone and siltstone forms the south boundary of the Plains. The Plains were formed by fluvial deposition by the Tutaekuri and Ngaruroro Rivers over the last 6,500 years. The Tukituki River contributed to the deposition of the southeast part of the plain. Swamps and marshes developed in low-lying areas where the water table reaches ground surface.

Table 1: Major geological units in Hawke's Bay (in order of increasing age and strength) *(from Begg et al. 1994)*

Unit	Description	Age (years)	Strength	Location
Young deposits	Fine sand, silt, mud, peat, pumice, and clay with some interbedded gravel	< 6,000	Very soft to stiff	Estuaries, swamps, and low-lying alluvial plains and lakes
Soil mixes	Gravel and sand	< 3 million	Loose to dense	Alluvial plains
Rock	Sandstone, siltstone, mudstone, limestone, and minor conglomerate	3 to 75 million	Very weak to moderately strong	Hill country to the east of the axial ranges
Sedimentary rock	Greywacke sandstone, conglomerate, siltstone, mudstone, and minor volcanic and chert (volcanic rocks[1] of the Taupo Volcanic zone)	> 110 million except for volcanic rocks (<1 million)	Moderately strong to very strong	Western boundary of the region, the axial ranges

[1] Included with this unit because they are generally lithified

The coast in Hawke's Bay is the product of the interaction of sea level fluctuations, sediment input into the coastal regime, adjustment to tectonic processes, and human activities in recent time (e.g., river diversions which affect sediment transport, the construction of the Napier breakwater, etc.). Prior to the establishment of the present sea level, the sea extended inland to a maximum distance of 12 km to the west of Hastings. The Ahuriri Lagoon formed at least 4,500 years ago due to accumulation of a strip of dense gravels along the coast. Thirteen hundred hectare of Ahuriri Lagoon was uplifted above sea level following the 1931 Hawke's Bay earthquake. Prior to the 1931 event, Napier Hill was partly isolated from the mainland by marshes and lagoon. The beach from Whirinaki (to the north) to Napier Hill is gravel and sand with no obvious source of sediment supply besides a small input from the Esk River. The beach from Clifton (16 km south of Napier) to Napier Hill is formed from gravel and sand from the Tukituki, Ngaruroro, and Tutaekuri Rivers and from the erosion of the cliffs from Clifton to Cape Kidnappers. In this study, the soil up to 20 m depth is critical to the

liquefaction evaluation. The quaternary geology of the Heretaunga Plains is shown in Figure 6.

Hawke's Bay is located on the continental shelf with nearshore water depths of approximately 10 m and water depths of approximately 200 m at the edge of the continental shelf. The Bay's sea bed is mostly featureless without significant bedforms or other geomorphological features other than in the area of the Lachlin Ridge located 20 km from the coastline (Dravid and Brown 1997).

2.3.3 *The 1931 Hawke's Bay Earthquake*

The Hawke's Bay earthquake caused widespread damage in the region and had an official death toll 256 lives (Callaghan 1933). The main event occurred on 3 February 1931 at 10:47 am New Zealand local time, and the magnitude was estimated to be M_s7.8 (Dowrick and Smith 1990; Haines and Darby 1987). The estimated moment magnitude, M_w, for the event varies from reference to reference but is generally in the range of M_w7.4-7.8. Several moderate shocks were felt in Napier during the 1929 and 1930, but no major foreshocks occurred prior to the 3 February main shock. A large number of aftershocks followed the main event (596 aftershocks in February 1931: Adams et al. 1933). Table 2 presents general information on the main shock and largest aftershocks.

Table 2: Earthquake facts *(from Doser and Webb 2003)*

Event	**Date (yymmdd)**[1]	**Epicenter**[2]		**M_s**	**M_w**
		Latitude	Longitude		
Main shock	310203	-39.69°	176.73°	7.8	7.4-7.6[3]
AS1[4]	310204	-39.3°	177.0°	5.7	5.8
AS2	310208	-39.2°	177.0°	6.3	6.4-6.5
AS3	310213	-39.43°	177.48°	7.3	7.3-7.5

[1] NZ local time
[2] After Doser and Webb (2003) from Smith and Downes (1997)
[3] Lower bound magnitude
[4] AS stands for aftershock

Scientific investigations performed shortly after the earthquake include studies of seismology (Adams et al. 1933; Bullen 1938), geology (faulting, uplift, and subsidence) (Henderson 1933; Marshall 1933), and building damage (Brodie and Harris 1933). The 1933 volume of the New Zealand Journal of Science and Technology constitutes the most complete account of the event.

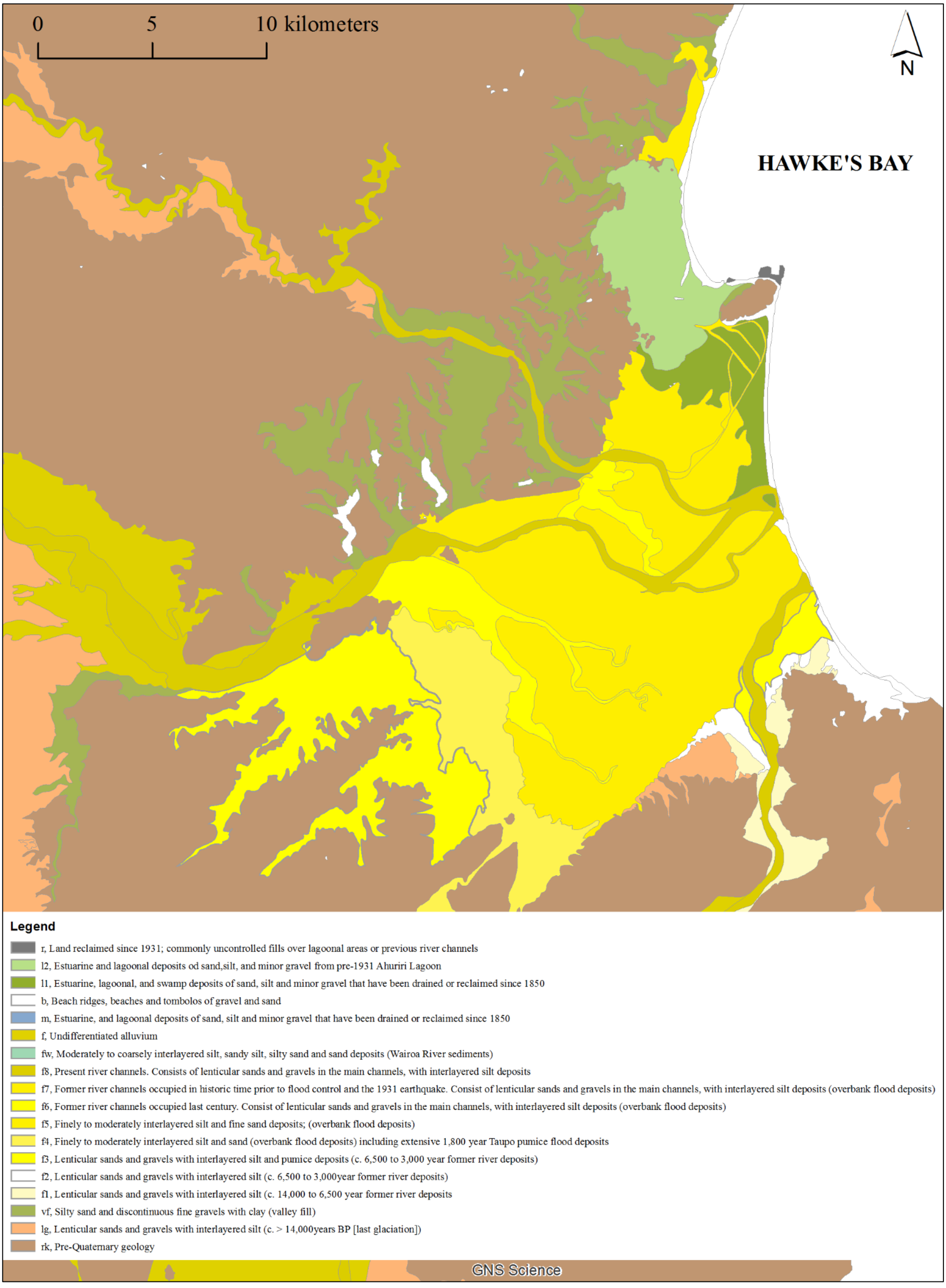

Figure 6: Quaternary geology of the Heretaunga Plains *(after Dravid and Brown 1997)*

Only one complete time series of the main shock motions was recorded, by the Imamura strong motion seismograph in Takaka (Adams et al. 1933). Bullen (1938) carried out an analysis of the travel times of P- and S-waves recorded at both distant and near stations in an attempt to understand the seismology of the 1931 event. The main shock resulted from three large slips near the focus; the second and third slips followed the first by 6 sec and 14 sec, respectively. Bullen (1938) pointed out the epicenter of the event is located at approximately 39.3º S, 176.6º E (±0.2º), 32 km northwest of Napier; the location of the epicenter was relocated in subsequent studies to 25 km NNE of Napier: 39.3º S, 177.0º E (Dowrick 1998). Based on the study of recurring aftershocks, Adams et al. (1933) suggested that the focal depth of the main event was ~15 to 20 km.

The 1931 event was mainly a thrust event generated by a slip on a reverse fault dipping steeply to the northwest under Hawke's Bay. It was also accompanied by a strike-slip movement. Angular changes from triangulation networks surveyed from 1926 to 1931 were analyzed by Walcott (1978) and revised by Haines and Darby (1987). Dislocation models from Haines and Darby (1987) that best explain the surface deformation pattern and geodetic data estimated the movement along the fault as 6 to 8 m dip slip and 4 to 8 m strike slip at a 59-68° northwest dip. The rupture had a length of 80 km and extended 40 km under the sea northeast of Napier and 40 km southwest (McGinty et al. 2001). Doser and Webb (2003) reported a total unilateral rupture length of 105 to 120 km. This is comparable to the length of the deformation zone (>90 km long and 17 km wide) reported by Hull (1990). The source extended from the subduction interface (25-35 km deep) to within 5 km of the surface but did not reach the surface (Figure 7). Surface faulting was constrained to the southwestern end of the deformation zone where near-surface rocks accommodated the shear failure due to their strength and the orientation of pre-existing plane weaknesses. To the northeastern end of the deformation zone, surface faulting was not observed due to a change in the rock type along the fault. Near-surface rocks had a lower strength and fractured at depth, not allowing the rupture to propagate to the surface. Ruptures seen at the surface were secondary (Haines and Darby 1987), resulting in fault scarps up to 4.6 m vertical displacement and 1.8 m right lateral strike-slip (horizontal) movement.

The epicenters of a large number of aftershocks imply that the stress concentration on the faults in the region moved in the direction of Mahia Peninsula and likely lead to the September 1932 Wairoa earthquake. The largest aftershock occurred on 13 February (ten days after the main shock) and had an estimated magnitude of M_w7.3. It was generated by a strike-slip movement offshore from Oldman Bluffs and ruptured within the Australian plate. The location of the epicenter (50 km east of the main shock's epicenter) suggests that this aftershock occurred on a different fault from the main shock, which is likely why the magnitude of this aftershock approached that of the main shock. The bilateral fault length was estimated to be 70 km which is comparable with the fault length in McGinty et al. (2001). No onshore faulting was observed for this aftershock.

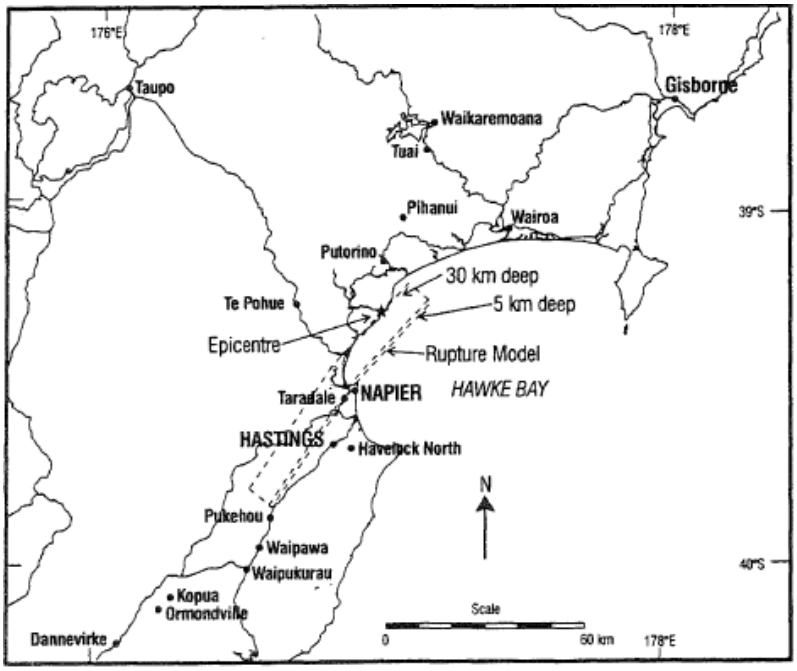

Figure 7: Elastic dislocation model for the main event by Haines & Darby (1987) *(from Dowrick 1998)*

Source parameters in Table 3 for the main shock and the three largest aftershocks were obtained from the analysis of several seismograms (Doser and Webb 2003) and are in accord with the displacement model obtained by McGinty et al. (2001).

Table 3: Source parameters for the faulting mechanism *(from Doser and Webb 2003)*

Event	**Focal mechanism**[1]			**Moment x10^{18} (N m)**	**Depth (km)**
	Strike	Dip	Rake		
Main shock	225±20	70±10	165±15	220±80	15±3
AS1	215±10	50±5	70±10	0.6±0.15	8±3
AS2	225±20	70±20	180±10	4.5±0.6	15±6
AS3	203±20	78±14	176±7	92±4	16±352

[1] Values are the first set of parameters in Table 2 of Doser and Webb (2003) obtained from the Baker and Doser (1988) method

2.3.4 *Characterization of Ground Elevation*

2.3.4.1. Post-Earthquake Changes in Land Elevation

Surface deformation during the Hawke's Bay earthquake was manifested in a zone of uplift trending northeast and extending from southwest at Hastings to northeast of the Mohaka River mouth. As a result of this deformation, the Ahuriri Lagoon was uplifted and the bed of the lagoon was visible at the surface. Also, the Tutaekuri River, which in the past flowed into the southern part of the lagoon, changed course and now bypasses the lagoon to the south. The projection of the rupture plane to the surface is

the line of zero vertical displacement to the south of Napier and continues offshore in a northeastern trend.

A maximum uplift of 2.7 m occurred near Oldmans Bluff (northeast of Napier), and a maximum subsidence of 1 m occurred at Hastings. Hull (1990) suggested that the aftershocks located offshore of Oldmans Bluff led to the observed maximum uplift in this locality. Marshall (1933) reported an increase in tidal levels in the Ngaruroro and Clive Rivers near the coast. Figure 8 shows the changes in elevation as a result of the earthquake. Elevation data were compiled by Henderson (1933) and Marshall (1933) from the relevelling of stop banks along the low-lying Heretaunga Plains and from the relevelling of the Wellington-Gisborne railway. Elevation changes continued for up to a year after the event. The elevation changes shown in Figure 8 (particularly in the zone of uplift) are the net result of co-seismic uplift and post-seismic movement (<0.5 m down-drop adjustments) (Hull 1990). A study of the change in levels shows that the northern part of the Heretaunga Plains was uplifted and the southern part was subsided.

Marshall (1933) studied the coastline between Wairoa and Cape Kidnappers (south Hawke's Bay) and estimated the height change from tide-gauge data and pre-earthquake high-tide levels. Shortly after the earthquake, the wave action increased due to the emptying of the Ahuriri Lagoon. The lagoon was shallow and dry during low water levels as a result of deposition of silts from streams. Examination of the shore showed changes in coastal levels starting from the mouth of the Tukituki River. The strip between the Tukituki and Ngaruroro Rivers was approximately 0.3 m lower after the earthquake, resulting in saltwater intruding into marshes and lagoons which previously did not occur. The subsidence was attributed to the settlement of loose deposits subjected to earthquake shaking. North of the Ngaruroro River mouth, the beach seemed more affected and ridges could be seen. For half a mile north, saltwater marshes increased in the area, implying a 0.1 m downward movement. Beyond half a mile north of the mouth of the Ngaruroro River, a gradual increase in elevation could be noticed as Napier was approached. Further north of Napier, the breakwater was little affected by the earthquake, but it rose 1.8 m. The Ahuriri Lagoon which was shallow and flat prior to the earthquake was uplifted by 1.8 m, resulting in 13 km^2 of dry land being reclaimed. The amount of uplift gradually increased from the town of Tangoio (1.8 m) to Moeangiangi River (2.7 m) near Oldmans Bluff. North of Oldmans Bluff, the uplift was quite small and landslides took place. A total of 30 km^2 were uplifted by the earthquake in 2 minutes and 30 seconds.

2.3.4.2. Present Ground Digital Elevation Model (DEM)

In 2003, Hawke's Bay Regional Council performed a LiDAR survey of the Heretaunga and Ruataniwha Plains. The accuracy of the LiDAR is roughly 1.8 m and the datum is 10 m above mean sea level (MSL). For this study, the terrain was processed to produce a Digital Elevation Model (DEM). The DEM shown in Figure 9 was cropped to the extent of the present study area, expressed in terms of MSL and reshaped to a 25 m × 25 m raster.

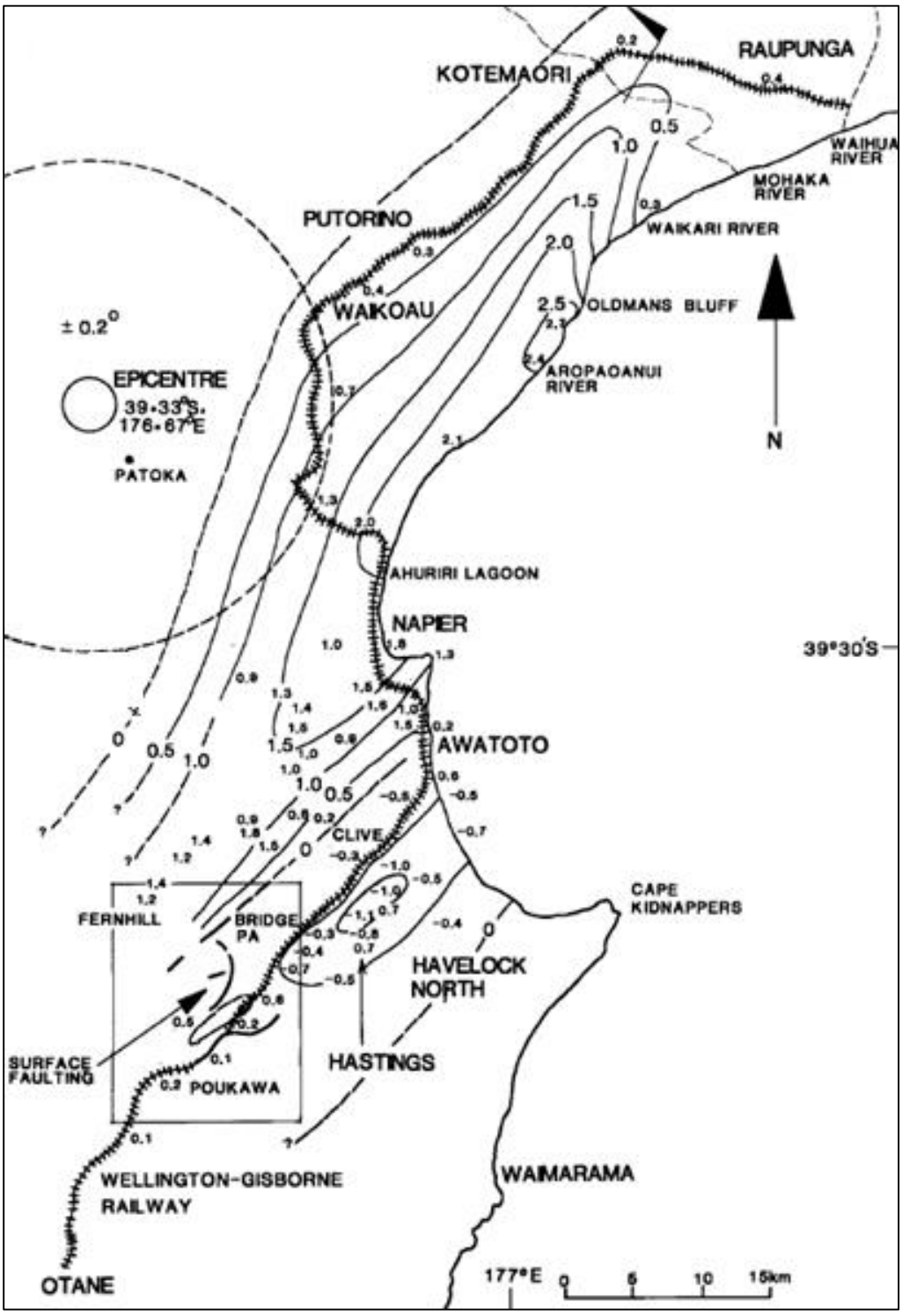

Figure 8: Tectonic movement after the 1931 Hawke's Bay earthquake and its 13 February aftershock *(from Hull 1990).* Note the older location for the epicenter.

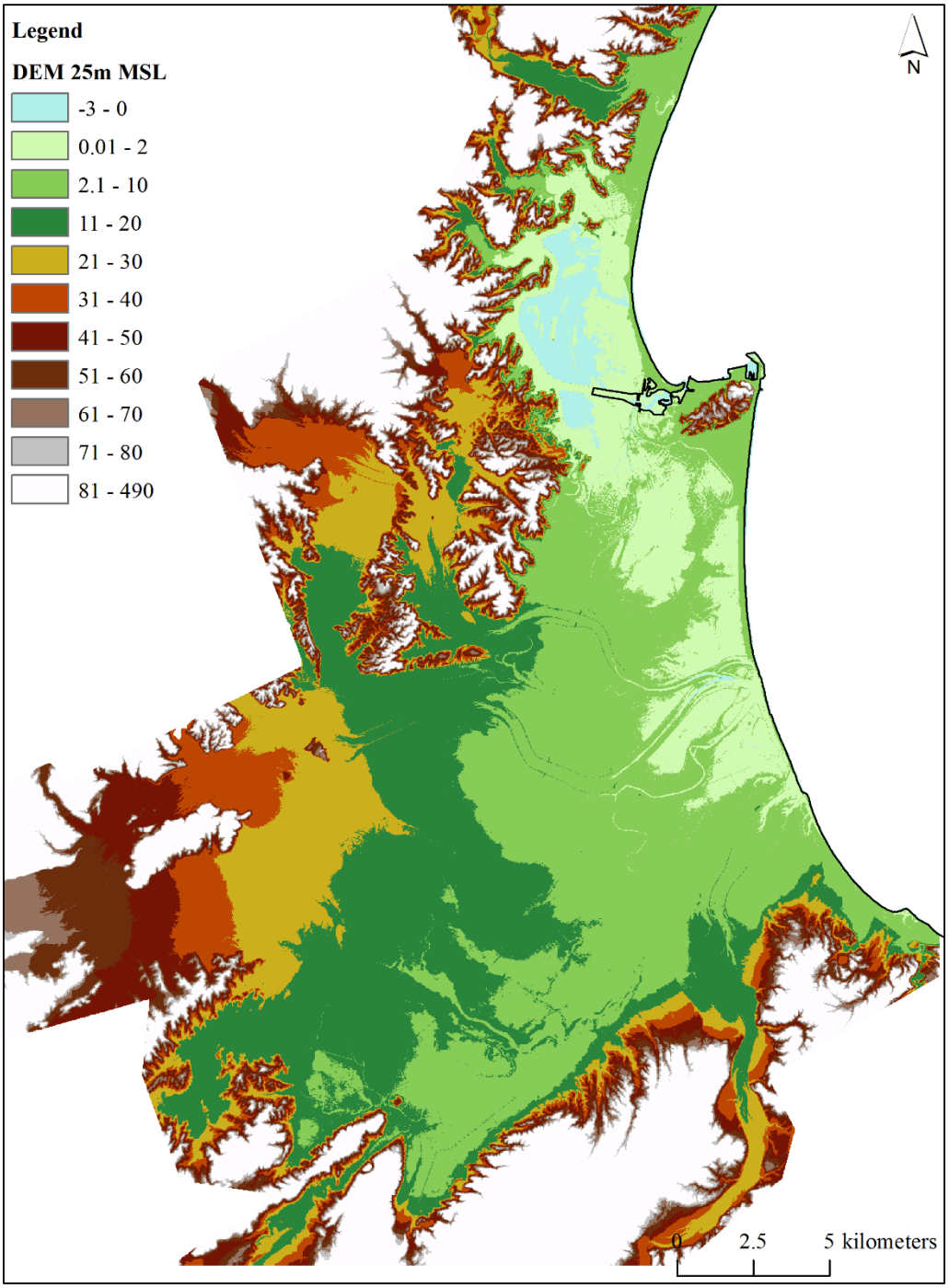

Figure 9: Digital Elevation Model for the Heretaunga Plains

2.3.5 *Characterization of 1931 Ground Shaking*

The ground shaking from the Hawke's Bay earthquake was felt throughout much of New Zealand, except in areas far North (Auckland) and far South (Otago). Dowrick (1998) defined the extent of MMI based on the 1996 New Zealand intensity scale. The study presents an overview of the damage to the built environment and the MMI intensities for the 1931 event. Based on the severity of the damage at different locations around Hawke's Bay, Dowrick (1998) developed isoseismal maps for the event. The effects of the earthquake were greatest in the towns of Napier and Hastings (MMI X). Yet, other towns in Hawke's Bay experienced major damages such as Eskdale, Greenmeadows, Petane, Tangoio, and Taradale (MMI X), Awanui, Bay View, Bridge Pa, Clive, Havelock North, Mohaka, and Poraiti (MMI IX), and Fernhill, Poukawa, and Te Aute (MMI IIX).

The criteria that were used to estimate the shaking intensities were entirely based on damage to buildings. In Napier, an assessment of building damage was hampered by the significant number of buildings that were damaged by post-earthquake fires (total of 130). Thus, the assessment of the intensities of shaking was based on damage to the remaining buildings (total of 520). Similarly in Hastings, 11 buildings were destroyed by fire, and the effects of shaking were established from the remaining 255 buildings. Additional details on the assignments of MMI can be obtained from Dowrick (1998). From the assignment of MMI intensities, isoseismals were derived and are shown in Figure 10.

Peak ground acceleration (PGA) is a more useful parameter in assessing liquefaction hazard than MMI intensities. The ground motions for the 1931 Hawke's Bay earthquake were simulated by Bayless et al. (2017) using the Southern California Earthquake Center (SCEC) Broadband Strong Ground Motion Simulation Platform (BBP). Based on historical data from the 1931 Hawke's Bay earthquake, the velocity and density model as well as the earthquake source were characterized. A shallow crustal earthquake source model was used for the simulation. The earthquake was not recorded on ground motion instruments, but the isoseismal map from Dowrick (1998) was used to compare the simulated PGAs with the MMI map. To establish this comparison, simulated PGAs were converted to intensities using the Ground Motion Intensity Conversion Equation (GMICE) from Caprio et al. (2015). The converted intensities were checked against the MMI intensities from Dowrick (1998) and the 2 sets of intensities were in good agreement (Bayless et al. 2017). The resulting ground motion or PGA map for the Hawke's Bay earthquake is shown in Figure 11, and as discussed in subsequent sections of this paper was used in the liquefaction hazard study of the region. More details on the PGA map in Figure 11 are given in Appendix A.

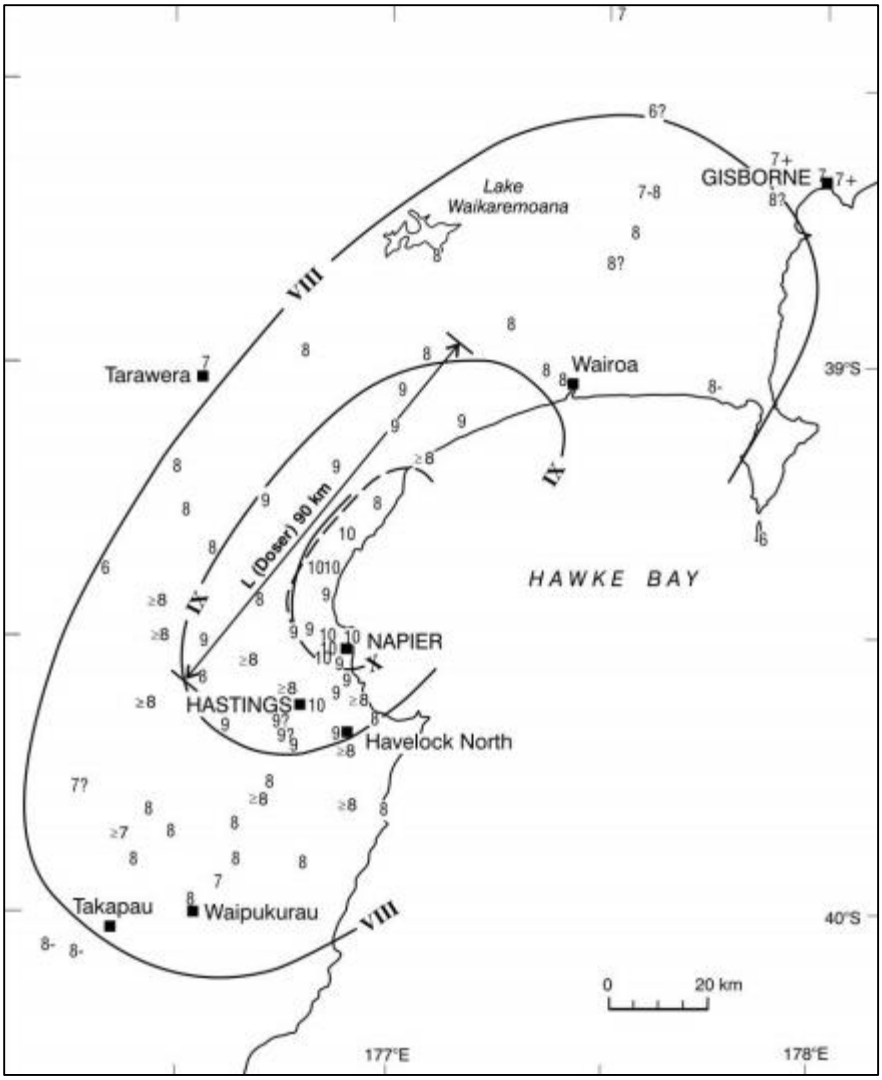

Figure 10: MMI isoseismals of the 1931 Hawke's Bay earthquake based on observations. *(from Dowrick 1998)*

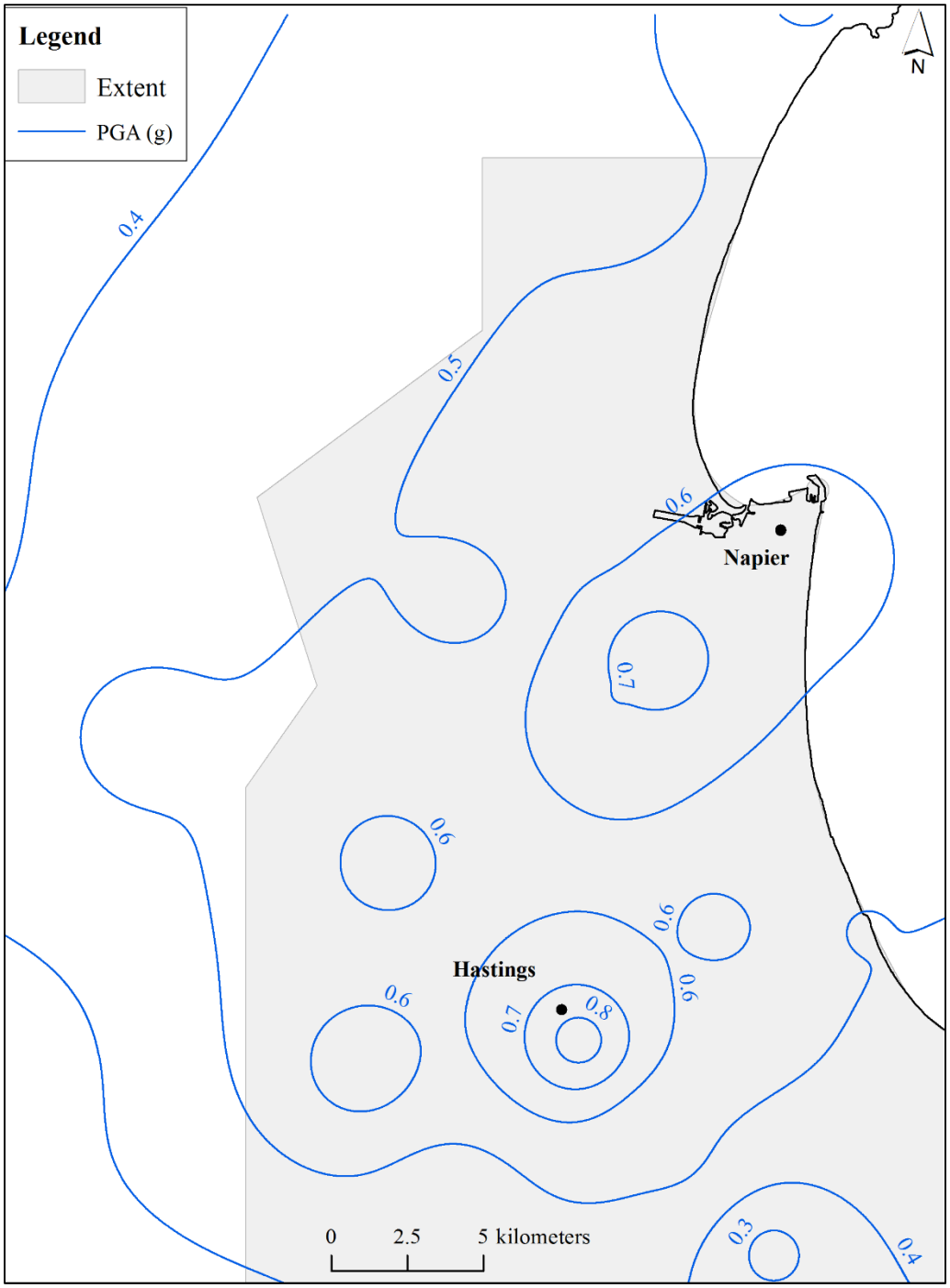

Figure 11: Ground motion characterization based on PGA from MMI

2.3.6 *Documentation of Liquefaction during the 1931 Event*

As stated previously, the 1931 event was accompanied by well-documented changes in elevation, faulting, liquefaction, and landslides (Callaghan 1933; Dowrick 1998; Hull 1990; Marshall 1933). Liquefaction occurred over wide areas in Hawke's Bay and was

documented in historical photographs (e.g. Figure 12), personal accounts, books, and newspaper clips. Additionally, published journal articles after the event provide scientific description of liquefaction, although the phenomenon was not fully understood at the time. Callaghan (1933) reports observations of liquefaction manifestations during his inspection after the earthquake, and Fairless and Berrill (1984) report liquefaction effects in Heretaunga Plains, Taradale, Clive, Esk Valley, Mohaka, Tangoio, Petane, and Gisborne. The reported ground damage included sand boils or mud spouts or sand geysers, cracks and fissures, differential settlement, and lateral spreading.

Figure 12: Sand boils at Petane *(from the archives of the MTG Hawke's Bay Museum)*

2.4 Liquefaction Hazard Study

As stated previously, the overall objective of this study is to provide insights on the liquefaction hazards in Napier and Hastings based on the assessment of data from the 1931 Hawke's Bay earthquake. Towards this end, CPT-based liquefaction triggering evaluations are used within LPI and LSN frameworks to predict the severity of the surficial liquefaction manifestations for the 1931 Hawke's Bay earthquake scenario. The required inputs for the analyses include the soil profile characteristics across the study area, the estimates of PGA from the 1931 Hawke's Bay earthquake, and the approximate groundwater depths at the time of the event.

The steps followed to achieve the research objectives were:

1. Collect liquefaction observations from 1931 archives. These observations serve as a validation tool to the results of the liquefaction analysis described hereafter.
2. Develop an understanding of the soil profile in Napier and Hastings and gather CPT sounding to be used in the analysis. The tip resistance (q_c) and the sleeve

friction (f_s) are used in the liquefaction triggering assessment to characterize the soil at each CPT location.

3. Characterize the distribution of PGAs across Napier and Hastings using the PGA model developed by Bayless et al. (2017). The PGAs are used to evaluate the liquefaction triggering potential at sites of interest.
4. Develop a groundwater model to estimate the ground water depth (GWD) at the time of the earthquake. The GWDs are used to evaluate the liquefaction triggering potential at sites of interest.
5. Perform a liquefaction vulnerability assessment of the region using the CPT-based simplified liquefaction evaluation procedure proposed by Boulanger and Idriss 2014 within the LPI and LSN frameworks. The inputs for the evaluation include data from the CPT sounds, estimates of the PGAs, and estimates of the GWDs at the time of the earthquake (as obtained above).
6. Compare predicted surficial liquefaction manifestation severity with the field observations made following the 1931 Hawke's Bay earthquake. Considerable effort was spent compiling and geo-referencing historical accounts relating to the liquefaction response in Napier and Hastings.
7. Identify regions where the predictions are and are not accurate.

2.4.1 *Collection of 1931 Liquefaction Records*

As stated previously historical photographs, personal accounts, books, newspaper clips, and journal articles provide documentation of the occurrence of liquefaction during the 1931 Hawke's Bay earthquake. These sources were used to develop a database of liquefaction manifestations during the 1931 earthquake. The reported ground damage included sand boils or mud spouts or sand geysers, cracks and fissures, differential settlement, and lateral spreading in Heretaunga Plains, Taradale, Clive, Esk Valley, Mohaka, Tangoio, Petane, and Gisborne. Based on these accounts, a database was compiled and was used to assess the validity of the severity predictions. An example of the collection of observations is shown in Figure 13.

This task was divided into 2 parts based on the sources of information. The first part covered liquefaction observations obtained from a literature review. Information on occurrences of liquefaction around Hawke's Bay was compiled by Brodie and Harris (1933), Callaghan (1933), Dellow et al. (2003), Dowrick (1998), Fairless and Berrill (1984), Henderson (1933), and Marshall (1933). The second part involved a visual study of photographs, newspaper clips, and personal accounts from 1931 from the archives of the MTG Hawke's Bay Museum & Art Gallery, Napier Public Library, and Hastings District Libraries, from published books on the history of Hawke's Bay, and from personal communications with the local historian Mr. Michael Fowler (Fowler 2007, 2013).

The quality and spatial distribution of the liquefaction observations are highly variable, partly due to the lack of understanding of the liquefaction phenomenon at the time and partly due to the low population densities of the region. Early observers did not explicitly search for liquefaction manifestations, and hence, historical cases of

liquefaction had to be inferred from available information that is undoubtedly incomplete. Thus, it is probable that occurrences of liquefaction have not been identified. More details on the liquefaction observations in Hawke's Bay and particularly in our area of study are described in Appendix B.

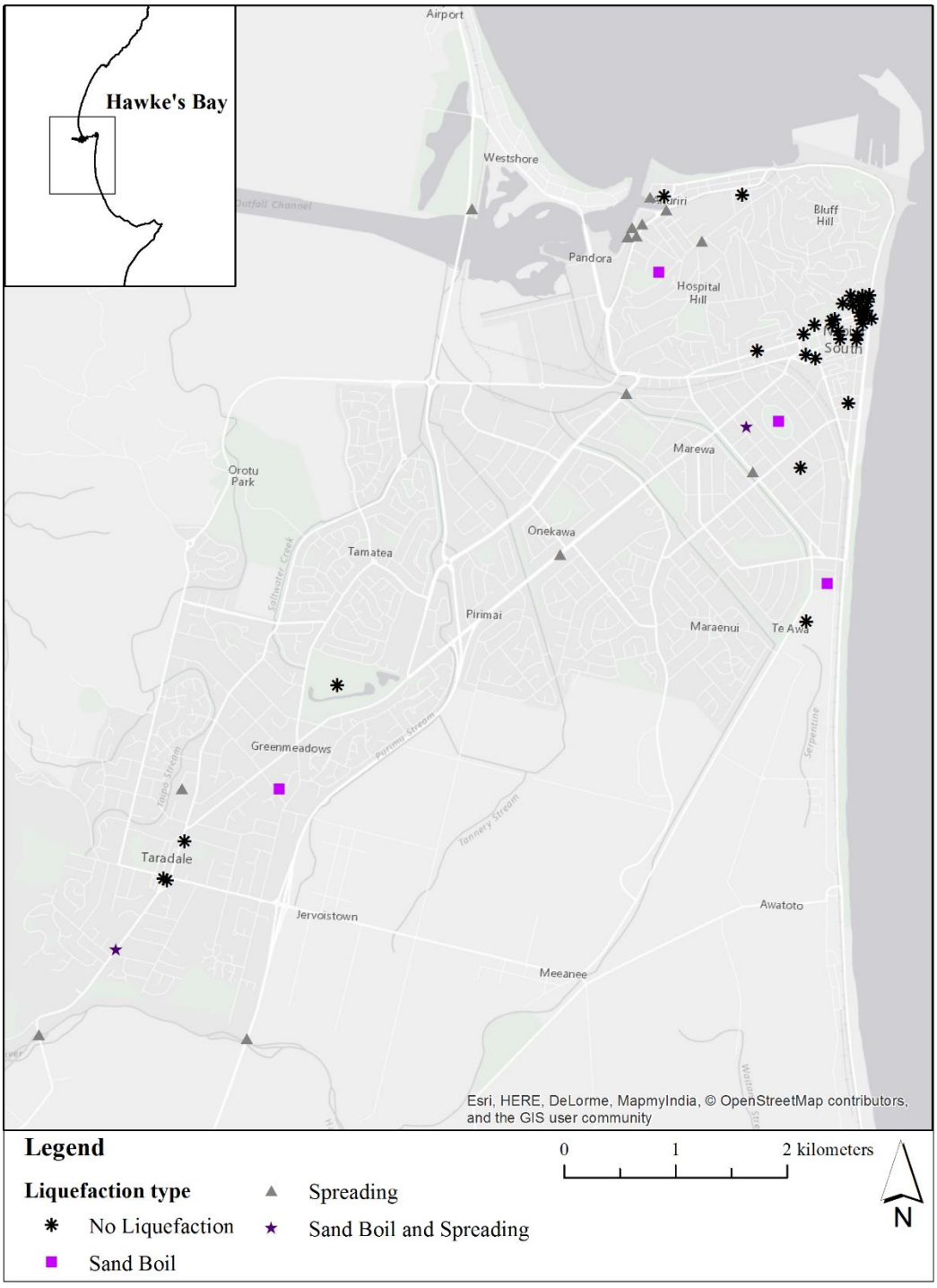

Figure 13: Overview of liquefaction observations around Napier

2.4.2 *Characterization of the Soil Profile using Subsurface Site Investigations*

Subsurface site investigation data in Hawke's Bay are available from the New Zealand Geotechnical Database (NZGD) and Tonkin and Taylor Geotechnical Database (TTGD). At present, there are 65 boreholes (BHs) and 897 CPT soundings for Napier and Hastings. The borehole logs were digitized in the TTGD and most of the CPT soundings were already in digital format in the database.

Examination of the BHs in Napier City reveals that the soil profiles vary across the city. In general, the profiles consist of alluvial deposits underlain by beach deposits underlain by a dense gravel layer. The alluvial deposits are thicker along the coast, with their thickness decreasing landward such that the gravel layer at Taradale is 11 m deep. Also, going from the sea inland, the sand at Te Awa has a significant fraction of clayey material. Closer to the Napier Central Business District (CBD), the sand in Napier South is silty and a medium dense gravel layer is encountered at a depth of ~2 m. Farther west, in Maraenui and Onekawa, a loose silty sand deposit that is interbedded with silt layers is up to 20 m thick and traces of gravel are present at approximately 15 m deep. In Taradale, silts dominate the soil profile, and a dense gravel layer is present at a depth of 11 m. In Napier, no boreholes were available, but hand auger logs show an intercalation of sands and silts.

Examination of BHs in Hastings reveals that the alluvial deposits are very thick. A 31 m borehole was drilled at the police station in Hastings, and there were no signs of a gravel layer. The deposits are loose to medium dense. The stratigraphy in Hastings is comprised of interbedded layers of sand and silt with a minor clay fraction. There is a continuous trace of pumice at a depth of 4 m in one location and at 8 m in other locations. The pumice is a byproduct of the last eruption of the Taupo volcanic zone and was transported to the Heretaunga Depression (where Hastings is located) by the meandering rivers.

897 CPT soundings were used in the Tonkin and Taylor liquefaction calculator. A number of sounds were discarded because pre-drilling was performed to bypass buried utilities and extended into the liquefiable layers. Accordingly, the data obtained from the CPT (i.e., tip resistance, q_c, and sleeve friction, f_s) for this portion of the liquefiable layers are unreliable. Twenty-nine soundings were discarded because of pre-drilling.

As discussed subsequently, the LPI and LSN frameworks nominally require the CPT to be performed to full depth of liquefiable soils, for maximum depth of 20 m. However, this criterion was relaxed to a maximum depth of 10 m, otherwise the number of CPT soundings included in the analyses would have been very limited. Soundings between 5 and 10 m were also considered in the analyses by performing the analyses both with and without these "short CPTs" included in the database. The reason for this is because the CPT sounding may have been terminated between 5 and 10 m because the penetrometer hit refusal due to the presence of a denser material or gravel layer (e.g., the deeper layers were not liquefiable). In this case, the calculated liquefaction vulnerability index value for the short CPTs would be appropriate for use in assessing

liquefaction hazard. However, it is also possible that the CPT sounding was terminated at a shallow depth because characterization of the near surface is all that was needed for the project for which the sounding was being performed (e.g., static bearing capacity conditions for lightweight structures). In this case, the calculated liquefaction vulnerability index value for the short CPTs would not be appropriate for use in assessing liquefaction hazard. Since both scenarios are possible, the liquefaction hazard analyses were performed both with and without these "short CPTs" included in the database. The spatial distribution of CPT soundings is shown in Figure 14.

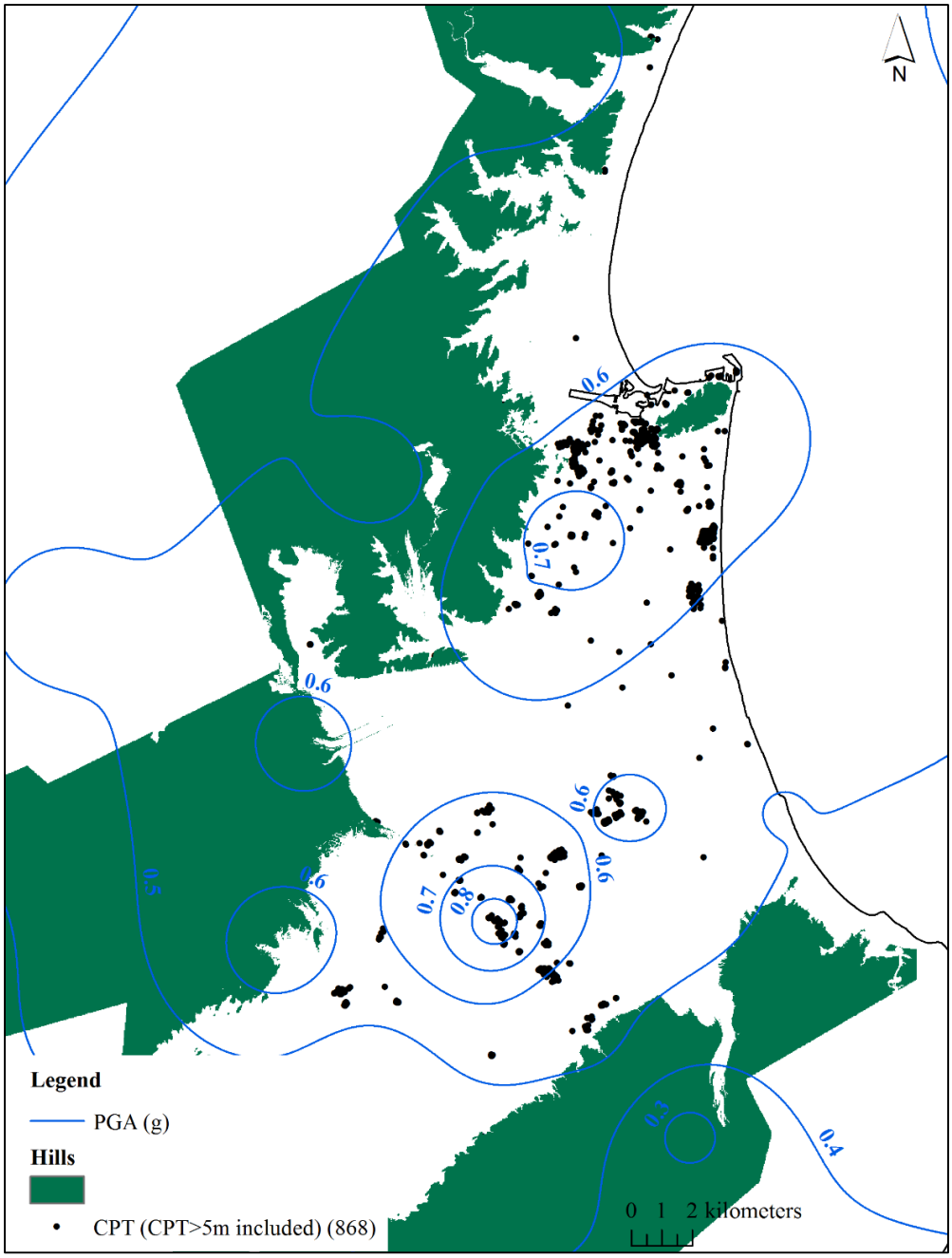

Figure 14: Spatial distribution of CPT soundings with depth greater than 5 m

2.4.3 *Estimation of Groundwater Elevations at the Time of the Earthquake*

Depth to the groundwater table at the time of the 1931 Hawke's Bay earthquake is needed as an input into the liquefaction hazard analyses. Specifically, the unconfined groundwater at shallow depth plays a key role in liquefaction triggering during earthquakes. This section outlines the development of a groundwater depth model that is used to estimate the GWD at the time of the 1931 earthquake.

A major fluvial gravel aquifer system underlies the Heretaunga Plains that is comprised of a postglacial gravel-marine transgression aquifer system and a peripheral limestone aquifer system. The aquifer system is mainly composed of saturated gravel sediments deposited by the rivers as a byproduct of recurring natural processes such as tectonic deformation and variation of sea levels during geologic periods. For the last 250,000 years, tectonic deformations in Hawke's Bay had major impacts on the hydrology of rivers in the area and the formation of aquifers in the Heretaunga depression. Most rivers in Hawke's Bay underwent course adjustments in response to this deformation: Mohaka, Esk, Tutaekuri, Tukituki, and Ngaruroro Rivers. Three rivers converge on the plains and recharge the interconnected aquifer system. The Ngaruroro and Tutaekuri Rivers enter the plains from the west (between the limestone hills) while the Tukituki River enters from the southeast. The Ngaruroro River deposited gravel in the center and southern part of the plains, the Tutaekuri River deposited gravel in the area from Napier south to Meeanee, and the Tukituki River, which entered the plains in the last 20,000 years, deposited gravel on the eastern part of the Heretaunga Plains. Dravid and Brown (1997) suggested that the erosion and deposition of river beds and flood channels similarly filled the Heretaunga depression with gravel over the last 6000 years. The Ngaruroro-Tutaekuri aquifer system underlies most of the plains (250 km^2) and thus, is the major aquifer system. It extends to a depth of 250 m and was formed by the Ngaruroro River. The aquifer system starts unconfined in the west and becomes gradually confined to the east. The main aquifer system merges with the peripheral system in the northern and eastern parts of the Heretaunga Plains.

2.4.3.1. Previous Studies on the Ground waters of the Heretaunga Plains

The hydrogeology of the Heretaunga Plains was studied previously. Grant (1972) compiled a report on the groundwater of the area based on flow data. Buckland (1974) built on this work and investigated the extent of the unconfined aquifer area of the Heretaunga Plains groundwater system and evaluated the possibility of water contamination by land use. McLellan (1988) described the basin configuration in western Heretaunga Plains. However, the most complete hydrological study of the Heretaunga Plains is by Dravid and Brown (1997). In an internal report completed in 2006, the Hawke's Bay Regional Council's Environmental Monitoring Section revisited the computer model of the Heretaunga steady-state groundwater done in 1997 (HBRC 2006).

2.4.3.2. Development of the groundwater model

Most of the data compiled by the Hawke's Bay councils is on the confined aquifers. Due to the scarcity of unconfined groundwater data, the dataset used herein to develop the GWD model is a combination of water level measurements from site investigations within the boundaries of the study area (i.e. boreholes and cone penetration tests CPTs), hydrostatic water levels from well drilling logs (only water table aquifers), and piezometers tapping unconfined aquifers. The initial dataset was further divided into data representing low flow and high flow conditions. The focus herein is on the low flow conditions for a couple reasons. First, the levels of surface water constraining the model inland typically represent low flow conditions (i.e. more data is available for the low flow condition). Second, the 1931 event occurred during the summer when typical low flow conditions prevail; thus for the analysis and observations to be comparable, similar conditions should be considered in the liquefaction assessment. In the same line of thought, it is assumed that no precipitation occurred before or at the time of the earthquake because Hawke's Bay District "was experiencing the mild drought conditions of midsummer" (Callaghan 1933). Also, due to the lack of information, the effect of pumping on groundwater could not be estimated.

There are a number of uncertainties in the static water levels described above. The water levels from the Hawke's Bay Regional Council consist of a series of wells drilled over a period spanning from the 1920s to present day. Therefore, the measurements were taken at a given point in time (typically at the time of drilling of the well) and may not represent the general trend of the groundwater table due to effects of drilling, pumping, and not allowing time for the water table to restore to equilibrium conditions. Also, the quality of the data is highly variable due to the advances in instrumentation from 1920s until present and potential measurement or recording errors at the time of drilling. Consequently, the data is treated as having ± 1 m accuracy. In addition, there are no records of groundwater level responses (i.e. temporal or permanent change in water level) due to the earthquake, and thus, a positive offset (i.e. a permanent increase groundwater level) cannot be inferred from the data, although such offsets have been documented in more recent earthquakes: the 2010 M_w7.1 Darfield earthquake, the 2011 M_w6.2 Christchurch earthquake (Gulley et al. 2013), the 2011 M_w5.8 Mineral, Virginia earthquake (Roeloffs et al. 2015) and the 2016 M_w5.8 Pawnee, OK, and M_w5.0 Cushing, OK, earthquakes (Kroll et al. 2017) .

Figure 15 summarizes the procedure used to develop the groundwater model. This procedure is detailed in Appendix C. The estimated GWD at the time of the earthquake using the model is mapped in Figure 16.

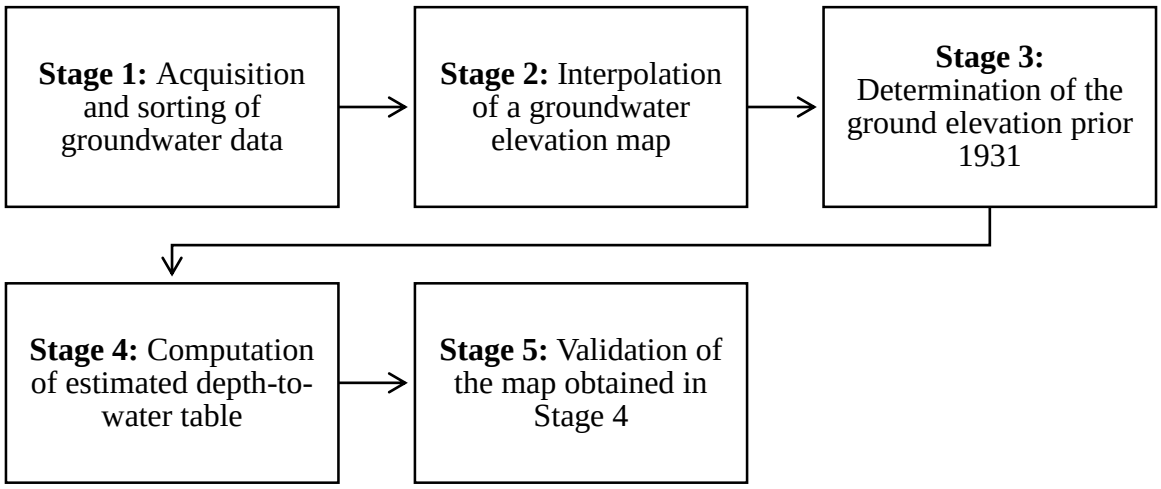

Figure 15: Procedure for the development of the groundwater model

The GWD model generates a smooth surface and consequently is an approximate fit of the regressed data. Based on the comparison of predictions and measurements, the model provides the most accurate estimates of groundwater elevation at the center of the study area. The prediction errors increase away from the center of the study area due to the reduction in the spatial density of available data. The areas of interest, Napier and Hastings, fall in the region of the model where the model yields the most accurate predictions. Thus, this model is satisfactory for use in the liquefaction hazard analyses. Nevertheless, further improvements can be made to the model by enhancing the quality of the well database and the number of groundwater monitoring wells.

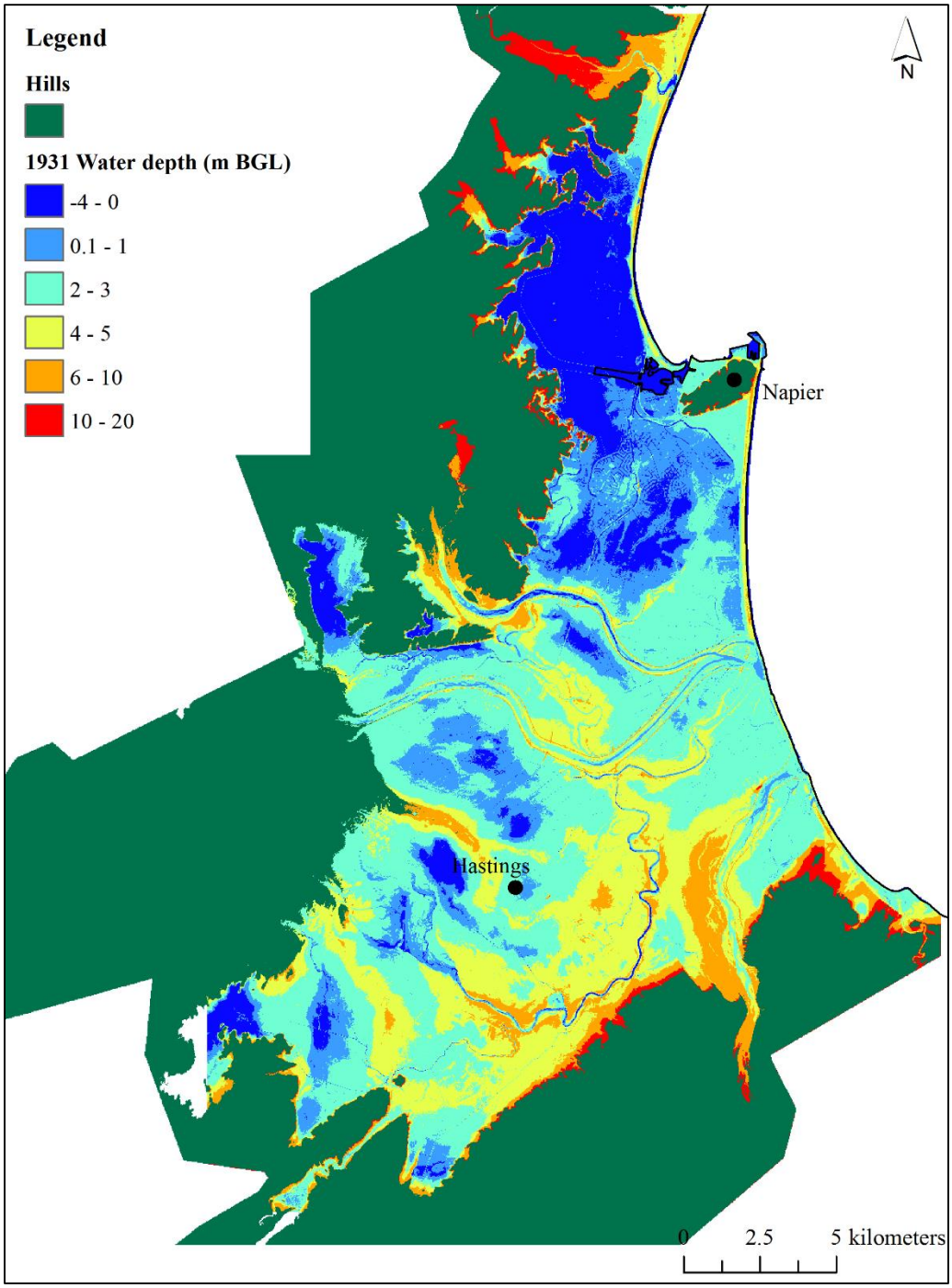

Figure 16: Estimated ground water depths at the time of the 1931 Hawke's Bay earthquake

2.4.4 *Liquefaction Triggering Assessment*

Using the inputs outlined above, to include PGAs from the Bayless et al. (2017) PGA model, the Boulanger and Idriss (2014) CPT-based simplified liquefaction triggering procedure was used to compute the factor of safety against (FS) liquefaction. The additional input parameters needed for the analyses are listed in Table 4.

Table 4: Input parameters for the liquefaction triggering analysis *(partially reproduced from Tonkin and Taylor, 2013)*

Input parameter	**Default value adopted**	**Comments**
Soil Unit weight	18 kN/m^3	Not sensitive to the typical variability in soil density in Christchurch (Tonkin and Taylor 2013)
FC - I_c correlation	CFC = 0.0	Assumption in line with appropriate upper bound value for Christchurch soils (Leeves et al. 2015)
I_c - cutoff	I_c cutoff = 2.6	Assumption in line with appropriate value for Christchurch soils (Leeves et al. 2015)
Level of earthquake shaking	M_w = 7.4, estimated PGA from the 1931 earthquake (see Section 2.3.5)	PGA model (Bayless et al. 2017)
Probability of Liquefaction (P_L)	Deterministic CRR curve (i.e., PL = 15%)	Based on standard engineering design practice
Depth to Groundwater (GWD)	Estimated groundwater levels at the time of the earthquake (see Section 2.4.3)	Two key assumptions associated with GWD are: - The groundwater profile is hydrostatic below the ground water surface - The soils are fully saturated below the groundwater surface

2.4.5 *Overview of Liquefaction Severity Indices*

While the Boulanger and Idriss (2014) simplified procedure predicts the FS at a given depth in a soil profile, it does not predict the severity of surficial liquefaction manifestations, which is of interest to this study. However, the FS is used as an input into the LPI (Iwasaki et al. 1978, 1982) and LSN (van Ballegooy et al. 2014) liquefaction vulnerability assessment frameworks which account for the cumulative liquefaction response of the profile down to a maximum specified depth to predict the severity of surficial liquefaction manifestations. Both of these frameworks have been

widely used in practice (van Ballegooy et al. 2014; Holzer et al. 2006; Maurer et al. 2014, 2015a; b; Papathanassiou et al. 2005; Sonmez 2003). The LPI is computed as:

$$LPI = \int_0^{20m} F \cdot w(z)dz \tag{1}$$

where: F = 1 – FS for FS ≤ 1 and F = 0 for FS > 1; and $w(z)$ = 10 – 0.5z where z = depth in meters below ground surface (Iwasaki et al. 1978, 1982). Per Eq. 1, computed LPI values can range from 0 to 100, with the severity of the predicted surficial liquefaction manifestation increasing with increasing LPI value (Table 5). The computed LPI value is proportional to the thickness of the liquefied layers, the amount by which FS is less than one in the layers, and the proximity of the layers to the ground surface.

While the LPI framework is widely used in practice, it was found to have a misprediction rate that is higher than desirable (van Ballegooy et al. 2014; Beyzaei et al. 2017; Cox et al. 2017; Cubrinovski et al. 2017; Maurer et al. 2014, 2015b). Three of the identified shortcomings of the LPI framework are: (1) the linear depth weighting factor ($w(z)$) may not properly account for the influence of layer depth on severity of surficial liquefaction manifestations; (2) by only considering FS, independent of the density of the soil, on severity of surficial liquefaction manifestations the contractive/dilative tendencies of the soil are not fully taken into account; and (3) layers having a FS greater than one are considered not to have an influence on surficial liquefaction manifestation, which is not in accord with laboratory tests (Ishihara and Yoshimine 1992). As a result, the LSN framework was proposed as an alternative (van Ballegooy et al. 2014). LSN is defined as:

$$LSN = 1000 \int \frac{\varepsilon_v}{z}\, dz \tag{2}$$

where: ε_v is the calculated volumetric reconsolidation strain per Zhang et al. (2002); and z is the depth to the layer in meters below the ground surface. As may be observed from Eq. 2, the depth weighting factor is hyperbolic (i.e., 1/z). Additionally, ε_v is both a function of FS and the density of the soil, and thus accounts for the contractive/dilative tendencies of the soil, and has a value greater than zero for FS < 2. As with LPI, the severity of the predicted surficial liquefaction manifestation increases with increasing LSN value (Table 6).

Table 5: LPI values used for damage classification *(reproduced from Maurer et al. 2014)*

Severity classification	**Expected LPI range**
No liquefaction	LPI < 4
Marginal	4 ≤ LPI < 8
Moderate	8 ≤ LPI < 15
Severe	LPI ≥ 15

Table 6: LSN values used for damage classification *(reproduced from Tonkin &Taylor 2016)*

Severity classification	Expected LSN range
No liquefaction	LSN < 16
Medium	16 ≤ LSN < 25
High	25 ≤ LSN < 35
Very high	LSN ≥ 35

Although the LSN was specifically developed to overcome shortcomings in the LPI framework, it has not been scrutinized by the geotechnical earthquake engineering community to the extent that the LPI framework has. As a result, it undoubtedly has its own shortcomings and should not be expected to yield perfect predictions for all scenarios (e.g., Green and Maurer 2017). Accordingly, both the LPI and LSN frameworks are used herein to predict the severity of surficial liquefaction manifestations in Napier and Hastings for the Hawke's Bay earthquake scenario. This is discussed in more detail in Section 2.4.7. It is important to note, however, that lateral spreading is a distinct form of liquefaction manifestation that can be very damaging to infrastructure. The severity of lateral spreading cannot be deduced from LSN and LPI indices because neither of these frameworks incorporate topographic factors that significantly influence the severity of lateral spreading (e.g. height of the nearest free-face, distance from the free-face, and ground slope) (van Ballegooy et al. 2014; Green and Maurer 2016; Maurer et al. 2014). However, if the FS > 1 for the full depth of the soil profile, then it can be reasonably assumed that the severity of lateral spreading will be none.

2.4.6 *Uncertainties of the Input into the Liquefaction Analysis*

Given the uncertainties in the estimated MMI-based PGAs (Section 2.3.5), two sets of values were used in the analyses. The first set consisted of the PGA values obtained directly from the Bayless et al. (2017) MMI-based model and the second set were the Bayless et al. (2017) model PGAs multiplied by 0.5. Additionally, the influence of the "short CPTs" was also considered in the analyses by performing the analyses both with and without these soundings included in the database (refer to Section 2.4.2 for additional discussion of the short CPTs). Accordingly, four sets of analyses, referred to as Cases 1-4, were performed to examine the effect of input parameters on the results (Table 7). The results for Case 1, which is considered to represent unbiased predictions, are presented and discussed in the next section; the results of the remaining cases are included in Appendix D.

Table 7: Sensitivity analysis on PGA and inclusion of short CPTs

Case	PGA	Short CPTs
1	PGA	Excluded
2	PGA	Included
3	0.5 × PGA	Excluded
4	0.5 × PGA	Included

The uncertainty in GWD was also considered for incorporation in the case matrix in Table 7. Figure 17 is a plot of computed LPI values as a function of GWD for each of the CPT locations for Case 1. As may be observed from this figure, there is a general trend of decreasing LPI values as GWD increases; note that LSN values were also computed and show a similar trend. This implies that the shallower the GWD, the more severe the expected surficial liquefaction manifestations. However, the large scatter in the data suggests that factors other than GWD have a more significant influence on potential liquefaction severity and that the uncertainty in the GWD is not a primary controlling factor. Hence, the decision was made not to incorporate GWD into the case matrix in Table 7.

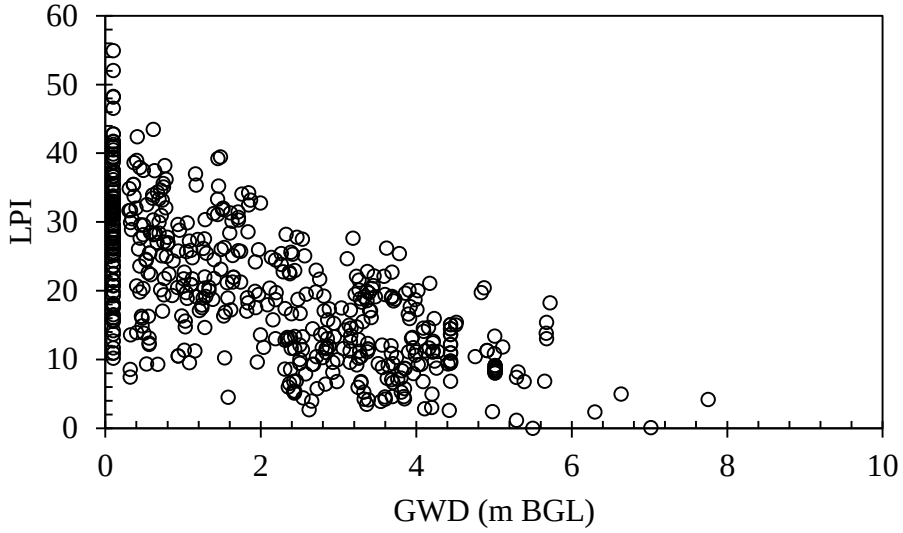

Figure 17: Variation of LPI with respect to GWD (LPI results taken from Case 1)

2.4.7 *Results*

Maps of computed LPI and LSN for Napier and Hastings are shown in Figure 18 and Figure 19, respectively. The maps in Figure 18a and 18c and Figure 19a and 19c are overlain by the PGA contours used in the analyses. The locations of CPT soundings where liquefaction severity indices were computed are shown in these figures. The maps in Figure 18b and 18d and Figure 19b and 19d are overlain with liquefaction observations made shortly after the 1931 earthquake, to facilitate comparisons of predicted versus observed liquefaction manifestations.

Per Figure 18a, Napier and its suburbs are predicted to have experienced severe liquefaction during the 1931 Hawke's Bay earthquake (red colored CPTs), except for some locations in Ahuriri, Napier CBD, Tamatea, Maraenui, and Taradale where liquefaction is predicted to be less severe per LSN (Figure 18c). The lower severity predictions are possibly related to the soil density or depth distribution of liquefiable layers captured by LSN only. Compared to the mapped liquefaction severity, Figure 18b and 18d show that both LPI and LSN predict more severe liquefaction than was observed after the earthquake.

Per Figure 19, the severity of liquefaction in Hastings is predicted to have been less severe than in Napier. Per the LPI map (Figure 19a) marginal to moderate surficial liquefaction manifestations are predicted to have occurred during the Hawke's Bay earthquake, while the no liquefaction to medium severity is predicted to have occurred per the LSN map (Figure 19c).

Despite the similarity in the PGA values for Napier and Hastings (MMI X), the predicted severity of liquefaction is less for Hastings than it is for Napier. Possible reasons for this are the shallow depth of the ground water table in Napier relative to Hastings and that most of Napier sits on poorly compacted sands and silts that were used to reclaim swampland, resulting in profiles that are very susceptible to liquefaction during earthquake shaking. Areas that were reclaimed prior to the 1931 earthquake liquefied during the earthquake. For example, Napier South was reclaimed in 1908 and the Ahuriri port area was reclaimed in 1878. Both of these areas experienced liquefaction and lateral spreading during the 1931 earthquake, which resulted in significant damage to the quay at the Ahuriri port.

Maps of LPI and LSN for Cases 2, 3, and 4 are included in Appendix D. In general, the inclusion of short CPTs (Case 2) results in a closer prediction of observed liquefaction severity than for Case 1, at least in Napier and Hastings CBDs. However, this observation does not imply that the inclusion of shorter CPTs improves predictions, but rather it could be the result of compensating errors (i.e., over-prediction of liquefaction of severity due to shortcomings in the analysis frameworks and under-prediction of liquefaction severity as a result of including CPT soundings that do not characterize the full depth of the potentially liquefiable soils in a profile). Further work is needed to sort the CPT soundings based on why the CPT was terminated at a shallow depth (i.e. refusal due to the presence of dense strata versus terminated early for other reasons). Only CPT soundings that were terminated at shallow depths that characterize the full-depth of the liquefaction potential of the profile should be included in the analyses.

Maps of LPI and LSN for Case 3 predict less severe liquefaction than Case 1 as a result of the reduction in the PGA (i.e. 0.5 × PGA). Yet, using the reduced PGA does not result in a significant reduction in the predicted liquefaction severity when Cases 2 and 4 are compared. However, it is difficult to properly interpret this comparison until the reasons for the shallow terminations of the short CPTs are better understood.

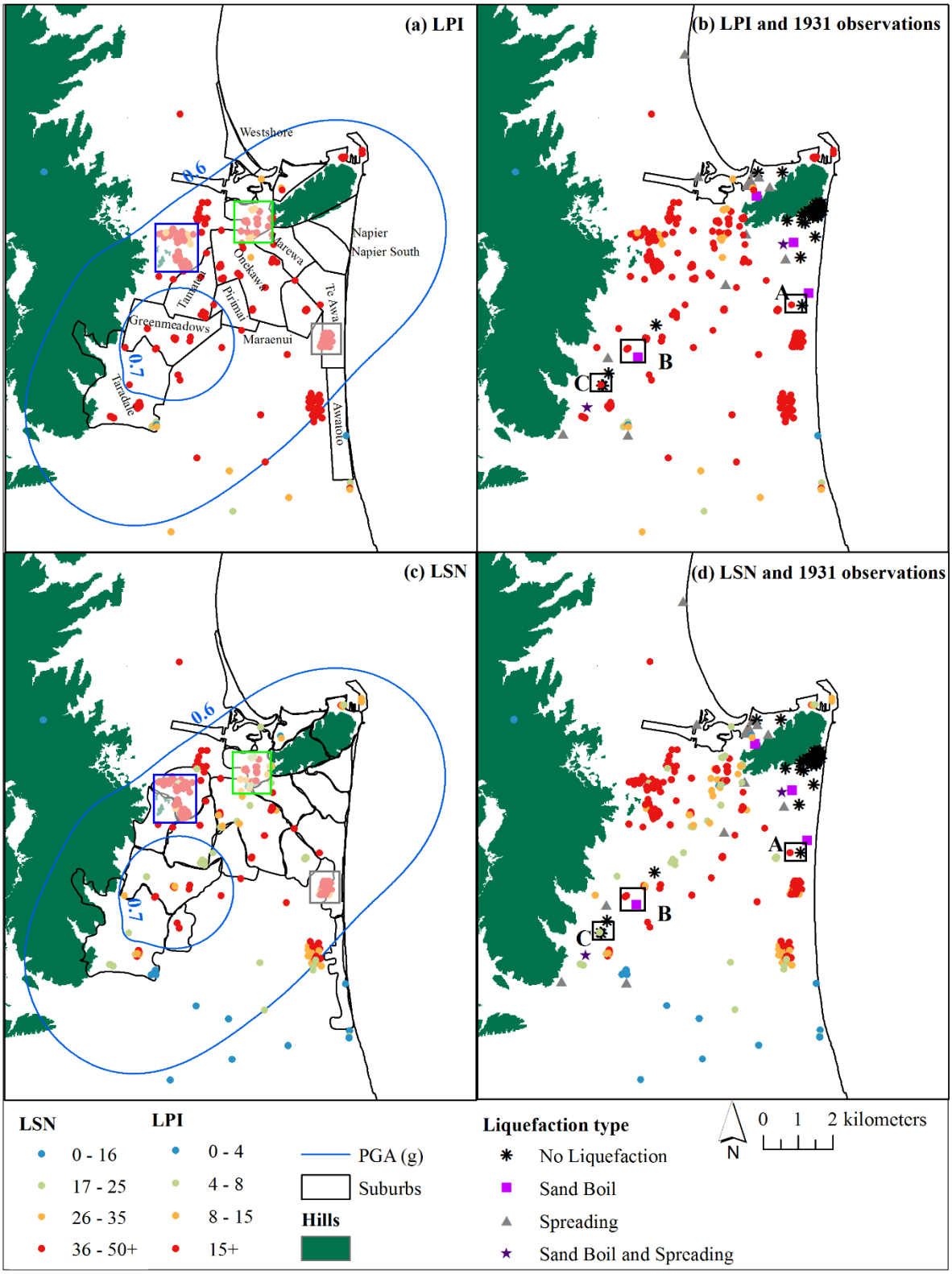

Figure 18: Computed liquefaction severity indices for Napier- Case 1 (a) LPI, (b) LPI overlaid with 1931 observations, (c) LSN, (d) LSN overlaid with 1931 observations (colored boxes referred to in the text)

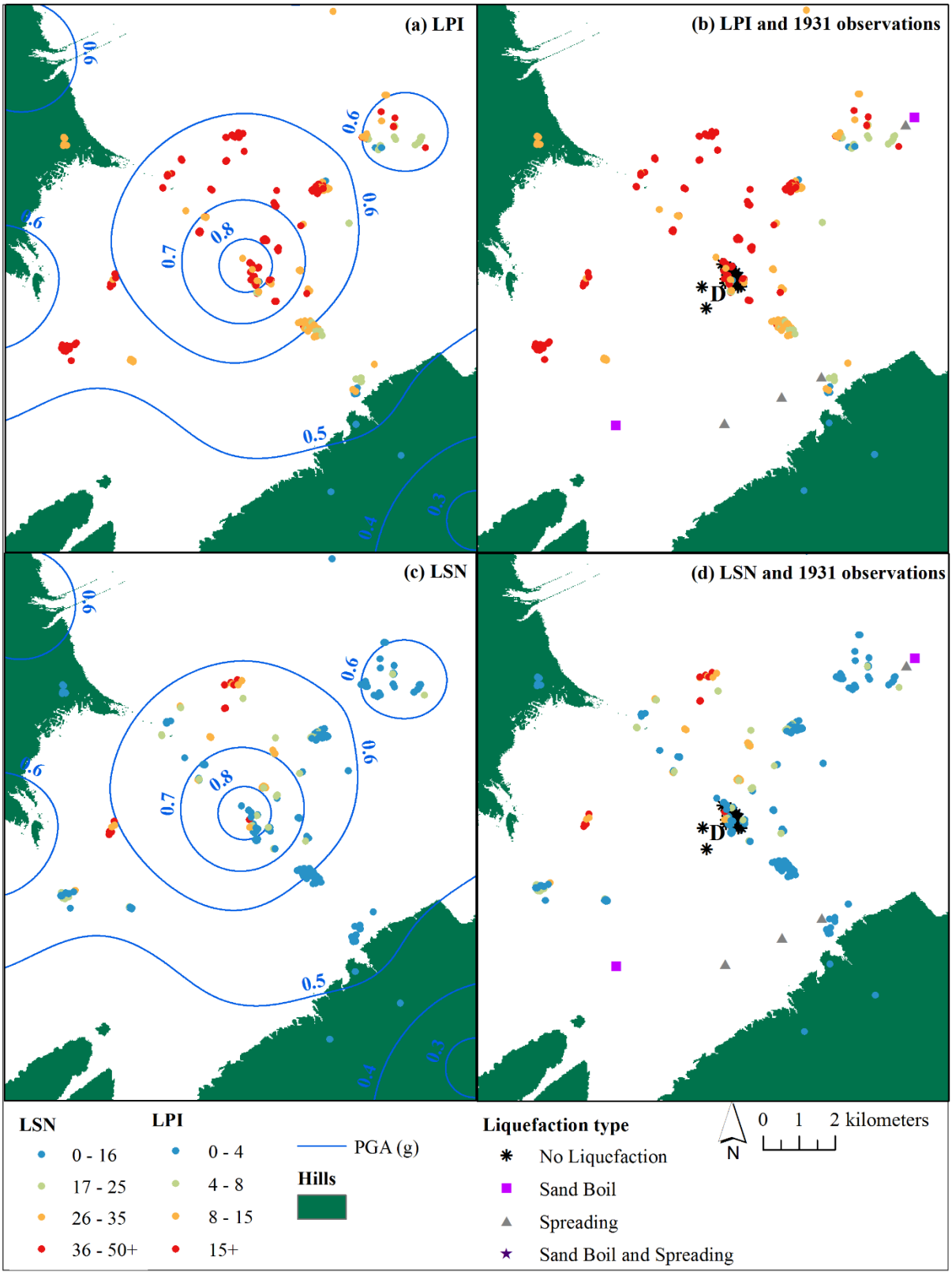

Figure 19: Computed liquefaction severity indices for Hastings- Case 1 (a) LPI, (b) LPI overlaid with 1931 observations, (c) LSN, (d) LSN overlaid with 1931 observations

Based on the above results, the simplified liquefaction evaluation procedure-liquefaction vulnerability framework combination seemingly over-predicts the liquefaction severity in Napier and Hastings for the 1931 Hawke's Bay earthquake. To gain insights into the reasons for the over-predictions, the characteristics of the soil profiles are examined in more detail. Specifically, the Soil Behavior Type Index (I_c) proposed by Robertson (1990) is used to quantify the percentage of various soil types in the upper 10 m of the profiles.

Soil Behavior Type Index is computed from CPT data and is defined by Robertson and Wride (1998) as:

$$I_c = [(3.47 - Q)^2 + (log\, F + 1.22)^2]^{0.5} \quad (3a)$$

where:

$$Q = \left(\frac{q_{c-\sigma_v}}{P_a}\right)\left(\frac{P_a}{\sigma'_{v0}}\right)^n \quad (3b)$$

And

$$F = \left[\frac{f_s}{(q_c - \sigma_v)}\right] 100 \quad (3c)$$

In these expressions: q_c is the cone tip resistance; f_s is the cone sleeve friction; σ_v and σ'_{v0} are the total and effective overburden stresses, respectively; P_a is atmospheric pressure in consistent units with the variables; and the exponent n is typically equal to 1. The relationship between I_c and soil behavior type is given in Table 8. Robertson and Wride (1998) state that it is reasonable to assume that, in general, soils having I_c > 2.6 are not susceptible to liquefaction.

Table 8: Relationship between Soil Behavior Type Index (I_c) and Soil Behavior Type *(after Robertson 1990)*

Soil Behavior Type Index, I_c	Soil Behavior Type
I_c < 1.30	Gravelly sand to dense sand
1.31 < I_c < 2.05	Sands: clean sand to silty sand
2.05 < I_c < 2.60	Sand mixtures: silty sand to sandy silt
2.60 < I_c < 2.95	Silt mixtures: clayey silt to silty clay
2.95 < I_c < 3.60	Clays: silty clay to clay
I_c > 3.60	Organic soils: peats

The percentages of the different soil behavior types in the upper 10 m of the profiles across the study area are shown in Figure 20. As may be observed from this figure, the soil behavior types are grouped by I_c < 2.05, 2.05 < I_c < 2.60, 2.60 < I_c < 3.60, and I_c > 3.60, where the soils falling in the first two groups are considered susceptible to

liquefaction, while the soils falling in the latter two groups are not. Color coding is used in this figure to represent the percentage of the soils in the upper 10 m that fall in each of these groupings.

As may be observed from Figure 20, the soils in the upper 10 m of the profiles in Napier are composed of a greater percentage of clean sand than the profiles in Hastings. For example, the green and blue boxes near Napier Hill in Figure 20a show that 50 to 100% and 15 to 50% of the profiles in these respective regions are composed of clean sand. The grey box in Te Awa shows that 15 to 30% of the profile is composed of clean sand. Figure 20b shows that the profiles in these three regions are composed of 15 to 30% of sand mixtures (silty sand and sandy silt). The green box near Napier Hill in Figure 20c shows that the profile is composed of a small fraction of clay, the blue box shows a higher percent of clay in this area (30-100%) and the grey box in Te Awa also shows a higher percent of clay (30-70%). Figure 20d shows that the profiles are composed of very little high plasticity silts, clays and organic soils (0-15%). In Hastings, it seems that the proportions of clean sand and plastic soils in the profiles are comparable. Sand mixtures are limited to 0 to 15% of soil composition.

As may be observed from Figure 18a and 18c, the predicted liquefaction potential in the green box near Napier Hill is severe. This is likely a result of the large percentage of clean sands in the upper 10 m of the soil profiles in the area and the shallow groundwater table. The predicted liquefaction potential in the blue box near Napier Hill is also severe, yet Figure 18 shows that there is a significant percent of clay (non-liquefiable) in the profiles in the area. This suggests that the liquefaction potential in this area may be being over-predicted. The predicted liquefaction potential in the grey box in Te Awa is also severe, but the profiles in the area are composed of 30 to 70% non-liquefiable soil. Also, post-earthquake observations at the Napier Boys High, located in the vicinity of this group of CPTs, showed no evidence of liquefaction in this locale. Therefore, the liquefaction severity is being over-predicted in this area. These examples led to a more in-depth examination of specific sites which were selected based on their proximity to 1931 post-earthquake observations. This is detailed in the subsequent section.

In Hastings, the predicted liquefaction potential based on the LPI map is more severe than that based on LSN (Figure 20). This is likely due to the depth distribution of dense clean sands and plastic soils. A site-specific analysis is required to confirm this finding.

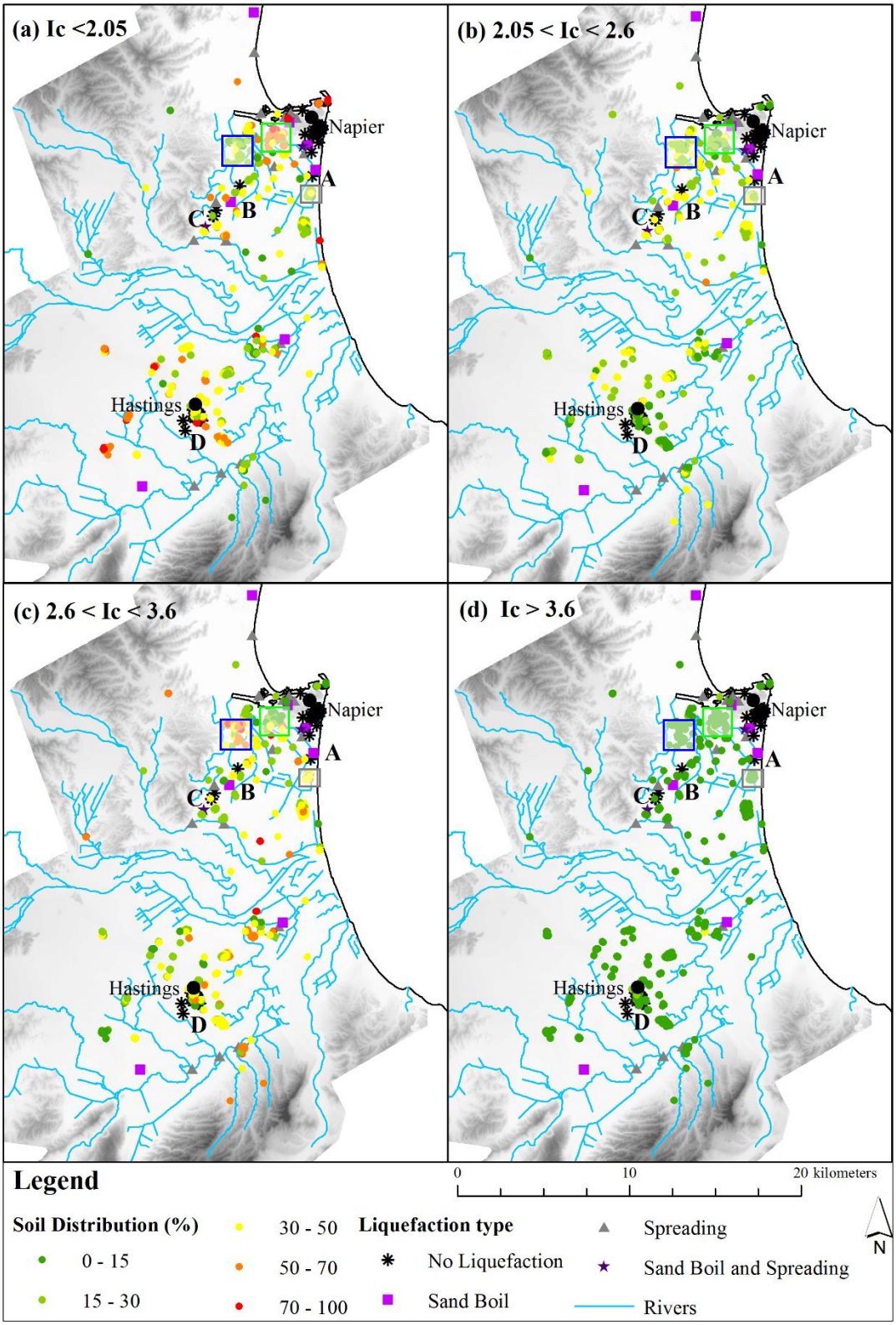

Figure 20: Distribution of soil types in the upper 10 m in the soil profiles based on the soil behavior type index I_c (colored boxes referred to in the text)

2.4.8 *Discussion*

Given the geomorphology of the soil deposits in Napier and Hastings and the seismic hazard of the region, liquefaction and its consequences need to be considered in emergency management planning of the region. In general, the simplified liquefaction evaluation procedure-liquefaction vulnerability framework combination tends to over-predict liquefaction severity of the area of study: Napier and Hastings. To provide insights into trend, four sites denoted as A, B, C and D in Figure 18-22 are examined in more detail. Due to the limited robustness of liquefaction observations following the 1931 event and the limited available geotechnical subsurface investigations, most locations where observations were made do not coincide with locations where subsurface data is available. Thus, for the purpose of the comparison, any CPT data within the proximity of a post-earthquake observation were examined. Information on A, B, C and D is summarized in Table 9. One limitation of maps in Figure 20 is their inability to provide insights about the depths at which the different types of soil were encountered. To fill this knowledge gap, Figure 21 and Figure 22 give additional information on the stratigraphy of the profiles by showing the median value of I_c at 1-m depth intervals from 0 to 10 m.

There are no CPT data to use to assess the liquefaction hazard in Napier CBD, thus further testing is needed in this area. However, the liquefaction assessment over-predicts the liquefaction severity in the Hastings CBD, especially using the LPI framework. Site D in Figure 19 and 20 is located in the Hastings CBD, where no liquefaction manifestations were observed following the 1931 event. Thus, the "no liquefaction" observation is discussed hereafter.

Table 9: Comparison between predicted and observed liquefaction at 4 sites within the area of study

Site	**Location**	**Observation**	**Predicted liquefaction**			
			LPI	Classification	LSN	Classification
A	Te Awa	No liquefaction	15+	Severe	36+	Severe
B	Greenmeadows	Sand boil	15+	Severe	36+	Severe
C	Taradale	No liquefaction	15+	Severe	4-8	Medium
D	Hastings	No liquefaction	15+	Severe	0-16	No liquefaction

Site A

The location of the CPT sounding where the liquefaction severity indices were computed is ≈320 m from where the location of the post-earthquake observations were made. LPI and LSN predict severe liquefaction at this site whereas no liquefaction was observed in 1931 (Figure 18 and Table 9). This case is referred to as a "false-positive" (i.e., liquefaction is predicted but was not observed). Based on I_c, the upper 10 m of the soil profile is composed of 33.5% (or 3.35 m) of clean sand, 31.7% (or 3.17 m) of sand mixtures, and 34.8% (or 3.48 m) of plastic soils. From Figure 21 and Figure 22, sand mixtures are encountered at the surface of the profile down to 1-m depth. Then, plastic soils and sand mixtures are intercalated down to a depth of 10 m. Possibly, lenses of clean sand are present at depths of 5 to 6 m and 9 to 10 m. Given this stratigraphy, a

possible explanation of the "no liquefaction" observation is that liquefaction might have triggered at depth, but was not able to manifest at the surface. Also, the intercalation of sand and plastic soils may have increased the cyclic resistance of the soil to liquefy at a given depth.

Site B

The location of the CPT sounding where the liquefaction severity indices are computed is ≈400 m from where the location of the post-earthquake observations were made. LPI and LSN predict severe liquefaction at this site and a sand boil was observed after the 1931 event (Figure 18 and Table 9). This case is referred to as "true-positive" (i.e., liquefaction is predicted and was observed). Based on I_c, the upper 10 m of the soil profile is composed of 34.8% (or 3.48 m) of clean sand, 46.6% (or 4.66 m) of sand mixtures and 18.6% (or 1.86 m) of plastic soils. Compared to Site A, there are less plastic soils at this site. From Figure 21 and Figure 22, plastic soils are encountered at the surface of the profile down to 2-m depth. There is a 1 m lens of clean sand underlain by 4 m of sand mixtures, underlain by clean sand down to the cutoff depth. The thin plastic crust was not able to prevent the surficial manifestation of liquefaction, which occurred in the deeper sand or sand mixture stratum.

The LPI and LSN frameworks predict the same level of liquefaction severity at Sites A and B. More inland, however, the severities predicted by the two frameworks deviate, with LPI predicting more severe liquefaction than LSN. Seemingly, the sensitivity of the predictions to the density of the soil becomes more pronounced, resulting in lower severity predictions by the LSN framework.

Site C

The location of the CPT sounding where the liquefaction severity indices are computed is ≈30 m from where the location of the post-earthquake observations were made. LPI and LSN predict severe and medium severity liquefaction, respectively. No liquefaction was observed at this site following the 1931 event (Figure 18 and Table 9). As with Site A, this case is a "false-positive". Based on I_c, the soil profile is composed of 24.8% (or 2.48 m) of clean sand, 31.6% (or 3.16 m) of sand mixtures and 43.6% (or 4.36 m) of plastic soils. Compared to Sites A and B, the soils in this profile have a higher plasticity. From Figure 21 and Figure 22, there is intercalation of plastic soils and sand mixtures from the surface to a depth of 9 m. At 9 m, a clean sand layer is present down to the cutoff depth. The LPI framework seems to significantly over-predict liquefaction at this site, while the LSN framework slightly over-predicts liquefaction severity.

Site D

The location of the CPT sounding where the liquefaction severity indices are computed is ≈30 m from where the location of the post-earthquake observations were made. LPI and LSN predict severe and no liquefaction, respectively. No liquefaction manifestations were observed at this site following the 1931 event (Figure 18 and Table 9). This case is a "false-positive" for LPI and a "true-negative" for LSN (i.e., no liquefaction is predicted and none was observed). Based on I_c, the soil profile is

composed of 28.8% (or 2.88 m) of clean sand, 14.6% (or 1.46 m) of sand mixtures, 55.6% (or 5.56 m) of plastic soils and 1% (or 1 m) of organic soils. Compared to Sites A-C, the majority of the soils in the upper 10 m of this profile are plastic. From Figure 21 and Figure 22, high plasticity silts or clays form an 8-m deep layer underlain by clean sand up to the cutoff depth at 10 m. the thick, plastic crust likely mitigated the surficial manifestation of liquefaction if it did occur in the deep clean sand layer.

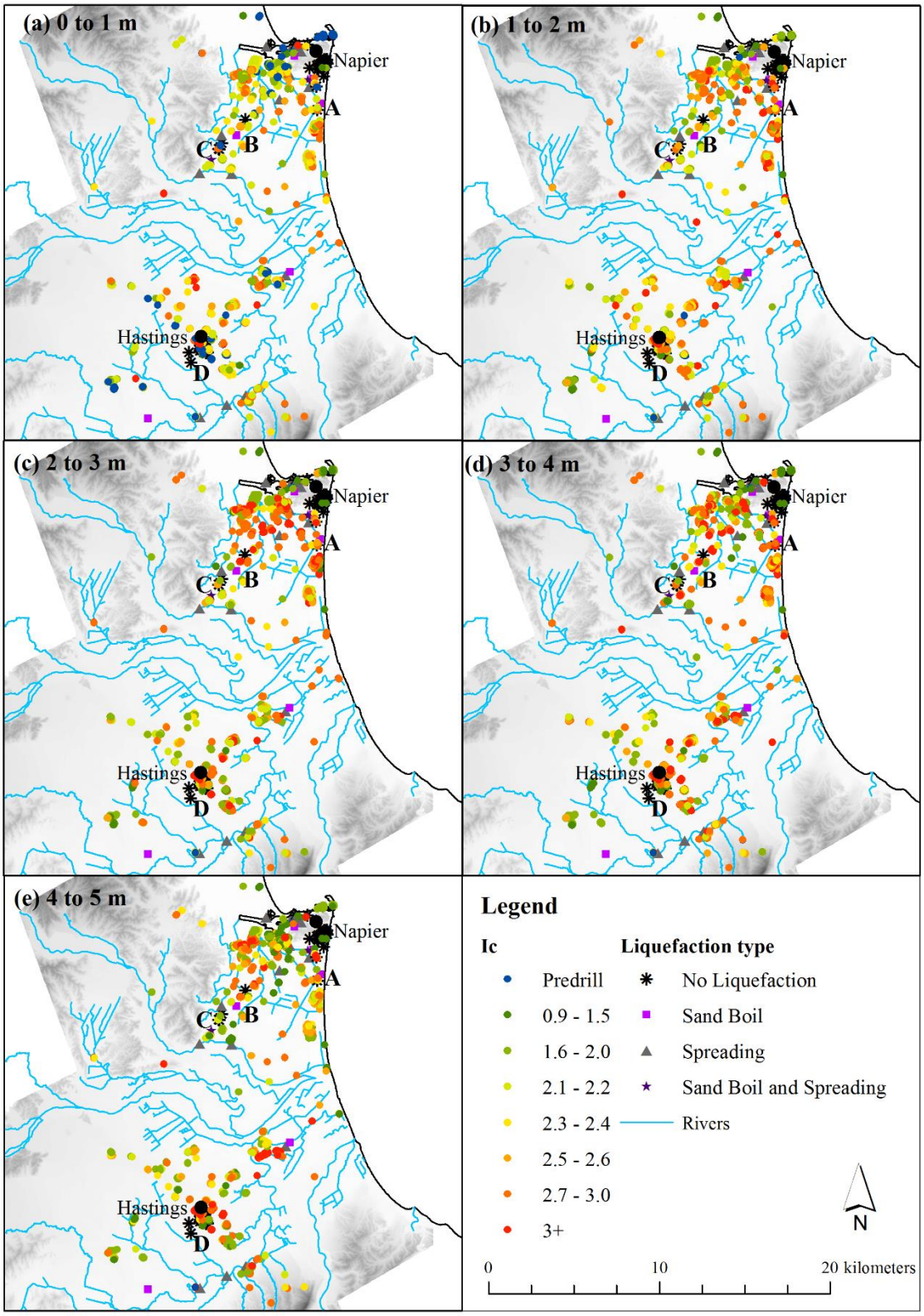

Figure 21: Average I_c values at 1-m depth intervals for depths of 0 to 5 m

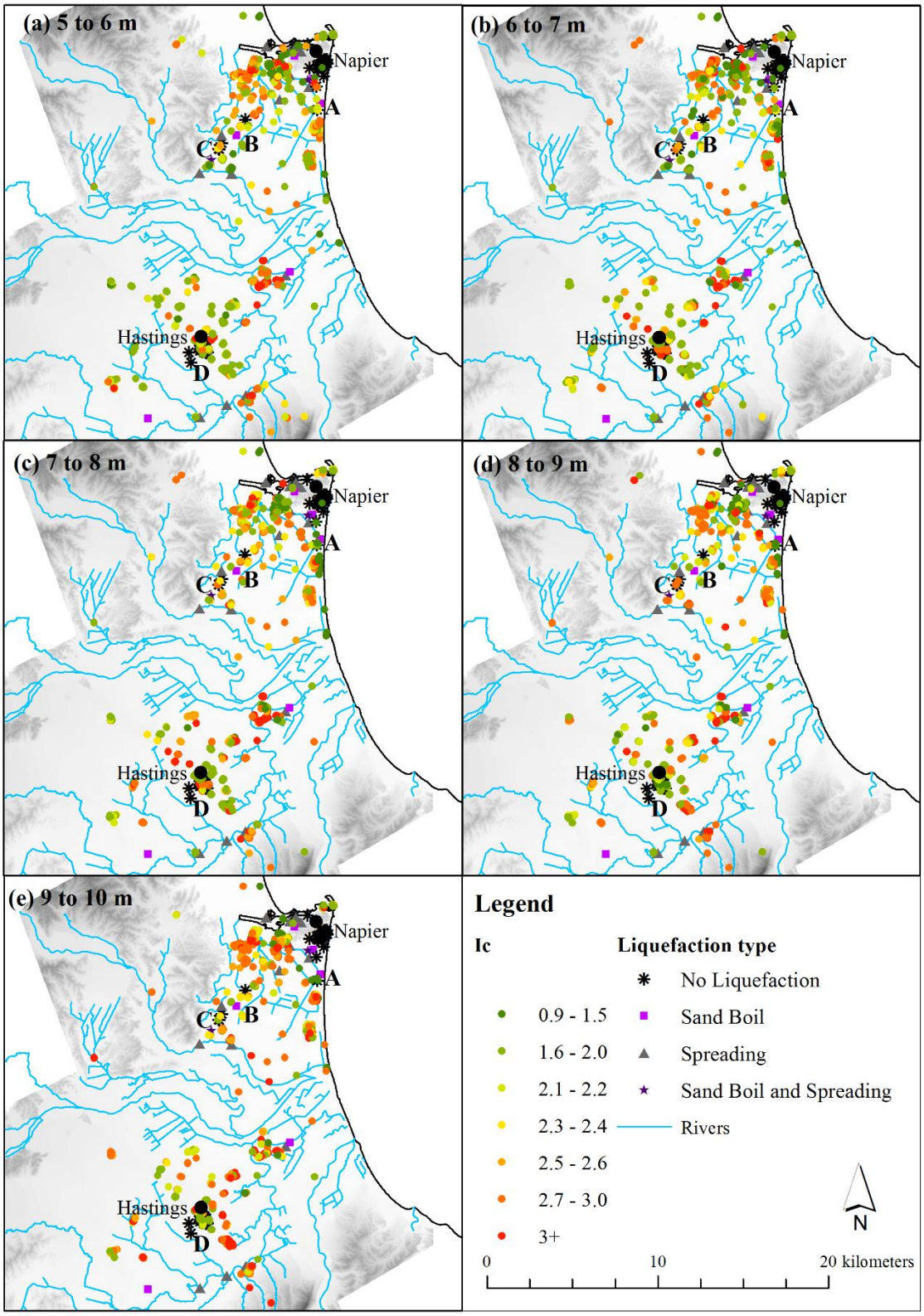

Figure 22: Average I_c values at 1-m depth intervals for depths of 5 to 10 m

The examples above suggest that the liquefaction triggering assessment over-predicts the liquefaction potential. The predictions range from slightly over-predicting at Site C to significantly over-predicting at Site A.

Possible reasons for this are:

- Neither the LPI nor LSN frameworks fully account for the thickness of the non-liquefiable crust on the severity of surficial liquefaction manifestations. However, the thickness of the overlying crust has been shown to influence the severity of the surficial liquefaction manifestations (e.g., Ishihara 1985; Maurer et al. 2015b).
- As a result of depositional processes during the formation of the Heretaunga Plains, most deposits in Hawke's Bay consist of interbedded layers of sand, silt, and clay. This makes it difficult to properly interpret CPT data (Robertson and Wride 1998). Additionally, interbedded silts and clay layers in sand deposits significantly impede the surficial manifestation of liquefaction (Beyzaei et al. 2017; Bray and Sancio 2006; Cox et al. 2017; Leeves et al. 2015; Maurer et al. 2015a).
- Compositional characteristics of soil are not fully considered in the liquefaction triggering procedure. Factors influencing liquefaction susceptibility include particle size and shape among other factors. Angular particles exhibit higher shear strength than rounded particles. Close examination of sand samples need to be performed to confirm the shape of particles. Also, coarser sands exhibit higher shear strength than finer sands because larger grains have a bigger contribution from friction to resist deformation. Over the course of time, rivers had high gradients and deposited coarser material in the Plains. As rivers widen and currents slow, finer materials were deposited. This needs to be further checked by performing sieve analyses on soil samples. Thus, angular particles and coarser sands are less likely to liquefy (Ishihara 1985)
- In the liquefaction triggering procedure, it is assumed that the soil is saturated below the groundwater table. However, detailed field investigations of profiles in Christchurch, New Zealand, show that this is not always the case, especially in regions that experience large fluctuations in the GWD (Stokoe et al. 2014). Partially saturated soils have a higher resistance to liquefaction with the decrease in the degree of saturation. Their behavior is comparable to a saturated dense sand (Okamura and Soga 2006; Yoshimi et al. 1989)

The factors listed above can significantly add to the cyclic resistance of soils to earthquake loading and inhibit the severity of surficial liquefaction manifestation. At present, there are no means to quantify the influence of these factors on the predicted liquefaction hazard in Hawke's Bay.

To refine the present study, further work is needed to improve the GWD model. The diversion of the Tutaekuri River after the earthquake is not accounted for in the present groundwater model. The influence of this variation is expected to be minimal and limited to the former course of the river which flowed into the former lagoon. However, it is recommended to investigate this variation to the groundwater model in future work. Development of a high flow conditions GWD model (i.e. shallower groundwater table, mostly coinciding with the ground surface in Napier) was attempted. However, the model did not provide reasonable results due to the inconsistencies in the high flow data. Thus, a practical solution to this problem is to

represent high flow conditions by reducing the GWD estimated using the low flow conditions model by a constant amount over the study area. A reduction of the GWD by 1 to 2 m is suggested. A reduction of 2 m results in the groundwater table being at the ground surface, which would be a worst case scenario from a liquefaction hazard perspective. This approximate range of water level fluctuation was also reported in Dravid and Brown (1997). The liquefaction hazard can be reanalyzed using this shallower groundwater table, with the expectation that the severity of the predicted liquefaction hazard to increase.

Another improvement to the analyses performed herein that can be made is to examine the short CPT soundings. As discussed previously, the inclusion or exclusion of the short CPTs from the sounding database analyzed can have a major impact on the computed liquefaction hazard, with the computed hazard decreasing if inclusion of the short CPTs in the analyzed database can be justified. The presence of the shallow gravel layer under Napier CBD is important for the analysis and explains the lack of CPT data in this area. A couple of CPT soundings were available in the surroundings of the CBD and it is important to manually check the reason behind their shallow termination in order to strengthen the explanation of why Napier CBD did not liquefy.

Additional recommendations for improving upon the study presented herein:

- Better characterize the profiles where the current analyses over-predict the severity of liquefaction manifestations. The goal of this effort is to understand whether the over-prediction is due to shortcomings with the profile data used in the analyses or with analyses framework, or both
- Better account for the uncertainties in PGA and groundwater depth. The goal of this effort is to determine whether the over-predictions are due to uncertainties in the input parameters for the analyses
- Examine the CPT database to determine whether the short CPTs characterize the full-depth of the liquefaction potential of the profile or not

2.4.9 *Summary and Conclusions*

Following the Canterbury Earthquake Sequence (CES), the liquefaction hazard of other seismically active regions of New Zealand (e.g., Hawke's Bay) has become a concern. Previous studies assessed the liquefaction hazard of Hawke's Bay, but none validated their analysis framework using liquefaction data from historic regional earthquakes. This study provides insights into the liquefaction hazards in Napier and Hastings based on the assessment of data from the 1931 Hawke's Bay earthquake. The Hawke's Bay earthquake is particularly important because it is the deadliest and one of the most damaging earthquakes in New Zealand's history. This study starts with an overview of relevant background information on Hawke's Bay and the 1931 Hawke's Bay earthquake. Then, it presents the work performed on the collection of liquefaction observational data from the 1931 event. Later, the study expands on the development of input parameters to the analysis framework (e.g. CPTs, PGA model, and groundwater model). The liquefaction triggering assessment is performed using the deterministic variant of the Boulanger and Idriss (2014) CPT-based simplified procedure.

Analysis of the results from the LPI and LSN frameworks show that for the 1931 Hawke's Bay earthquake scenario, MMI X in both Napier and Hastings, the liquefaction hazard in Napier is greater than in Hastings. Possible causes are the loose, sandy fill material in Napier used to reclaim swampland and the shallow groundwater table. The inclusion of "short CPTs" in the analyzed database tends to reduce the computed liquefaction hazard. Further work is needed to determine whether the short CPTs characterize the full-depth of the liquefaction potential of the profiles or not. A parametric study was performed to gain insights about the effect of short CPTs, as well as uncertainty in the PGA, on the computed liquefaction hazard. Comparing the LPI and LSN distributions to the post-earthquake observations showed that the analysis framework over-predicted the liquefaction hazard in several areas of Napier and Hastings. This is an important finding for emergency management planners because if the same analysis framework is used to predict the liquefaction hazard for future events, the hazard may also be over-predicted. Possible causes for the over-prediction might be to the lack of accounting for a non-liquefiable crust on mitigating liquefaction manifestations, the depositional and compositional characteristics of the soil may differ from those used to developed the simplified liquefaction evaluation procedure, and the soils may be partially saturated few meters below the groundwater table. In light of these findings, further laboratory and in-situ testing is recommended in Hawke's Bay at sites of where the liquefaction severity is being over-predicted to determine whether the over-prediction is a result of shortcomings of the inputs used in the analyses or shortcomings in the computational framework used to compute the liquefaction hazard.

2.5 References

Adams, C.E., Barnett, M.A.F., and Hayes, R.C. (1933). "Seismological Report of the Hawke's Bay Earthquake of 3rd February, 1931." *The NZ Journal of Science and Technology*, (XV), 93–107.

van Ballegooy, S., Malan, P., Lacrosse, V., Jacka, M.E., Cubrinovski, M., Bray, J.D., O'Rourke, T.D., Crawford, S.A., and Cowan, H. (2014). "Assessment of liquefaction-induced land damage for residential Christchurch." *Earthquake Spectra*, 30(1), 31–55.

Bayless, J., Hosseini, M., Skarlatoudis, A., and Somerville, P. (2017). *Validation of strong ground motion simulations of two historical New Zealand subduction zone earthquakes on the SCEC broadband strong ground motion simulation platform*. AECOM (Architecture, Engineering, Consulting, Operations, and Maintenance), New Zealand.

Begg, J.G., Hull, A.G., and Downes, G.L. (1994). *Earthquake hazards in Hawke's Bay: initial assessment*. Lower Hutt, New Zealand.

Beyzaei, C., Bray, J., van Ballegooy, S., Cubrinovski, M., and Bastin, S. (2017). "Depositional Environment Effects on Observed Liquefaction Performance in Silt Swamps during the Canterbury Earthquake Sequence." *Soil Dynamics and Earthquake Engineering (under review)*.

Bland, K.J., and Kamp, P.J.J. (2006). "Geological Structure of the Forearc Basin in Central Hawke's Bay, Eastern North Island." *Proceedings of New Zealand Petroleum Conference 2006*, Auckland, New Zealand, 6-10 March, 13.

Boulanger, R.W., and Idriss, I.M. (2014). *CPT and SPT Based Liquefaction Triggering Procedures*. *Center for Geotechnical Modeling*, Department of Civil and Environmental Engineering, University of California at Davis, Davis, CA.

Bray, J.D., and Sancio, R.B. (2006). "Assessment of the Liquefaction Susceptibility of Fine-Grained Soils." *Journal of Geotechnical and Geoenvironmental Engineering*, 132(9), 1165–1177.

Brodie, A., and Harris, B.E. (1933). "Damage to buildings, part of report on Hawke's Bay earthquake of 3rd February, 1931." *The NZ Journal of Science and Technology*, (XV), 108–114.

Buckland, A.H. (1974). *Heretaunga Plains Underground Water Technical Committee Report*.

Bullen, K.E. (1938). "An analysis of the Hawke's Bay earthquakes during February 1931." *The NZ Journal of Science and Technology*, 497–519.

Callaghan, F.R. (1933). "The Hawke's Bay Earthquake- General Description." *The NZ Journal of Science and Technology*, (XV), 3–38.

Caprio, M., Tarigan, B., Bruce Worden, C., Wiemer, S., and Wald, D. J. (2015).

"Ground motion to intensity conversion equations (GMICEs): A global relationship and evaluation of regional dependency." *Bulletin of the Seismological Society of America*, 105(3), 1476–1490.

Cox, B.R., McLaughlin, K.A., van Ballegooy, S., Cubrinovski, M., Boulanger, R.W., and Wotherspoon, L. (2017). "In-situ Investigation of False-positive Liquefaction Sites in Christchurch, New Zealand: St Teresa's School Case History." *Proc. 3rd Intern. Conf. on Performance-Based Design in Earthquake Geotechnical Engineering (PBDIII)*, Vancouver, Canada, 16-19 July. *(in press)*

Cubrinovski, M., Rhodes, A., Ntritsos, N., and van Ballegooy, S. (2017). "System Response of Liquefiable Deposits." *Proc. 3rd Intern. Conf. on Performance-Based Design in Earthquake Geotechnical Engineering (PBDIII)*, Vancouver, Canada, 16-19 July. *(in press)*

Dellow, G.D., Barker, P., Beetham, R., and Heron, D. (2003). *A Deterministic Method For Assessing The Liquefaction Susceptibility Of The Heretaunga Plains , Hawke's Bay , NZ.* Lower Hutt, New Zealand.

Doser, D.I., and Webb, T.H. (2003). "Source parameters of large historical (1917 – 1961) earthquakes, North Island, New Zealand." *Geophysical Journal International*, 152, 795–832.

Dowrick, D.J. (1998). "Damage and intensities in the magnitude 7.8 1931 Hawke's Bay, New Zealand, earthquake." *Bulletin of the New Zealand National Society For Earthquake Engineering*, 31(3), 139–163.

Dowrick, D.J., and Smith, E.G.C. (1990). "Surface wave magnitudes of some New Zealand earthquakes 1901-1988." *Bulletin of the New Zealand National Society For Earthquake Engineering*, 23(3), 198–210.

Dravid, P., and Brown, L. (1997). *Heretaunga Plains Groundwater Study: Volume 1-Findings*. Hawke's Bay Regional Council (HBRC) and Institute of Geological and Nuclear Sciences Ltd (GNS), Napier, New Zealand.

Fairless, G.J., and Berrill, J.B. (1984). "Liquefaction During in Historic Earthquakes in New Zealand." *Bulletin of the New Zealand Society for Earthquake Engineering*, 17(4), 280–291.

Grant, P.J. (1972). *Groundwaters of the Heretaunga Plains, Hawke's Bay*. Hawke's Bay Regional Council (HBRC), Napier, New Zealand.

Green, R.A., and Maurer, B.W. (2016). "Evaluating Risk Due to Liquefaction: Lessons Learned from Recent Earthquakes and New Developments." *Proc. 1st Intern. Symposium on Soil Dynamics and Geotechnical Sustainability* (E. G. Wang, G. Zhang, and D. Huang, eds), Hong Kong University of Science and Technology (HKUST), Hong Kong, China, 8-9 August, 20–23.

Green, R.A., and Maurer, B.W. (2017). "Use of volumetric strain in liquefaction damage index frameworks." *Proc. U.S.-N.Z.-Japan International Workshop on Liquefaction-Induced Ground Movements Effects*, PEER Report 2017/02, Pacific

Earthquake Engineering Research Center, Berkeley, CA, Appendix A, 39-40.

Gulley, A.K., Dudley Ward, N.F., Cox, S.C., and Kaipio, J.P. (2013). "Groundwater responses to the recent Canterbury earthquakes: A comparison." *Journal of Hydrology*, Elsevier B.V., 504, 171–181.

Haines, A. J., and Darby, D. J. (1987). *Preliminary dislocation models for the 1931 Napier and 1932 Wairoa earthquakes*, New Zealand Geological Survey Report.

HBRC. (n.d.). "Hawke's Bay Emergency Management." <http://www.hbemergency.govt.nz/hazards/earthquake> (Jan. 1, 2017).

HBRC. (2006). *Heretaunga Steady-State Ground-Water Model*. Hawke's Bay Regional Council, Napier, New Zealand.

Henderson, J. (1933). "The Geological Aspects of the Hawke's Bay Earthquakes." *The NZ Journal of Science and Technology*, (XV), 38–75.

Hengesh, J.V., Heron, D., Brown, L., and Hull, A.G. (1996). *Stage II- Earthquake hazard analysis: Part II- evaluation of liquefaction potential in the Hawke's Bay region*. Institute of Geological and Nuclear Sciences Ltd (GNS), Lower Hutt, New Zealand.

Holzer, T.L., Bennett, M.J., Noce, T.E., Padovani, A.C., and Tinsley, J.C. (2006). "Liquefaction hazard mapping with LPI in the Greater Oakland, California, area." *Earthquake Spectra*, 22(3), 693–708.

Hull, A.G. (1990). "Tectonics of the 1931 Hawke's Bay earthquake." *New Zealand Journal of Geology and Geophysics*, 33(2), 309–320.

Ishihara, K. (1985). "Stability of natural deposits during earthquakes." *Proceedings of the eleventh international conference on soil mechanics and foundation engineering*, San Francisco, CA, USA, 12-16 August, 321–376.

Ishihara, K., and Yoshimine, M. (1992). "Evaluation of Settlements in Sand Deposits Following Liquefaction During Earthquakes." *Soils and Foundations*, 32(1), 173–188.

Iwasaki, T., Tatsuoka, F., Tokida, K., and Yasuda, S. (1978). "A Practical Method for Assessing Soil Liquefaction Potential Based on Case Studies at Various Sites in Japan." *Proceedings of the second international conference on microzonation for safer construction-Research and application*, San Francisco, CA, USA, 26 November-1 December, 13.

Iwasaki, T., Tokida, K., Tatsuoka, F., Watanbe, S., Yasuda, S., and Sato, H. (1982). "Microzonation for soil liquefaction potential using simplified methods." *Third International Earthquake Microzonation Conference Proceedings*, Seattle, Washington, USA, 28 June-1 July, 1319–1330.

Kroll, K. A., Cochran, E. S., and Murray, K. E. (2017). "Poroelastic Properties of the Arbuckle Group in Oklahoma Derived from Well Fluid Level Response to the 3 September 2016 M_w5.8 Pawnee and 7 November 2016 M_w5.0 Cushing

Earthquakes." *Seismological Research Letters*, 88(4), 1–8.

Lee, J., Bland, K., Townsend, D., and Kamp, P. (2011). *Geology of the Hawke's Bay area: scale 1:250,000*. Institute of Geological and Nuclear Sciences Ltd (GNS), Lower Hutt, New Zealand.

Leeves, J., Ballegooy, S. Van, Lees, J., and Wentz, F. (2015). "Effect of Fines Content Correlations and Liquefaction Susceptibility Thresholds on Liquefaction Consequence." *6th International Conference on Earthquake Geotechnical Engineering*, Christchurch, New Zealand, 1-4 November 2015, 9.

Marshall, P. (1933). "Effects of Earthquake on Coast-line near Napier." *The NZ Journal of Science and Technology*, (XV), 79–92.

Maurer, B.W., Green, R.A., Cubrinovski, M., and Bradley, B.A. (2014). "Evaluation of the liquefaction potential index for assessing liquefaction hazard in Christchurch, New Zealand." *Journal of Geotechnical and Geoenvironmental Engineering*, 140(7), 1–11.

Maurer, B.W., Green, R.A., Cubrinovski, M., and Bradley, B.A. (2015a). "Fines-content effects on liquefaction hazard evaluation for infrastructure in Christchurch , New Zealand." *Soil Dynamics and Earthquake Engineering*, Elsevier, 76, 58–68.

Maurer, B.W., Green, R.A., and Taylor, O.D.S. (2015b). "Moving towards an improved index for assessing liquefaction hazard: Lessons from historical data." *Soils and Foundations*, 55(4), 778–787.

McGinty, P., Darby, D., and Haines, J. (2001). "Earthquake triggering in the Hawke's Bay, New Zealand, region from 1931 to 1934 as inferred from elastic dislocation and static stress modeling." *Journal of Geophysical Research*, 106(B11), 26593–26604.

McLellan, C. (1988). *Re-evaluation of basement contour beneath the Heretaunga Plains recharge area*.

Okamura, M., and Soga, Y. (2006). "Effects of Pore Fluid Compressibility on Liquefaction Resistance of Partially Saturated Sand." *Soils and Foundations*, 46(5), 695–700.

Papathanassiou, G., Pavlides, S., and Ganas, A. (2005). "The 2003 Lefkada earthquake: Field observations and preliminary microzonation map based on liquefaction potential index for the town of Lefkada." *Engineering Geology*, 82(1), 12–31.

Robertson, P. K. (1990). "Soil classification using the cone penetration test." *Canadian Geotechnical Journal*, 27(1), 151–158.

Robertson, P., and Wride, C. (1998). "Evaluating cyclic liquefaction potential using the cone penetration test." *Canadian Geotechnical Journal*, 35(3), 442–459.

Roeloffs, E.A., Nelms, D.L., and Sheets, R.A. (2015). "Widespread groundwater-level offsets caused by the M2 5.8 Mineral, Virginia , earthquake of 23 August 2011." *The Geological Society of America*, (Special paper 509), 117–136.

Sonmez, H. (2003). “Modification of the liquefaction potential index and liquefaction susceptibility mapping for a liquefaction-prone area (Inegol, Turkey).” *Environmental Geology*, 44(7), 862–871.

Stokoe II, K.H., Roberts, J.N., Hwang, S., Cox, B.R., Menq, F.Y., and van Ballegooy, S. (2014). “Effectiveness of inhibiting liquefaction triggering by shallow ground improvement methods: Initial field shaking trials with T-Rex at one site in Christchurch, New Zealand.” *Soil Liquefaction During Recent Large-Scale Earthquakes* (R. Orense, I. Towhata, and N. Chouw, eds.), Taylor & Francis Group, London, UK, 193–202.

Tonkin & Taylor. (2016). *Appendix A : Liquefaction vulnerability severity classification methodology*. Tonkin and Taylor Ltd, Auckland, New Zealand.

Tonkin and Taylor. (2013). *Liquefaction vulnerability study*. Tonkin and Taylor Ltd, New Zealand.

Walcott, R. I. (1978). “Geodetic strains and large earthquakes in the axial tectonic belt of North Island, New Zealand.” *Journal of Geophysical Research*, (83), 4419–4429.

Yoshimi, Y., Tanaka, K., and Tokimatsu, K. (1989). “Liquefaction resistance of a partially saturated sand.” *Soils and Foundations*, 29(3), 157–162.

Zhang, G., Robertson, P. K., and Brachman, R. W. . (2002). “Estimating liquefaction-induced ground settlements from CPT for level ground.” *Canadian Geotechnical Journal*, 39(5), 1168–1180.

CHAPTER 3 CONCLUSIONS

3.1 Summary

Following the Canterbury Earthquake Sequence (CES), the liquefaction hazard of other seismically active regions of New Zealand (e.g., Hawke's Bay) has become a concern. Previous studies assessed the liquefaction hazard of Hawke's Bay, but none validated their analysis framework using liquefaction data from historic regional earthquakes. This study provides insights into the liquefaction hazards in Napier and Hastings based on the assessment of data from the 1931 Hawke's Bay earthquake. The Hawke's Bay earthquake is particularly important because it is the deadliest and one of the most damaging earthquakes in New Zealand's history. This study starts with an overview of relevant background information on Hawke's Bay and the 1931 Hawke's Bay earthquake. Then, it presents the work performed on the collection of liquefaction observational data from the 1931 event. Later, the study expands on the development of input parameters to the analysis framework (e.g. CPTs, PGA model, and groundwater model). The liquefaction triggering assessment is performed using the deterministic variant of the Boulanger and Idriss (2014) simplified procedure.

3.2 Key Findings

Analysis of the results in the LPI and LSN frameworks show that for the 1931 Hawke's Bay earthquake scenario, MMI X in both Napier and Hastings, the liquefaction hazard in Napier is greater than in Hastings. Possible causes are the loose, sandy fill material in Napier used to reclaim swampland and the shallow groundwater table. The inclusion of "short CPTs" (i.e., CPT that terminated between 5 and 10 m depths) in the analyzed database produces a bias in the results and tends to reduce the computed liquefaction hazard. Further work is needed to determine whether the short CPTs characterize the full-depth of the liquefaction potential of the profiles or they were terminated at shallow depths for other reasons. A parametric study was performed to provide insights into the effect of short CPTs, as well as the uncertainty in PGA, on the computed liquefaction hazard. Comparing the LPI and LSN distributions to the post-earthquake observations showed that the analysis frameworks over-predicted the liquefaction hazard in several areas of Napier and Hastings. This is an important finding for emergency management planners because if the same analysis frameworks are used to predict the liquefaction hazard for future events, the hazard may also be over-predicted. Possible causes for the over-prediction might be to the lack of accounting for a non-liquefiable crust on mitigating liquefaction manifestations, the depositional and compositional characteristics of the soil may differ from those used to developed the simplified liquefaction evaluation procedure, and the soils may be partially saturated few meters below the groundwater table.

3.3 Recommendations for Future Work

Based on this study, the liquefaction hazard of Hawke's Bay is being overestimated by the current analysis frameworks and the causes can be attributed to multiple reasons. Recommendations for further clarification of this finding are:

- Better characterize the profiles where the current analyses over-predict the severity of liquefaction manifestations. The goal of this effort is to understand whether the over-prediction is due to shortcomings with the profile data used in the analyses or with analysis frameworks, or both
- Better account for the uncertainties in PGA and ground water depth. The goal of this effort is to determine whether the over-predictions is due to uncertainties in the input parameters for the analyses
- Examine the CPT database to determine whether the short CPTs characterize the full-depth of the liquefaction potential of the profile or not

APPENDIX A: PEAK GROUND ACCELERATION

The simulation of the ground motions and more specifically peak ground accelerations (PGA) from the 1931 Hawke's Bay earthquake is presented in Appendix A.

The simulations were performed using the Southern California Earthquake Center (SCEC) Broadband Strong Ground Motion Simulation Platform (BBP). Based on historical data from the 1931 Hawke's Bay earthquake, a 1D seismic velocity and density model was used. Hull (1990) determined that the earthquake was a shallow thrust reverse faulting in the accretionary wedge of the subduction zone and not at the plate boundary. Thus, a shallow crustal earthquake source model was used to characterize the earthquake source. The earthquake was not recorded on ground motion instruments, hence the isoseismal map from Dowrick (1998) was based upon to compare the goodness of the simulated PGAs with the Modified Mercalli Intensity (MMI) map. Simulations were performed at each MMI location and a 3-component acceleration time series was obtained and then adjusted for site effects. To establish a comparison between ground motions and intensities, simulated PGAs were converted to intensities using the Ground Motion Intensity Conversion Equations (GMICEs) from Caprio et al. (2015). The converted intensities were checked against the MMI intensities from Dowrick (1998). The 2 sets of intensity were found in good agreement (Bayless et al. 2017).
Points at which PGA values were simulated were made available for this study. The points are enumerated in Table A.1 and plotted on. These points were introduced to ArcMap (Figure A.1) and the PGA surface was interpolated using the interpolation tools. This PGA model serves as an input to the liquefaction triggering assessment.

Table A.1: Simulated PGA values at various locations in Hawke's Bay *(from Bayless et al. 2017 study)*

Site	Easting (m)	Northing (m)	MMI[1]	Simulated PGA (g)	PGA-based MMI[2]
Hastings	1929478	5605197	10	0.84	9.9
Taradale	1930826	5616597	10	0.70	9.7
Greenmeadows	1931991	5617763	10	0.80	9.9
Napier	1936436	5621219	10	0.69	9.1
PetaneValley	1932844	5629366	10	0.52	9.5
Eskdale	1931167	5632357	10	0.47	9.0
Tangoio	1936898	5639747	10	0.62	8.7
Pakipaki	1925346	5599679	9	0.44	9.0
Havelock North	1932524	5601642	9	0.51	9.6
Maraekakaho	1910440	5604641	9	0.35	8.2
BridgePa	1922358	5604399	9	0.66	9.8
Whakatu	1934190	5608981	9	0.62	9.9
Clive	1936314	5611116	9	0.55	9.8
Puketapu	1925833	5619798	9	0.46	9.3
Sherenden	1907418	5621061	9	0.36	8.9
PoraiteHills	1929956	5621909	9	0.59	9.2
BayView	1932949	5629433	9	0.55	9.4
TePohue	1917800	5648993	9	0.28	8.4
Tutira	1936136	5651188	9	0.45	9.1
Putorino	1946140	5660820	9	0.52	9.0
Mohaka	1938581	5666540	9	0.32	8.6
Kotemaori	1949639	5668593	9	0.51	8.8
Kopua	1879285	5558753	8	0.09	7.4
Norsewood	1874351	5559194	8	0.09	7.0
Waipukurau	1903691	5566687	8	0.15	7.8
Elsthorpe	1926123	5574520	8	0.22	8.4
Ongaonga	1892283	5576248	8	0.15	7.8
Otane	1910225	5577417	8	0.21	8.3
TeAute	1911062	5585136	8	0.20	8.0
Argyll	1904490	5585698	8	0.18	7.8
Tikokino	1895959	5586359	8	0.19	7.9
Waimarama	1941457	5585063	8	0.25	8.2
Maraetotara	1934678	5586335	8	0.21	8.3
Opapa	1914889	5588072	8	0.19	7.8
Poukawa	1919314	5592119	8	0.27	8.5
TeMata	1935833	5598201	8	0.28	8.3

Kereru	1893651	5607039	8	0.25	8.1
TeAwanga	1941558	5605326	8	0.44	9.3
Haumoana	1938865	5608804	8	0.50	9.4
Fernhill	1923079	5611090	8	0.63	9.6
Crownthorpe	1915049	5615254	8	0.53	9.1
Otamauri	1900931	5621639	8	0.27	8.6
Waiwhare	1899528	5628846	8	0.28	8.3
Rissington	1919563	5629317	8	0.41	9.1
Patoka	1910652	5638493	8	0.26	8.2
Pukutitiri	1905159	5645921	8	0.28	8.5
Turiroa	1934329	5646557	8	0.44	8.8
Pakaututu	1902328	5652264	8	0.21	8.0
Nuhaka	2010343	5667799	8	0.28	8.3
Wairoa	1982455	5670023	8	0.38	9.2
TeReinga	1992449	5692677	8	0.14	7.4
Tuai	1960178	5695931	8	0.17	8.0
Tiniroto	1996715	5698361	8	0.15	7.2
Manutuke	2027391	5707060	8	0.11	7.9
Weber	1881006	5522448	7	0.05	6.1
Hopelands	1850742	5529021	7	0.04	6.4
Woodville	1843425	5530953	7	0.04	6.5
Waitahora	1870232	5531558	7	0.06	6.7
Porangahau	1907002	5532477	7	0.07	6.7
Wallingford	1905715	5543044	7	0.09	7.6
Dannevirke	1863869	5544845	7	0.07	6.8
Matamau	1869054	5551748	7	0.09	7.1
Waipawa	1906709	5572554	7	0.16	7.6
Wanganui	1774992	5577994	7	0.04	6.4
Wakarara	1878749	5591149	7	0.14	7.5
Hangaroa	1992628	5705821	7	0.14	7.1
Gisborne	2036668	5708731	7	0.10	7.8
TeHapara	2035089	5709975	7	0.13	7.9
Patutahi	2025816	5713732	7	0.14	8.1
Wairakei	1870224	5720875	7	0.06	7.2
Rere	2001887	5724485	7	0.08	7.3
TeKaraka	2024627	5730855	7	0.05	6.9
Matawai	1996364	5744793	7	0.06	6.6
Motu	1997972	5756008	7	0.05	6.7
Tarawera	1906971	5763213	7	0.04	6.6

Masterton	1823661	5463277	6	0.02	6.1
Eketahuna	1828653	5497010	6	0.03	6.4
Nireaha	1823356	5501072	6	0.03	6.5
Foxton	1793793	5517313	6	0.03	6.6
Pahiatua	1840373	5517363	6	0.03	6.3
PalmersonNorth	1821502	5529873	6	0.04	6.6
Fielding	1818492	5543875	6	0.04	6.6
Hunterville	1819503	5576134	6	0.05	6.8
Rangiwahia	1848018	5579397	6	0.07	6.9
Mangaweka	1839310	5589936	6	0.05	6.3
Taihape	1840041	5604264	6	0.05	6.6
Raetihi	1796397	5633357	6	0.04	6.7
Ohakune	1806471	5634086	6	0.05	6.7
Kuripapango	1886752	5634047	6	0.19	8.1
PortlandIsland	2019818	5639358	6	0.18	7.7
Waitara	1707172	5682374	6	0.01	5.7
Taupo	1867055	5713625	6	0.08	7.3
TolagaBay	2062831	5739541	6	0.04	6.8
WaipiroBay	2068257	5778642	6	0.02	6.3
Opotiki	1976447	5784702	6	0.05	7.0
Makomako	1767370	5795712	6	0.02	4.9
Wellington	1748739	5427921	5	0.01	4.1
Martinborough	1806217	5434003	5	0.02	4.9
Carterton	1812148	5454937	5	0.01	5.6
Castlepoint	1871207	5467621	5	0.02	6.3
Levin	1793372	5500664	5	0.02	6.5
Marton	1802760	5561889	5	0.04	6.7
Hawera	1709876	5617150	5	0.02	6.1
Eltham	1711829	5634648	5	0.01	5.9
Horopito	1804771	5642288	5	0.04	6.7
Stratford	1710646	5645038	5	0.01	5.5
Inglewood	1704229	5665234	5	0.01	5.4
NewPlymouth	1693036	5676502	5	0.01	5.4
Taumaranui	1796091	5693750	5	0.04	6.4
Awakino	1741772	5720456	5	0.02	5.4
Otorohanga	1793528	5770921	5	0.02	6.5
Arapuni	1832316	5783129	5	0.02	5.9
TeTeko	1932951	5783344	5	0.07	7.7
Whakatane	1950673	5791836	5	0.04	6.3

Cambridge	1816948	5803396	5	0.02	5.6
Matata	1929899	5800079	5	0.03	6.2
EastCape	2088591	5814020	5	0.01	5.2
Tauranga	1879100	5824108	5	0.03	6.8
Patea	1726170	5598420	4	0.02	6.1
TeKuiti	1789094	5755024	4	0.02	6.3
Rotorua	1884824	5774009	4	0.06	7.4
Kawhia	1759265	5785038	4	0.01	4.9
TeAwamutu	1803054	5791006	4	0.03	5.6
Matamata	1844412	5811535	4	0.03	6.5
Hamilton	1800703	5815370	4	0.02	5.2
Paeroa	1836677	5859380	4	0.01	4.9
Ngaruawahia	1789522	5828913	3	0.01	4.8
Morrinsville	1823170	5829207	3	0.02	5.7
Waitoa	1832338	5835455	3	0.02	6.0
TeAroha	1839577	5841477	3	0.01	5.2
Mercer	1781563	5872197	3	0.01	4.5
Thames	1825731	5886740	3	0.01	4.3
Pukekohe	1768925	5881009	2	0.01	4.5

[1] From the isoseimal map by Dowrick (1998)

[2] Converted from PGA to intensity using the Ground Motion Intensity Conversion Equations (GMICEs) from Caprio et al. (2015)

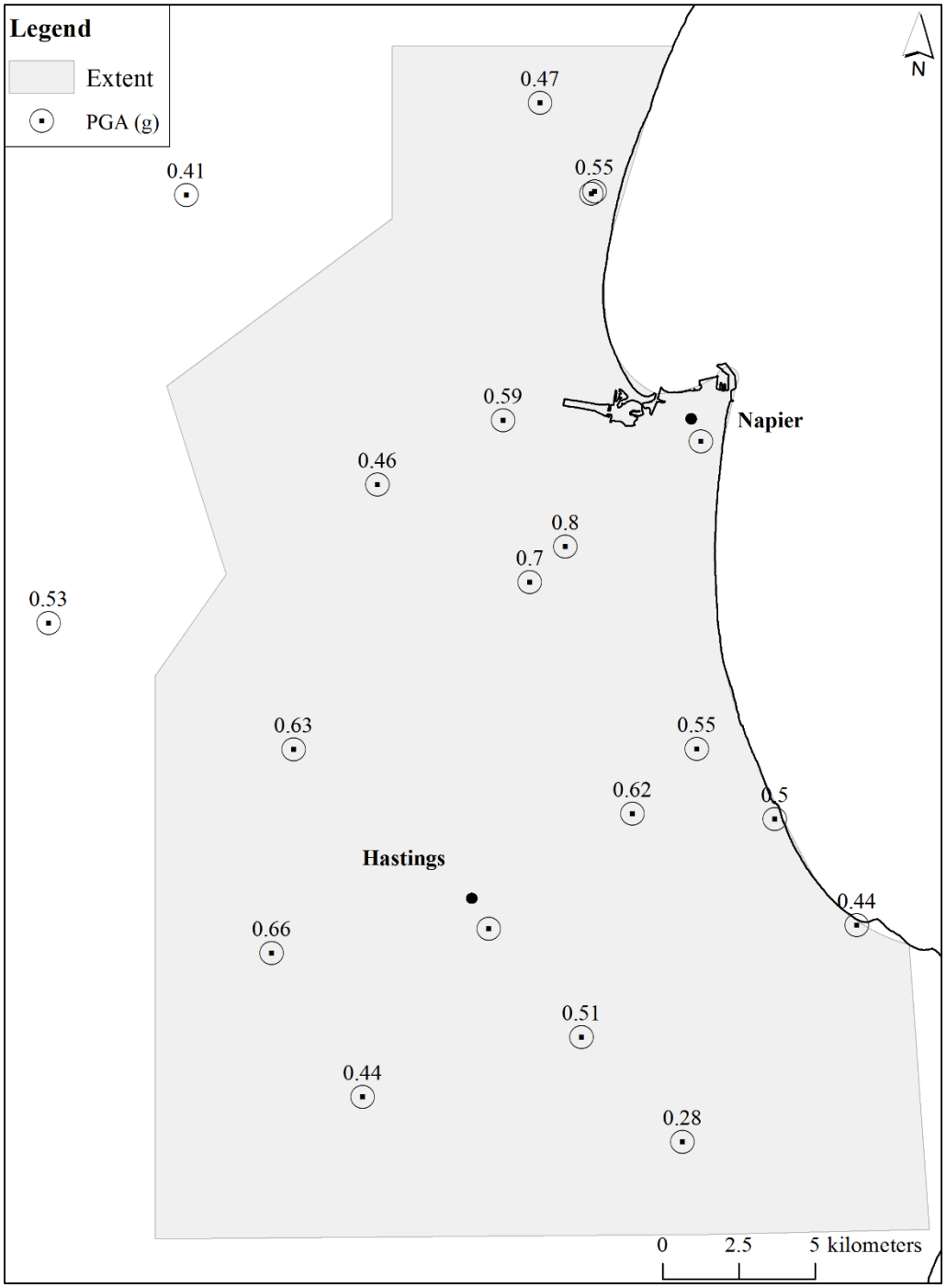

Figure A.1: Simulated PGA points within the extent of study area

APPENDIX B: HISTORICAL LIQUEFACTION RECORDS FROM THE 1931 EVENT

A detailed documentation of available liquefaction records from the 1931 Hawke's Bay earthquake is presented in Appendix B. The database created in this appendix is used in the comparison of the predicted versus the observed liquefaction occurrences following the 1931 event.

1. Written accounts and research

This study is based on written material. Written documents include published papers and reports, published books, personal accounts from archives and newspaper clips. Collectively, it provides an overview of the ground damage after the 1931 earthquake in Napier and its vicinity.

1.1 General Observations

Callaghan (1933) reports the "muddy water" which appeared around the vessels in the Hawke's Bay harbor (pp.16). Beaches of gravel and sand enclosing lagoons, swamps and flats were ridged at the mouths of streams due to the settlement of underlying mud. Mud spouts were formed on the alluvial flats (Henderson 1933, pp.48).

1.2 Napier (MM X)

Napier experienced the highest ground shaking (MM X) and the biggest damage following earthquake and fire. Fissures in the ground surface were conspicuous throughout the area between the Tutaekuri River, the Ahuriri lagoon and Taradale. In Napier, fissured ground was noticeable and the most pronounced fissures were along the original bed of the Tutaekuri River which formerly flowed in an arc through the center of Napier lying on the flats (Callaghan 1933, pp.12). At this locality, roads were fissured, water and sewer pipes were ruptured and in some places, the ground has moved about 3.5 m towards the open channel. In the former river channels, the fill consolidated and its surface sank. The Tutaekuri old channel can be traced through Napier and near the Boys' High School (Te Awa), settlement was about 0.5 to 1 m (Henderson 1933, pp.48). Most of the underground pipe systems were affected by the movement of the ground especially those laid on silt in Napier South for example. As a result, the water supply and the sewerage systems were put out of order (Callaghan 1933, pp.11 & Dowrick 1998, pp.145). Damage to roads and railways around Napier was greatest on reclaimed swamps (Dowrick 1998, pp.142). Napier South had been reclaimed in 1908 with silt from the Tutaekuri River and was badly affected by liquefaction during the earthquake. Sand boils and wooden foundation piles sinking and tilting were reported (Fowler 2013, pp.39, Evening Post, Feb 6, 1931). Based on several personal accounts (Ashcroft 1931; Spiller 1931), liquefaction was reported on George Drive. George Drive was a former channel for the Tutaekuri River and was diverted to discharge into the sea at its present location after the reclamation of Napier South (McGregor 1989). Along George Drive, the ground was covered in cracks up to 0.3 m wide and over 1 m deep. Houses were leaning at critical angles and foundations failed. Moreover, the earthquake caused damage to electricity supply systems at a substation in Taradale: foundations "sank unevenly". The most significant damage to electricity supply and telegraph systems was the critical leaning and sinking of distribution poles founded in old river beds and reclaimed lands (Dowrick 1998, pp.145-146, Robinson and Benjamin 1933).

1.3 Port Ahuriri and Westshore (MM X)

A considerable area extending from Battery Road to the entrance of the Inner Harbor has been reclaimed. On this reclaimed portion stand the business premises and stores of Port Ahuriri. A wharf was built on the shore facing the Inner Harbor. During the earthquake, severe liquefaction occurred on the supporting reclaimed land: "the piles, wharf decking and fillings became twisted, bent, and fissured to an extraordinary extent" (Callaghan 1933, pp.15). Historic photographs also show lateral spreading of the quay in the direction of the sea (Figure B.1). The Westshore causeway bypassing the Ahuriri flats was shockingly fissured and cracked making it impassable (Callaghan 1933, pp.15). It was constructed largely from mud and sand originating from the Ahuriri mud-flats, then covered with a meter of limestone rubble, 30 cms of concrete and sealed with 2.5 cms of asphalt (Fowler 2013, pp.39). Limestone blocks covered the faces of the embankment on both sides. It accommodated a road and a railway side by side. The foundations of the causeway consist of reinforced concrete girders sitting on reinforced concrete piles across the mud-flats. The causeway spread in parts, bulging out the limestone facing and it sank in parts down to the level of the mud-flat (Figure B.2). Due to unconsolidated mud in the swampy area, the pile groups at both ends were displaced and the girders at the south end were disconnected from the piles (Henderson 1933, pp.48). The railway to the north of Napier over the Westshore Bridge has suffered from fissures and cracks in the ground (Callaghan 1933, pp.24). One account of mud blowout at the Ahuriri Lagoon was reported (Daily Telegraph, Feb 2, 1981).

1.4 Hastings (MM X)

In Hastings, there is only one observation of fissures in the streets, fills and embankment (Callaghan 1933, pp.17). These were hard to detect in the photographs available in the archives. The water supply systems were very little damage excluding subsidence at bridges and earth fills (Dowrick 1998, pp.143).

Figure B.1: Lateral spreading of the wharf in Ahuriri (*from the archives of the MTG Hawke's Bay Museum*)

Figure B.2: Severe liquefaction and lateral spreading of the Westshore embankment *(from the archives of the MTG Hawke's Bay Museum)*

1.5 Heretaunga Plains (MM IX)

Roads and railways as far south as Waipukurau significantly suffered from fissures and cracks in the ground (Callaghan 1933, pp.19). The railway from Ormondville (south west of Hastings) to Hastings was badly damaged, the rails had bent and twisted, specifically those passing over swampy ground and embankments had failed (Callaghan 1933, pp.24). The damage to the railways from Hastings to Napier was not extensive. The roads and railway from Napier up to Bay View (north of Napier) along the seaside were twisted and bent. Then, both roads and railway were untouched for a considerable distance (Auckland Weekly News, Feb 25, 1931). Mud boils under the floorboards of Tuckers Woolscour (Clive) and at Longlands (west of Hastings in the old bed of the Ngaruroro River) were reported by Fairless and Berrill (1984) (Table B.1). The coastline between the Tukituki River and the Ngaruroro River was approximately 0.3 m lower than its pre-earthquake level and Marshall (1933) attributes this change in level to the settlement of loose deposits after the shaking (pp.80). Also, stop banks along the lower channels of the rivers slumped and were widely fissured (Callaghan 1933, pp.33).

1.6 Other districts in Hawke's Bay

Sand boils were reported in Tangoio (MM X), Petane (MM X), Bay View (MM IX) and Mohaka mouth (MM IX) (Henderson 1933, pp.49). Sand boils at Petane appeared near the coast (Figure B.3) (The Auckland Weekly News, March 4, 1931). At Bay View, "spouts of water arose from the ground during the earthquake and have left behind them deposits of a very fine grey sand" (Auckland Weekly News, Feb 25, 1931).

The earthquake caused differential settlements of machinery and buildings at the Wairoa freezing works and the dairy factory, north east of Napier. Buildings on the

banks of Wairoa river had leaned significantly, the roads in the vicinity had been fissured, one section of a road had subsided and shifted several feet towards the Wairoa River, and the bridge spanning the river had been badly bent (Callaghan 1933, pp.20). The spreading of the northern bank of the river pushed out the pier from the bank and the Wairoa road bridge failed (Dowrick 1998, pp.143). Also, sand boils were reported on the Wairoa flats (Henderson 1933, pp.49). In the vicinity of Gisborne (MM VII+), a "blowout from a mud spring" and "mud-pools" were observed at Hangaroa and Muriwai Beach, respectively (Callaghan 1933, pp.21). The Hangaroa mud blowout was described in details in Strong (1933). It is reported that ejecta covered an area of 9,100 m^2 and temporarily blocked the Hangaroa River. Serious observations of differential settlement were reported South of Napier: Pakipaki (MM IX) and Whakatu (MM IX) (Callaghan 1933, pp.19).

Figure B.3: Sand boils at Petane *(from the archives of the MTG Hawke's Bay Museum)*

Table B.1: Observations of liquefaction from the 1931 earthquake *(reproduced from Fairless & Berrill, 1984)*

Evidence	Area	Coordinates	Epicentral Distance [1]	Reference
Sea discolored in patches. "Penetrating marshwater"	Hawke's Bay. Seems widespread			Hayes (1953)
50% more water in streams	Mohaka area especially Mohaka Mouth	39.13°S 177.19°E	About 50 km	Eiby (1973b) Eiby (1980a) Eiby (1981)
Large quantities of water, sand and silt issued from holes in the ground	Tangoio Lagoon, Petane	39.34°S 176.92°E 39.43°S 176.87°E	22 km 19 km	Daily Telegraph (1981)
Buildings leaning	Taradale, Wairoa	39.53°S 176.85°E	27 km	Bullen (1938a)
Settlement and expulsion of sand and mud	Near mouth of Tutaekuri River (Ahuriri?) and in Heretaunga Plains	39.03°S 177.43°E 39.48°S 176.88°E	26 km	Callaghan et al (1933)
Spouts of sediment, Mud boils	Esk Valley	39.39°S 176.83°E	15 km	
Mud boils	Site of Princess Margaret Hospital	39.48°S 176.9°E	26 km	Daily Telegraph 02/02/81
Mud boils	Through floor boards of Tuckers Woolscour, Clive	39.6°S 176.90°E	36 km	Conly (1980)
"Blowhole"	Road near Taradale	39.53°S 176.86°E	28 km	Grayland (1942)
"Boiling mud pool"	Longlands	39.68°S 176.81°E	40 km	Daily Telegraph 17/02/31
"Geysers"	Gisborne Beach	38.69°S 178.04°E	140 km	21/02/31
"Blowouts"	Mohaka area			Grayland (1957) Jaggar (1931) Guthrie-Smith (1969)

[1] Based on 1938 epicenter location

2. Visual studies

Visual studies provided material to complement the above findings. Visual studies comprised historical photographs from the archives at the Hawke's Bay Museum & Art Gallery, Napier Public Library and Hastings District Libraries. The biggest collection of historical photographs was made available by the archives at the Hawke's Bay Museum & Art Gallery and it can conveniently be accessed electronically at their website (http://www.mtghawkesbay.com/museum-collection/). The collection and analysis of material consisted of 3 stages. First, the photographs were closely examined for liquefaction manifestations. Second, the photographs were cautiously located throughout the Hawke's Bay region. Old maps and plans were used, where available to pinpoint the photographs to their most probable location. Michael Fowler, a local historian and columnist, assisted in the identification of the location of some photographs. Several photographs couldn't be located due to the changes in planning and urbanization from 1931 to this present day. These photographs were not further investigated. Other photographs were broadly located in Hawke's Bay. These photographs were considered but their location is not known with confidence. The majority of photographs was identified at their exact locations based on the above aids. Third, the photographs were collected in a database and were classified into 5 categories indicative of liquefaction occurrence in order of increasing severity: unknown (where the photograph did not provide information on liquefaction or it was hard to tell), not liquefiable, sand boil, lateral spreading and sand boil and lateral spreading. Finally, the photographs were digitized on an aerial map in ArcGIS based on the identified location of individual photographs. The digitized liquefaction observations are summarized in Table B.2 and shown in Figure B.4, Figure B.5 and Figure B.6.

Table B.2: Additional observations of liquefaction from this study

Point ID	Site Description	Area	Liquefaction[2] Type	Certainty	Resource[3]
1	Camp	Ahuriri	NO LQF	Possible	PHOTO
2	Union Hotel	Ahuriri	NO LQF	Certain	PHOTO
3	Damaged road	Ahuriri	Spreading	Certain	PHOTO
4	Williams and Kettle Ltd	Ahuriri	Spreading	Certain	PHOTO
5	Nelson Quay	Ahuriri	Spreading	Certain	PHOTO
6	Post office	Ahuriri	Spreading	Possible	PHOTO
7	Battery Road	Ahuriri	Spreading	Possible	PHOTO
8	West Quay	Ahuriri	Spreading	Certain	PHOTO
9	Railway line	Ahuriri	Spreading	Certain	PHOTO
10	Barry brothers	Ahuriri	Unknown	Possible	PHOTO
11	Mud blowout	Ahuriri	Sand boil	Possible	NEWSCLIPS
12	Sand Geysers	Bay View	Sand boil	Certain	PHOTO
13	Water spouts with fine white sand	Bay View	Sand boil	Certain	PHOTO
14	Road and railway-seaside	Bay View	NO LQF	Certain	NEWSCLIPS
15	Clive Hotel	Clive	Unknown	Unknown	PHOTO
16	Tucker Woolscour	Clive	Sand boil	Certain	PUBPAPERS
17	Esk Valley bridge	Eskdale	Spreading	Possible	PHOTO
18	Cosy Theater	Hastings	NO LQF	Certain	PHOTO
19	Grand Hotel	Hastings	NO LQF	Certain	PHOTO
20	Methodist Church	Hastings	NO LQF	Certain	PHOTO
21	Post office	Hastings	NO LQF	Certain	PHOTO
22	Municipal theatre	Hastings	NO LQF	Possible	PHOTO
23	Municipal buildings	Hastings	NO LQF	Certain	PHOTO
24	Farmers Coop Association Ltd	Hastings	NO LQF	Certain	PHOTO
25	The Tribune Limited	Hastings	NO LQF	Certain	PHOTO
26	Racecourse	Hastings	NO LQF	Certain	PHOTO
27	Roachs'	Hastings	NO LQF	Certain	PHOTO
28	Land's bag Shop	Hastings	NO LQF	Certain	PHOTO
29	Karamu Road	Hastings	NO LQF	Certain	PHOTO
30	Williams and Kettle Ltd	Hastings	NO LQF	Certain	BOOKS
31	Police Station	Hastings	NO LQF	Certain	PHOTO
32	Tourist Motor Company	Hastings	NO LQF	Certain	PHOTO
33	Public Trust office	Hastings	NO LQF	Certain	PHOTO
34	Hastings High School	Hastings	NO LQF	Certain	PHOTO

35	Daily Telegraph	Hastings	NO LQF	Certain	BOOKS
36	Westerman & Co	Hastings	NO LQF	Certain	BOOKS
37	Commercial Bank of Australia	Hastings	NO LQF	Certain	PHOTO
38	Pacific Hotel	Hastings	NO LQF	Certain	PHOTO
39	De Pelichet, McLeod & Co	Hastings	NO LQF	Certain	PHOTO
40	Colonial Mutual Life Assurance Society Limited	Hastings	NO LQF	Certain	PHOTO
41	J G Martin automobile upholsterer	Hastings	NO LQF	Certain	BOOKS
42	HB Jockey Club	Hastings	NO LQF	Certain	BOOKS
43	Loach & Price Limited	Hastings	NO LQF	Certain	BOOKS
44	King's theater	Hastings	NO LQF	Certain	BOOKS
45	St Andrews Road	Havelock North	Spreading	Certain	PHOTO
46	Havelock Bridge	Havelock North	Spreading	Certain	PERSACC
47	Wrecked roads	Longlands	Spreading	Certain	BOOKS
48	Mud blowout	Longlands	Sand boil	Certain	PUBPAPERS
49	Mohaka River mouth	Mohaka	Sand boil	Certain	PUBPAPERS
50	Nelson Park	Napier	Sand boil	Certain	PHOTO
51	Te Awa School	Napier	Sand boil	Possible	PHOTO
52	Napier Post Office	Napier	NO LQF	Unknown	PHOTO
53	E&D building	Napier	NO LQF	Possible	PHOTO
54	Napier Technical College	Napier	NO LQF	Possible	PHOTO
55	St Paul Presbyterian Church	Napier	NO LQF	Certain	PHOTO
56	Dalgety & Company Ltd	Napier	NO LQF	Certain	PHOTO
57	Women's rest	Napier	NO LQF	Certain	PHOTO
58	Empire Hotel	Napier	NO LQF	Possible	PHOTO
59	Emerson Street	Napier	NO LQF	Certain	PHOTO
60	Caledonian Hotel	Napier	NO LQF	Certain	PHOTO
61	Central fire station	Napier	NO LQF	Certain	PHOTO
62	Kinross White Limited	Napier	NO LQF	Certain	PHOTO
63	Masonic hotel	Napier	NO LQF	Certain	PHOTO
64	Club hotel	Napier	NO LQF	Certain	PHOTO
65	Marine Parade	Napier	NO LQF	Certain	PERSACC
66	Williams and Kettle head office	Napier	NO LQF	Certain	PHOTO
67	Public Trust	Napier	NO LQF	Certain	PHOTO

68	Tennyson Street	Napier	NO LQF	Certain	PHOTO
69	Bank of New Zealand	Napier	NO LQF	Certain	PHOTO
70	Courthouse	Napier	NO LQF	Certain	PHOTO
71	HB County Council Office	Napier	NO LQF	Certain	PHOTO
72	Bate and Bell Limited	Napier	NO LQF	Certain	PHOTO
73	Telephone exchange	Napier	NO LQF	Certain	PHOTO
74	St Patrick's church	Napier	NO LQF	Certain	PHOTO
75	Napier Borough Council Waterworks bldg	Napier	NO LQF	Certain	PHOTO
76	Byron Street	Napier	NO LQF	Certain	PHOTO
77	Parker's Chambers	Napier	NO LQF	Certain	PHOTO
78	Hastings Street School	Napier	NO LQF	Certain	PHOTO
79	Band Rotunda	Napier	Spreading	Possible	PHOTO
80	Napier Boys High School[4]	Napier	NO LQF	Possible	PHOTO
81	George's drive	Napier	Spreading	Certain	PERSACC
82	Dr Moore's Hospital	Napier	Unknown	Possible	PHOTO
83	Breakwater Road	Napier	Unknown	Unknown	PHOTO
84	Blythes Building	Napier	Unknown	Unknown	PHOTO
85	Municipal Theatre	Napier	Unknown	Unknown	PHOTO
86	Outside St John's Cathedral	Napier	Unknown	Unknown	PHOTO
87	Remains of Central hotel	Napier	Unknown	Unknown	PHOTO
88	Napier breakwater	Napier	Unknown	Unknown	PHOTO
89	Collapsed building	Napier	Unknown	Unknown	PHOTO
90	Zenith Transport Company	Napier	Unknown	Unknown	PHOTO
91	Napier South	Napier South	Sand boil & Spreading	Certain	BOOKS
92	McLean Park	Napier South	NO LQF	Possible	PHOTO
93	Petane and Eskdale Road	Petane	Spreading	Certain	PHOTO
94	Petane Road	Petane	Spreading	Certain	PHOTO
95	Damaged road	Tangoio	Sand boil & Spreading	Possible	PHOTO
96	Blowhole	Taradale	Sand boil	Certain	PUBPAPERS
97	Gloucester Rd (possibly)	Taradale	Sand boil & Spreading	Certain	PERSACC
98	Anderson Park	Taradale	NO LQF	Certain	PHOTO
99	Town Hall	Taradale	NO LQF	Certain	PHOTO
100	Taradale Hotel	Taradale	NO LQF	Certain	PHOTO

101	Damaged house	Taradale	NO LQF	Certain	PHOTO
102	Kennedy Road	Napier	Spreading	Possible	PERSACC
103	Napier-Greenmeadows Rd	Taradale	Spreading	Certain	PHOTO
104	Buildings leaning	Taradale	Spreading	Certain	PUBPAPERS
105	Memorial clock tower	Taradale	Unknown	Unknown	PHOTO
106	Redcliff bridge	Waiohiki	Spreading	Possible	PHOTO
107	Bridge on Waiohiki Rd	Waiohiki	Spreading	Certain	PERSACC
108	Westshore Embankment Road	Westshore	Spreading	Certain	PHOTO
109	Railway bent and twisted	Westshore	Spreading	Certain	NEWSCLIPS
110	Railway and bridge damage	Whakatu	Spreading	Certain	PERSACC

[2] NO LQF: No liquefaction

[3] PHOTO: Historical photographs, NEWSCLIPS: Newspaper clips, PUBPAPERS: Published papers, PERSACC: personal accounts, BOOK: Historical books

[4] Henderson 1933, pp.48 reports settlement near the Boys' High School but it is not visible in the photographs. A site visit to the location was done and the foundations of the old building were found in place. Thus, it was classified as "no liquefaction"

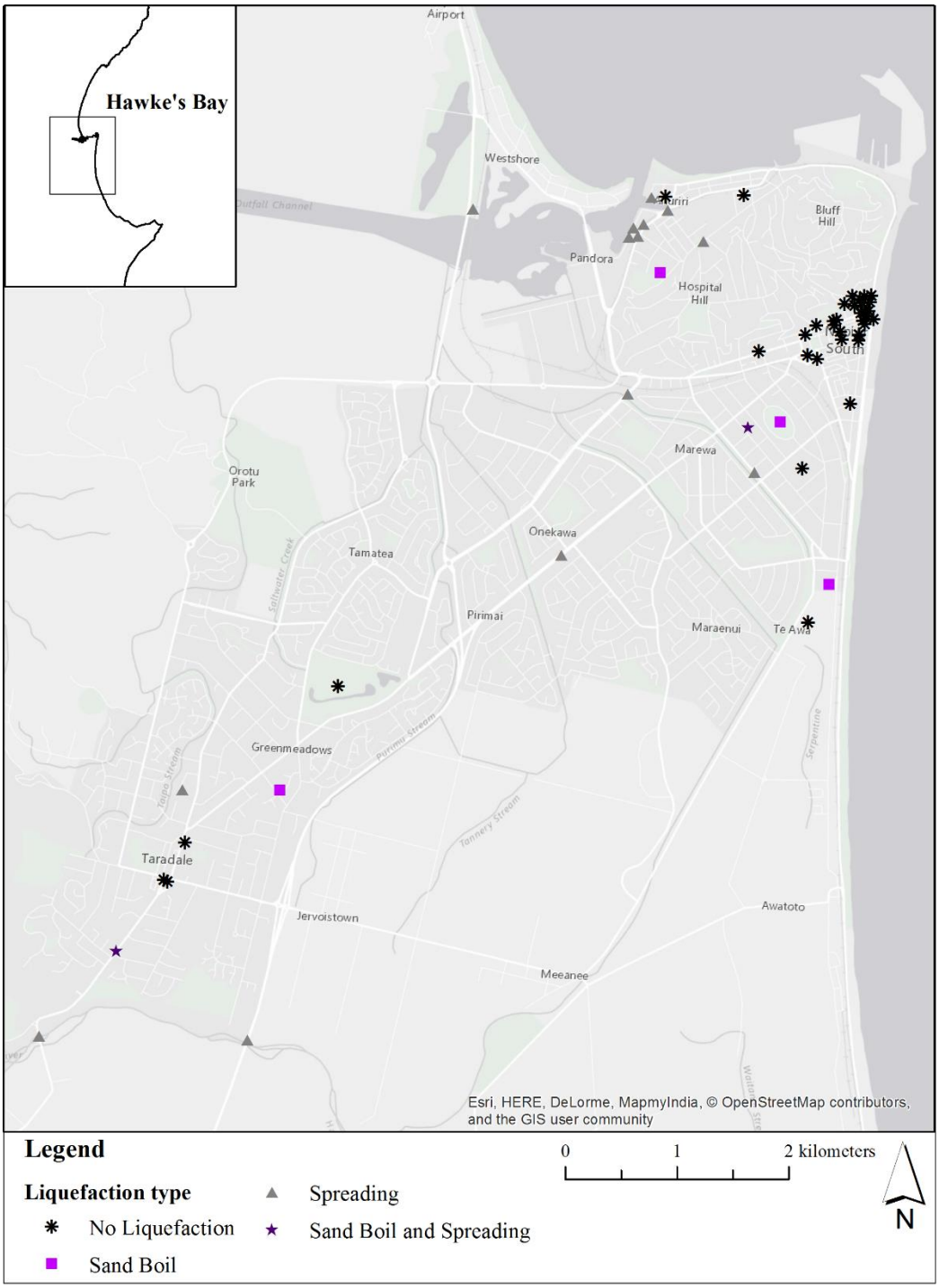

Figure B.4: Historical Liquefaction Sites – Napier/Ahuriri

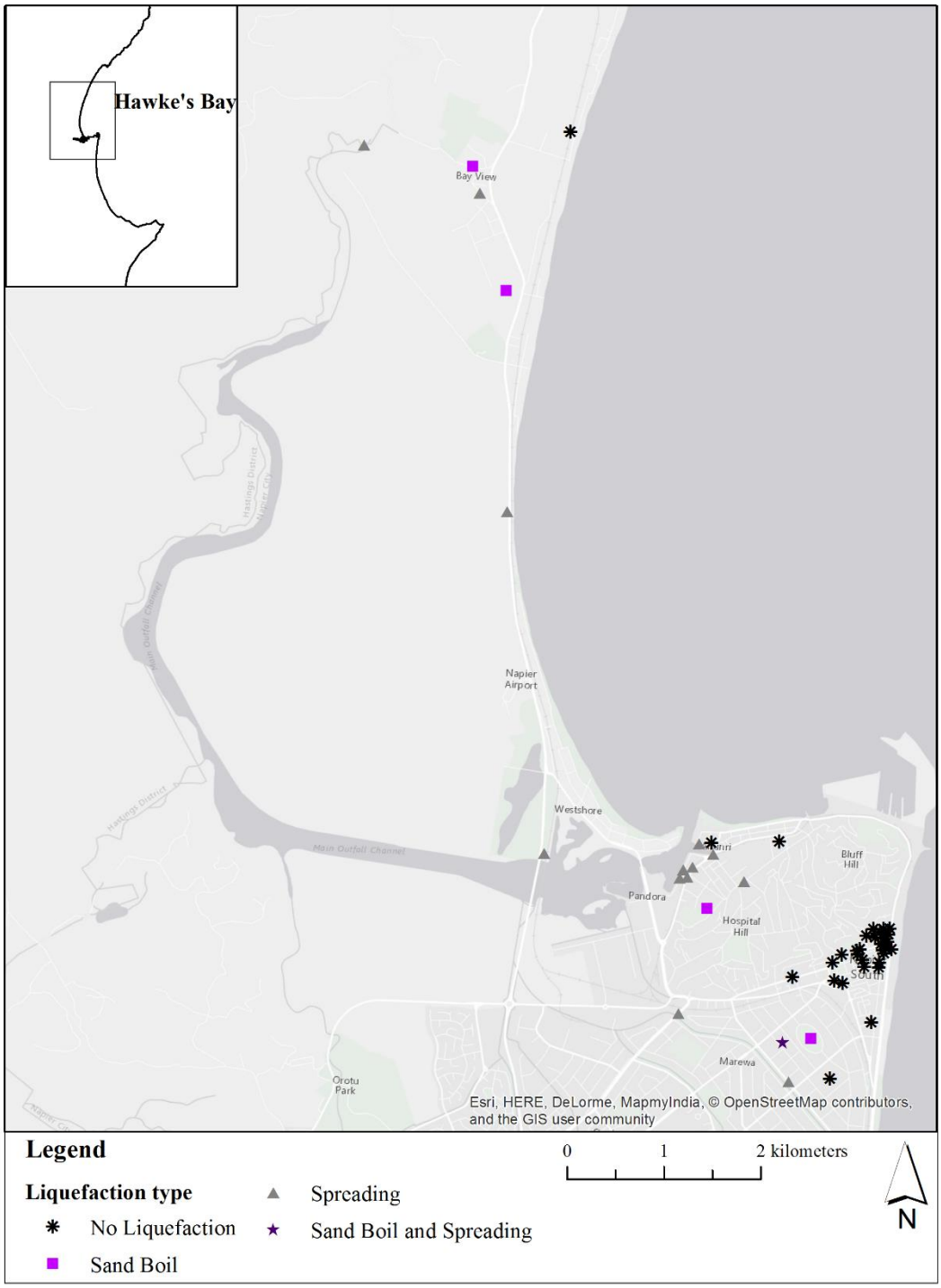

Figure B.5: Historical Liquefaction Sites – Westshore/BayView/Tangoio

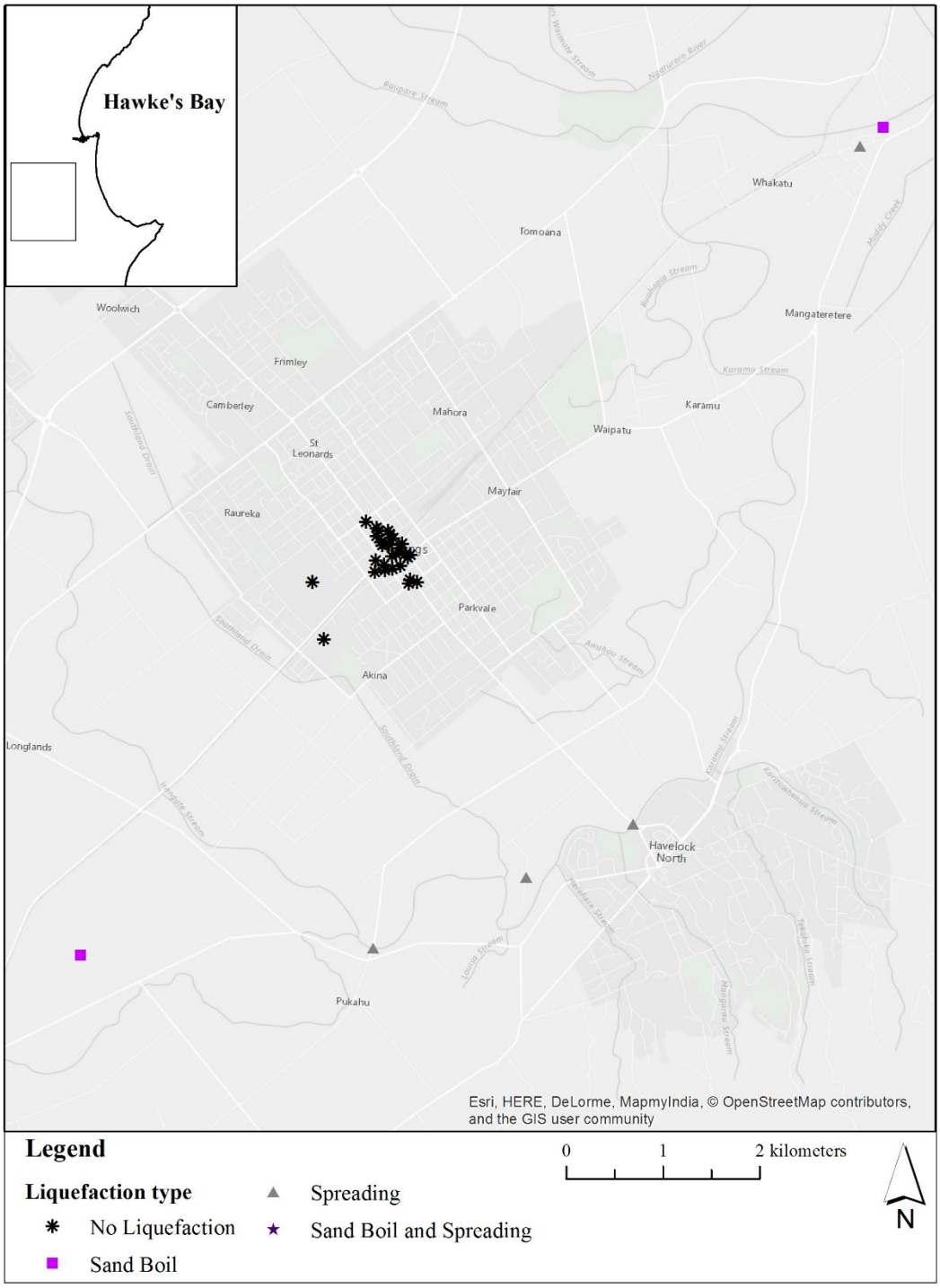

Figure B.6: Historical Liquefaction Sites – Hastings/Havelock North

3. References

"A Phenomenon of the Earthquake." (1931). *Auckland Weekly News*.

Ashcroft, B. (1931). "n.d." *Personal Accounts*.

"Boiling mud and water bubbled from the ground." (1981). *Daily Telegraph*.

Fowler, M. (2007). *From Disaster to Recovery: the Hastings CBD 1931-35*. Michael Fowler Publishing Ltd.

Fowler, M. (2013). *Michael Fowler's Historic Hawke's Bay*. Michael Fowler Publishing Ltd.

McGregor, R. (1989). *The Great Quake: The Story of the 1931 Hawke's Bay Earthquake*. Regional Publications Ltd, Napier, New Zealand.

"Post-quake trials." (1931). *Evening Post*, 9.

Robinson, I. R., and Benjamin, H. L. (1933). "Effects of Earthquakes on Electrical Supply Systems." *Proc. New Zealand Society of Civil Engineers*, 256–289.

Spiller, K. (1931). "n.d." *Personal Accounts*.

Strong, S. W. S. (1933). "The Sponge Bay Uplift, Gisborne, and the Hangaroa Mud Blowout." *The NZ Journal of Science and Technology*, 76–78.

"The Earthquake Area." (1931). *Auckland Weekly News*.

APPENDIX C: GROUND WATER MODEL

The input datasets and the construction of a model for the unconfined groundwater of the Heretaunga Plains is presented in Appendix C.

Based on unconfined groundwater data from geotechnical site investigations and the Hawke's Bay Regional Council (HBRC), an unconfined groundwater model is developed. Due to the limitations of groundwater data in general and specifically data pertaining to the 1931 era, all the available groundwater levels were used. The period of measurements ranges from the 1920s till present day, thus there exists some limitations and uncertainties amply discussed in this appendix. Groundwater data was sorted out based on the date of measurement. Measurements taken during the summer season were included in a low-flow-condition groundwater model. Measurements taken during the winter season were included in a high-flow groundwater model. However, this second set of measurements was largely inconsistent and the high-flow groundwater model was not pursued. An alternative is proposed herein to account for the seasonal fluctuations. The low-flow condition groundwater model comprises 3 main steps. First, a groundwater elevation model is interpolated by kriging the data points mentioned above. Second, the pre-1931 ground elevation is characterized using the detailed documentation of changes in elevation by Hull (1990). Third, the groundwater elevation is subtracted from the 1931 ground elevation and the depth-to-water table map is obtained. This groundwater depth model (GWD) serves as input to the liquefaction triggering assessment.

1. Groundwater Data Acquisition

1.1 Input Datasets

The majority of the available well data in Hawke's Bay belongs to confined aquifers. Yet, the intent of this work is to model unconfined groundwater. Thus, the data used in the model consider only unconfined groundwater measurements.

Datasets used in this model come from several sources:

- Site investigations within the study area and more specifically borehole logs and cone penetration logs (CPTs). Site investigations were retrieved from the Tonkin and Taylor Geotechnical Database TTGD (private access) and the New Zealand Geotechnical Database NZGD (public access)
- Well drilling logs from the Wellstor database (which contains well information) were made available by the Hawke's Bay Regional Council (HBRC). Wells in the database are classified in this study as tapping confined or unconfined aquifers based on the driller's notes at the time of drilling (also available from HBRC)
- Surface water features such as river levels, stream levels and drains were obtained from HBRC
- Time series data at monitoring stations recorded over a period of 3 to 22 years. HBRC holds this type of data
- Piezometric levels from different piezometers installed for groundwater monitoring during seasonal variations. The information is stored by the HBRC and was made available for this study

1.2 Data Limitations

Time series data recorded at monitoring stations give the best visualization of the variation of groundwater levels over the years. However, the majority of the data pertains to confined aquifers and was irrelevant for this model. Thus, static water levels were employed as input to the groundwater model. Considerable uncertainty arises from the utilization of static water levels from site investigations and well drilling information for a number of reasons. First, the water levels from boreholes and CPTs or wells are taken as a single measurement at a specific point in time which might be only representative of the conditions at that time. Second, the quality of the data is highly variable due to the advances in instrumentation from 1920s till present and potential measurement or recording errors at the time of drilling. Third, the water level for wells is measured during the drilling of the well following the pumping of water. The groundwater is not always given sufficient time to regain equilibrium condition. Fourth, it can be difficult to tell from the driller's notes whether water levels refer to confined or unconfined aquifers.

Furthermore, the HBRC recommends the cautious use of the data because there are some inconsistencies within the database being collected over the years. Mainly, there is no clear indication of the datum used for water measurement and ground elevation. The latter can be corrected for by using the ground elevations from LiDAR (developed in Section 2.3.4 of this manuscript) but there is no alternative for the datum taken for

the water levels. In this study, the datum or measurement point for the wells is taken at 0.4 m above the ground surface (as advised by HBRC). As such, all measurements will be treated to +/- 1m accuracy.

1.3 Data Processing

The datasets mentioned above are sorted out and only data representing unconfined groundwater is kept. The above datasets are further divided into 2 groups based on drilling dates and occasionally water level: data points measuring low-flow conditions (deeper groundwater table GWT) and data points measuring high-flow conditions (shallower GWT). The focus of this appendix is on the low-flow conditions, thus the data presented here pertains to the low-flow condition. Justification of the use of a low-flow groundwater model and recommendations for accounting for the seasonal fluctuations are given hereafter. Table C.1 summarizes the final input to the unconfined groundwater model under low-flow conditions.

Table C.1: Model input

Dataset	Total data points available	Data points fitting the purpose of study	Reason for elimination
Boreholes	64	25	No GWL[1] measurement (27 BHs), global outlier (1), duplicates (1), high-flow conditions (10)
CPTs	514	248	Out of area of study (6 CPTs), duplicates (3), high-flow conditions (257)
Wells	2,824[2]	57	Confined aquifers (2,687 wells), high-flow conditions (80)
Monitored wells[3]	43	1	Confined or no information available (39 wells), high-flow conditions (3)
Piezometers	1432	24	No reference to bore number[4] (1,059 piezometers), Confined or no information available (335), high-flow conditions (14)

[1] GWL: groundwater level

[2] 7,893 wells originally received from the Council from which 5,365 wells are within the area of study and further 2,541 wells have no water level record. Thus, the total data points reduced to 2,824 wells

[3] Reference datum for water levels in wells is unknown; the measuring point is assumed to be the top of a 0.4 m casing stick up above ground elevation

[4] Since there is no bore number in the database, the piezometers couldn't be classified as confined or unconfined based on drillers' notes

Since the data is not readily available in the format required for mapping, additional work is done to express water levels in terms of elevation above mean sea level (MSL). This is possible because the zero mean sea level has been constant for 6,500 years (Dravid and Brown 1997). Static water elevations less than MSL are concentrated close to the coastline especially in the former lagoon area. A negative elevation denotes that

the water level is lower than the mean sea level and as a result, there is intrusion of sea water into the edges of the plains. This discrepancy can be the result of wrong measurements and not allowing the water table to gain equilibrium between pumping and measurement. Thus, these instances were capped to -1; otherwise, there would be no potential for water to flow into the sea.

In addition to the data points, surface water levels such as rivers and streams are used to constrain the model spatially. The mean sea level (MSL) or the coastline (zero elevation) is used to constrain the model downstream. Data obtained for rivers are derived from multiple sources such as LiDAR, topographic maps, surveys and in some cases monitoring data, where available and is representative of typical low-flow conditions. The above datasets and the subsequent sections of this appendix are centered on the construction of a low-flow condition groundwater model for a couple reasons. First, the levels of surface water constraining the model inland typically represent low flow conditions (i.e. more data is available for the low flow condition). Second, the 1931 event occurred during the summer when typical low-flow conditions prevail; thus for the analysis and observations to be comparable, similar conditions should be considered in the liquefaction assessment. In the same line of thought, it is assumed that no precipitation occurred before or at the time of the earthquake because Hawke's Bay District "was experiencing the mild drought conditions of midsummer" (Callaghan 1933). Also, due to the lack of information, the effect of pumping on groundwater could not be estimated. Given the lack of rigorous data, it is suggested to account for the uncertainties in the groundwater levels. This was attempted in the present study through the construction of a groundwater model under high-flow conditions but did not provide reasonable results due to the inconsistency in the data for high-flow conditions.

2. Interpolation of Water Elevation Field Data

To define the spatial variation of field data over an area of study, each cell requires the availability of at least one data point. The lack of data in the groundwater field makes this task difficult. Thus, researchers have overcome this difficulty by the use of suitable interpolation techniques. ArcMap offers 2 types of interpolation techniques. Deterministic interpolation techniques create surfaces from measured points based on the extent of similarity (Inverse Distance Weighted) or the degree of smoothing (Radial Basis Functions). Geostatistical interpolation techniques employ the statistical properties and particularly the spatial autocorrelation of the predicted location and the measured points around it. All geostatistical methods rely on the similarity of nearby sample points. Kriging is the most commonly used technique in the field of hydrogeology and groundwater, especially (Elleithy et al. 2015; Hassan et al. 2016; Hussain et al. 2016; Marko et al. 2014). It is a statistical interpolation method which generates the best linear unbiased estimate for a random variable with some spatial autocorrelation defined by a semivariogram. A semivariogram is a measure of the change in the variable with changes in distance. Geostatistical methods work best when data is normally distributed and stationary (mean and variance do not vary significantly). To ensure a good interpolated surface is obtained, there are several steps in the kriging process. The first step is Exploratory Spatial Data Analysis (ESDA), the

second step is the fitting of a variogram model and spatial interpolation of water levels and the final step is the cross-validation of the prediction map. A flowchart describing the process is shown in Figure C.1.

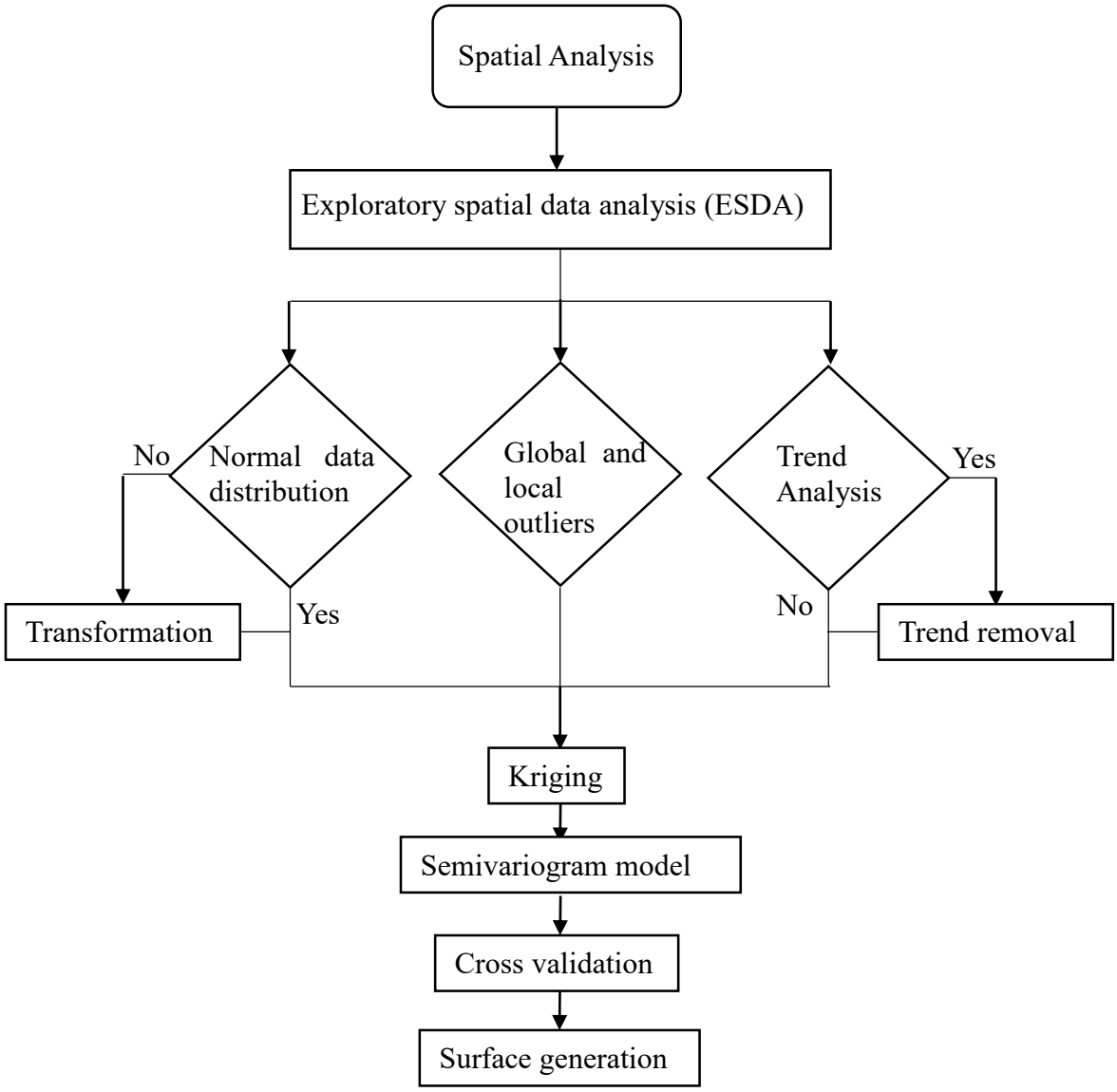

Figure C.1: Flow chart of Geostatistical analysis *(modified from Kumar, n.d.)*

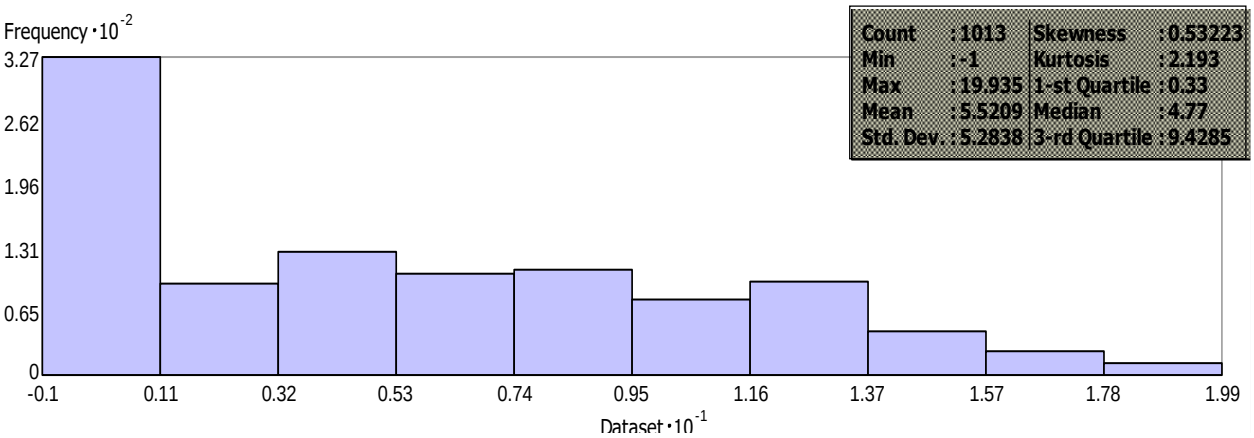

Figure C.2: Histogram, Transformation: none, Dataset: kriging points, Attribute: water elevation

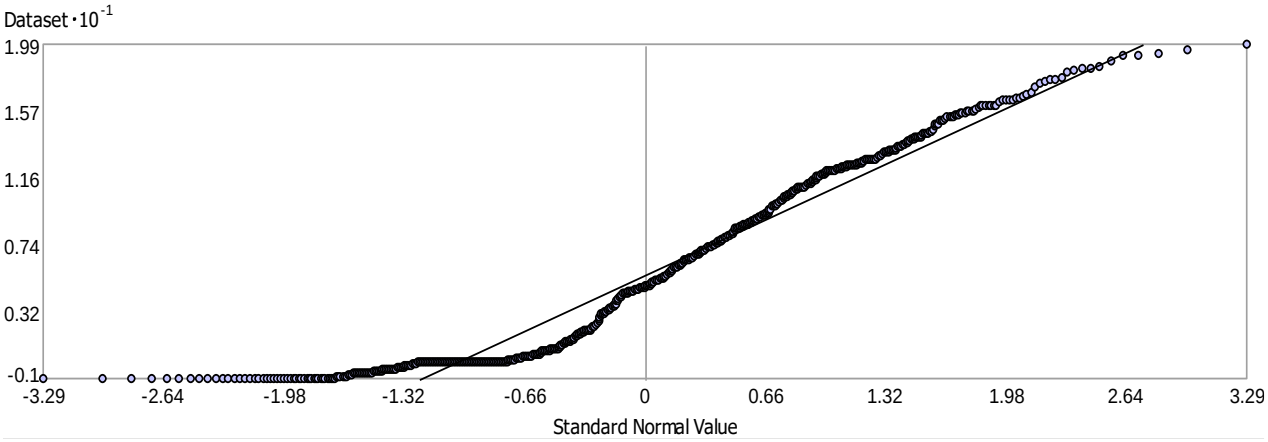

Figure C.3: Normal QQ plot, Transformation: none, Dataset: kriging points, Attribute: water elevation

2.1 Exploratory Spatial Data Analysis (ESDA)

ESDA tools in the Geostatistical Analyst toolbox are used to examine the distribution of the data, identify trends in the data, if any and understand the spatial correlation and directional influences.

The normality of the data is checked using the **histogram** (Figure C.2) and the normal QQ plot (Figure C.3). The distribution of the water elevation values is represented in the histogram using 10 classes. The x-axis represents the water elevation values rescaled 10^{-1} times (to fit on the histogram). The y-axis shows the frequency of the data represented by the height of each bar. The water elevation histogram shows that the data is unimodal and skewed right. The right tail identifies a relatively small number of data with high water elevations. These occur farther inland in the Heretaunga Plains and closer to the hills. The statistics on the top right corner of the histogram indicate a

low value of skewness. Thus, the data is close to a normal distribution and no data transformation is required.

The **quantile-quantile (QQ) plot** compares the distribution of the data to a standard normal distribution. Generally, the water elevation data are close to the 45-deg line except for the first portion of the line. The closer the points to the straight line, the closer the distribution to a normal distribution.

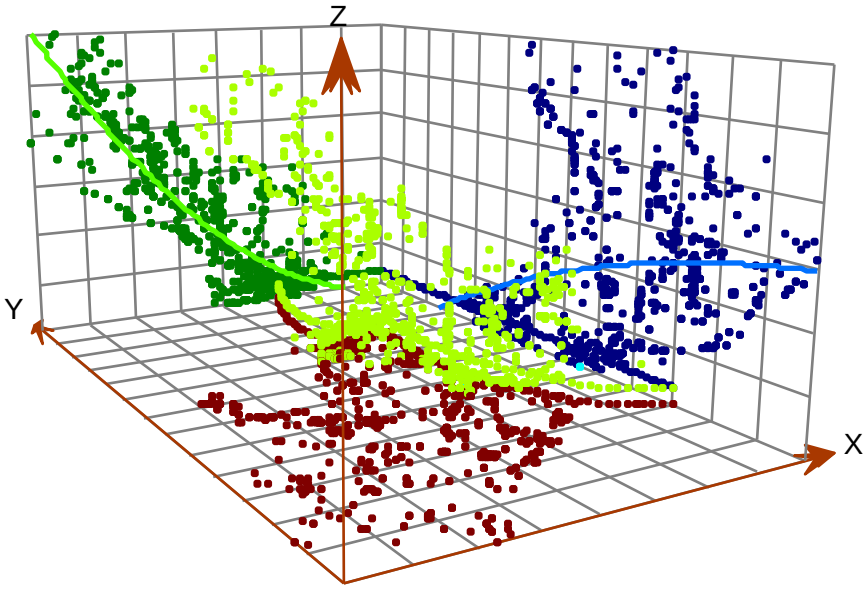

Figure C.4: Trend analysis, 2nd order polynomial, Dataset: kriging points, Attribute: water elevation

The **trend analysis** identifies the presence of a global trend in the data (Figure C.4). The trend analysis provides a 3-dimensional perspective of the data and projects the values on the xz and yz planes to allow a better visualization of the global trend. The trend is then fitted by a model and is removed. The interpolation is done on the residuals and then the global trend is added. Figure C.4 suggests that there may be a trend in the data. However, the trend is not strong for all the directions. Thus, the trend removal is not further investigated for two reasons. First, trend removal requires more parameters to be estimated. The more parameters to estimate, the less precise the model becomes. Second, the removal of the trend increases the accuracy of modeling residuals or random short-range variations which is not of concern in this study since the main interest is a more general smooth groundwater surface (Esri 2016).

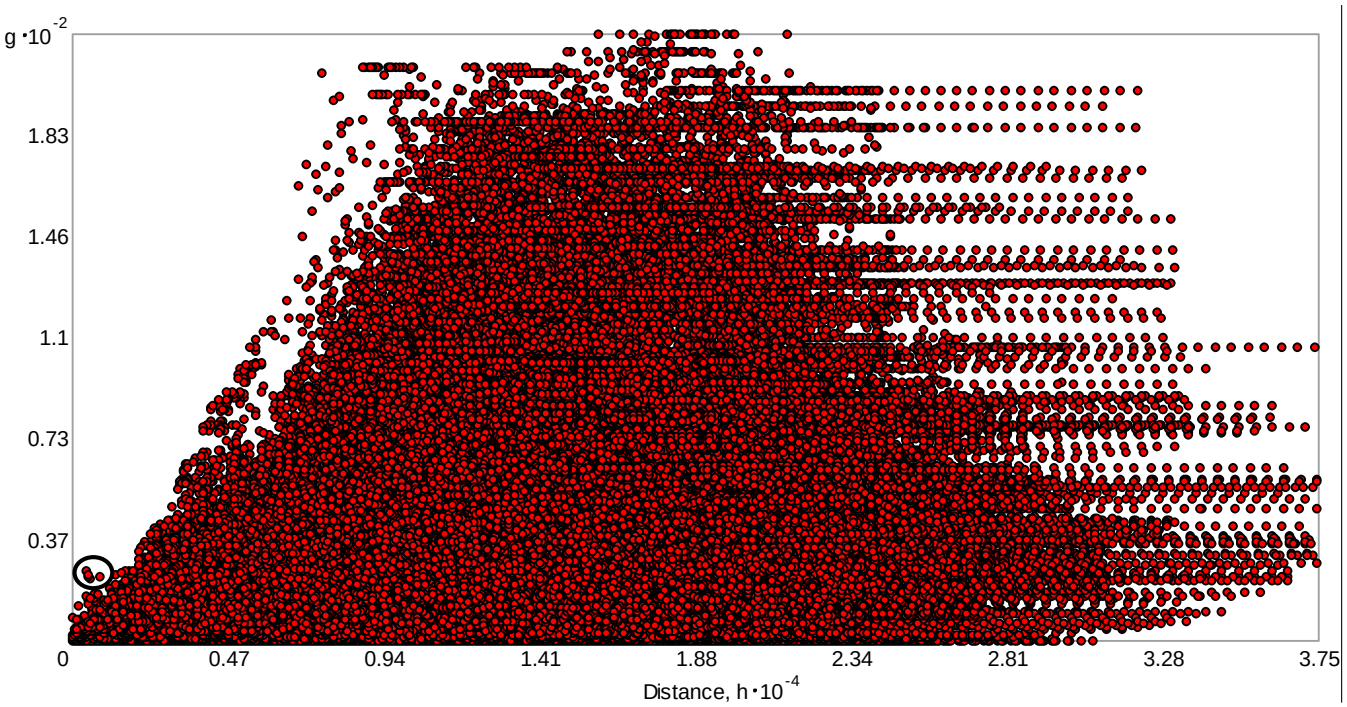

Figure C.5: Semivariogram cloud, lag:1500 m, number of lags: 25, Dataset: kriging points, Attribute: water elevation

The **semivariogram cloud** is a scatter which plots the semivariogram value γ on the y-axis with respect to the distance or lag on the x-axis. The points forming the cloud are pairs of points and not individual data points. The semivariogram value is the squared difference between the values of each pair of locations:

$$\gamma(h) = \frac{1}{2\,N(h)} \sum_{i=1}^{N\,(h)} [Z(x_i) - Z(x_i + h)]^2 \qquad \text{(C.1)}$$

Where $\gamma(h)$ is the semivariogram value for the lag distance (h), $N(h)$ is the total number of the variable pairs separated by a lag distance (h) and $Z(x)$ is the value of the variable.

The semivariogram is a measure of the dissimilarity between two values. Thus, the semivariogram value is smaller at short distances (around the origin) and increases as the distance between points increases (moving to the right of the plot). A departure from this general concept occurred at many locations in this dataset because the topography of the area has some abrupt changes in elevation from flat lands to hills. An example of this observation is the group of points circled in Figure C.5. These points are located south of the Heretaunga Plains where the ground slopes upward abruptly. Since liquefaction only occurs in flat lands and gentle slopes, data points with elevations greater than 20 m were not included in the model. Where the points flatten out, it means there is little spatial autocorrelation beyond this distance. In the area of

interest, the water elevations vary smoothly and thus there are no directional influences to be accounted for in the model.

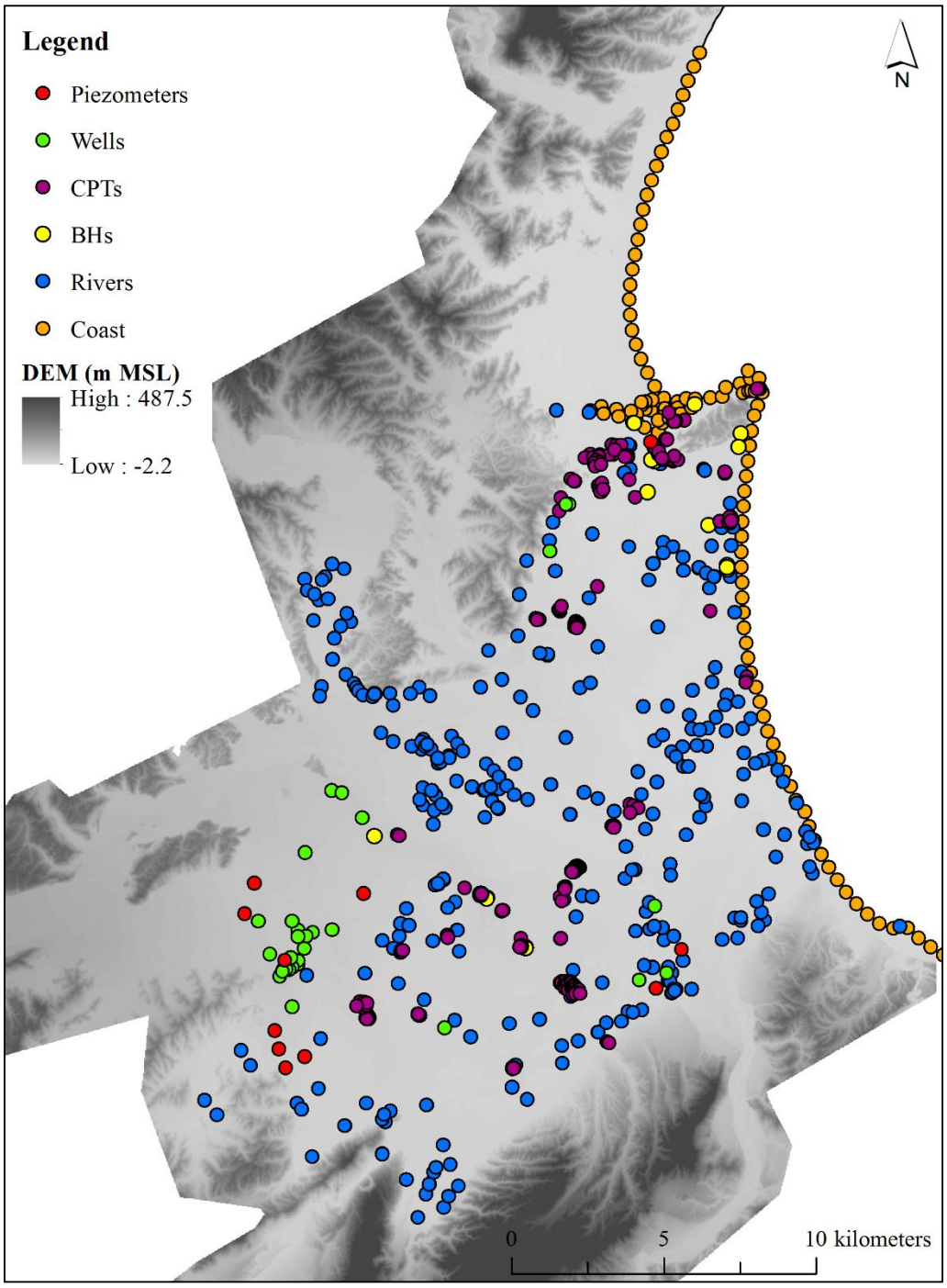

Figure C.6: Input data points for water elevation surface interpolation

2.2 Fitting of Variogram Model

There are many geostatistical methods: Kriging, Co-kriging and Empirical Bayesian Kriging. The last 2 methods were tried and did not yield good models, thus they won't be considered in this work. Kriging will be used in the development of the groundwater model. There are many types of kriging. The most widely used are ordinary, simple and universal. These types were tried for the construction of the ground water model. Ordinary and universal give comparable results. Ordinary kriging is simpler and more used than universal kriging and hence, is used for this model. Input datasets for the ground water level surface under low-flow conditions are shown in Figure C.6. River and coast polylines were converted into points in order to restrain the model spatially and downstream at the coastline. Geostatistical Analyst determines a convenient lag size for grouping semivariogram values. The lag size is the size of the distance class used to group pairs of locations. Thus, the red dots in the empirical variogram in Figure C.5 are binned into lags and then averaged (Figure C.7). The averaged points (blue crosses) are fitted with different models and lag sizes. The best fit model (blue line in Figure C.7) is Gaussian with a lag size of 1500 m. The goal of this model is to characterize a global GWT and thus, inexact data fitting at measured samples is performed to obtain a smooth GWT. Thus, the search neighborhood was set to smooth with a smooth factor of 1.

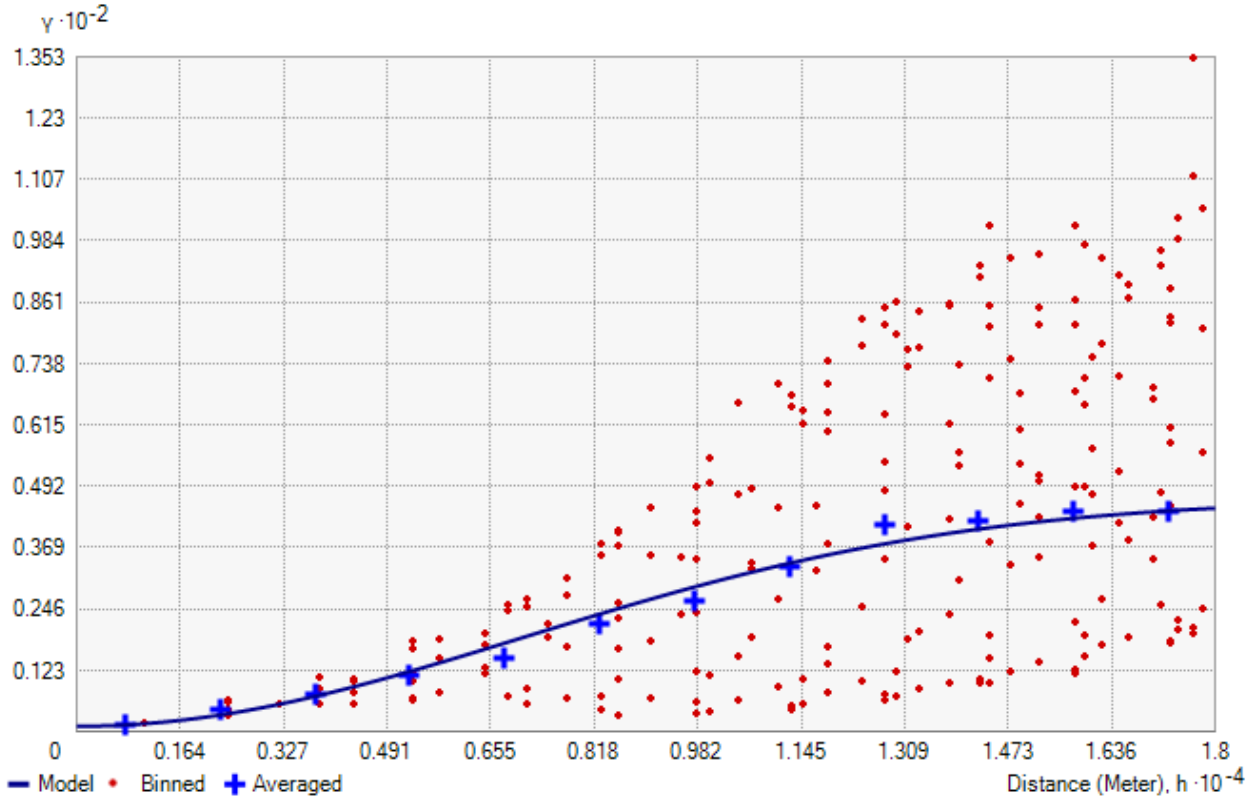

Figure C.7: Semivariogram model

The best fit model results in the water elevation surface shown in Figure C.8.

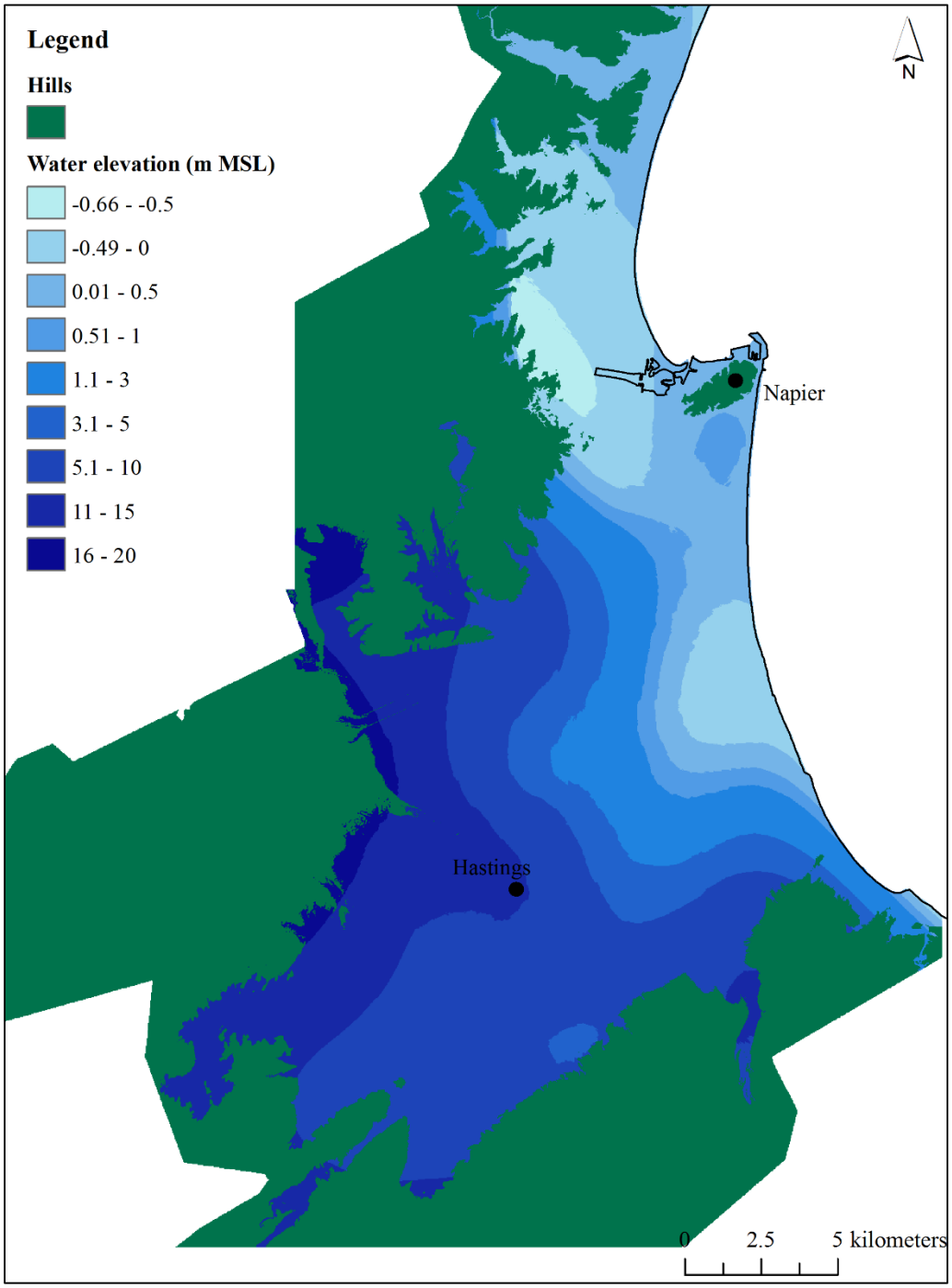

Figure C.8: Water elevation map for the Heretaunga Plains

2.3 Cross-Validation

Cross-validation is an important step in the kriging process. It gives a measure of how well the model is performing at unsampled locations and thus helps making a decision on which model provides the best predictions. This is done by a close examination of plots and prediction errors statistics.

$$prediction\ error = predicted\ value - measured\ value \tag{C.2}$$

Figure C.9a provides a graphical comparison between the predicted and the measured values. A good model should have a fit close to the 1:1 line which is approximately the case in this model (0.96 slope of regression line). Another measure of goodness of fit and normality of the data is the normal QQ plot. The QQ plot shows the quantiles of the difference between predicted and measured and the corresponding quantile of a normal distribution. Figure C.9b shows that the predictions follow a normal distribution except for the deviation at small values.

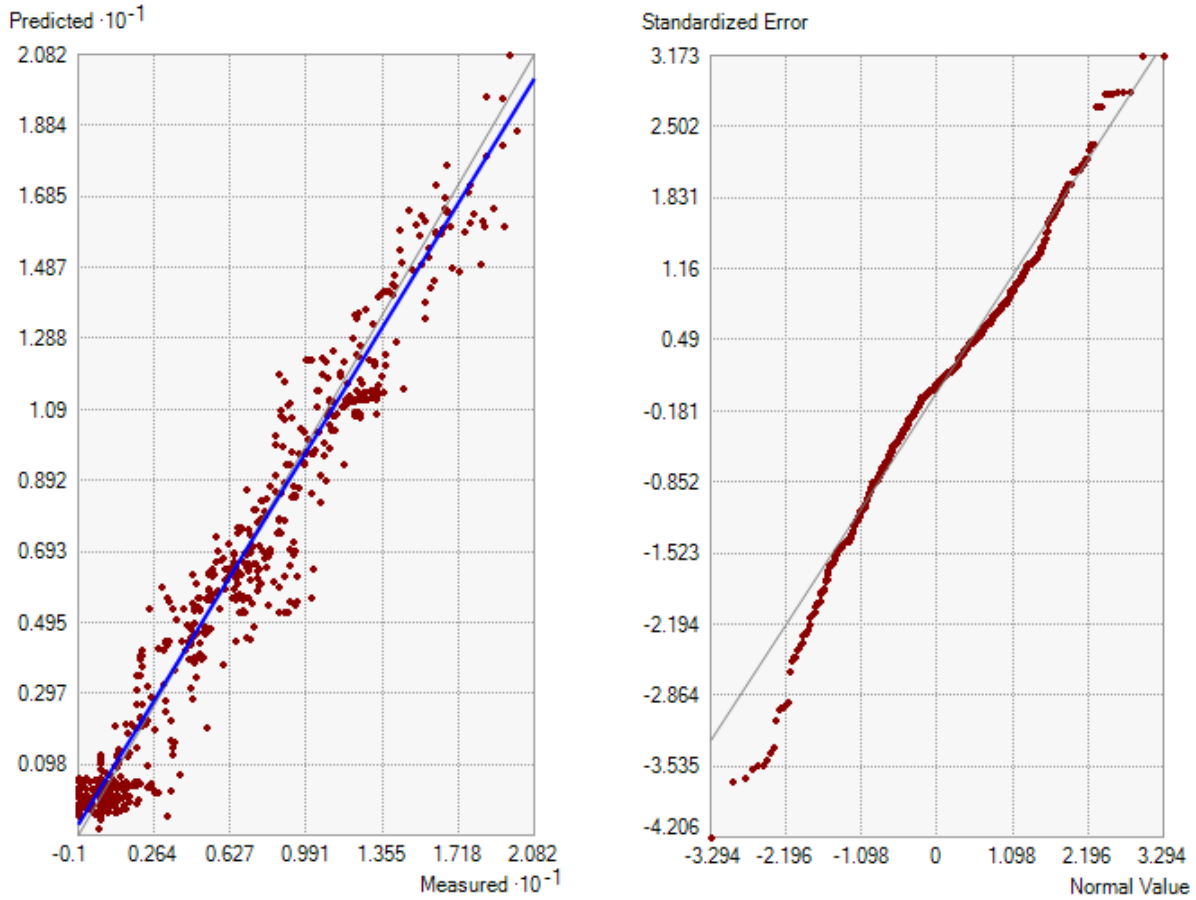

(a) (b)

Figure C.9: (a) Comparison between predicted and measured values, (b) normal QQ plot

Table C.2: Model predictions errors statistics

Prediction errors	Value
Mean	-0.0081
Root-Mean-Square	1.095
Mean Standardized	-0.0068
Root-Mean-Square Standardized	1.036
Average Standard Error	1.057

A model which provides accurate predictions should have the following prediction error statistics (Table C.2):

- The mean prediction error and the mean standardized prediction error should be equal to 0. This indicates that predictions are unbiased.
- The root mean square error and the average standard error should be close and as small as possible. This indicates that the predictions do not deviate largely from the measured values.
- The root mean square standardized error should be close to 1. This indicates that the prediction standard errors are accurate.

Based on the validation of predictions at measured locations, the model provides good estimates of groundwater elevation towards the center of the study area. The prediction errors increase away from the center which is explained by the reduction in the density of available data points. As mentioned above, the use of this model presets the generation of a smooth surface and consequently, inexact data fitting. Thus, the difference between the predicted values from the smooth surface and the measured values is expected to show as error. The standard error prediction is shown in Figure C.10. The areas of interest, Napier and Hastings, fall in the region of the model where valid predictions are done. Thus, this model is deemed satisfactory for the liquefaction triggering assessment.

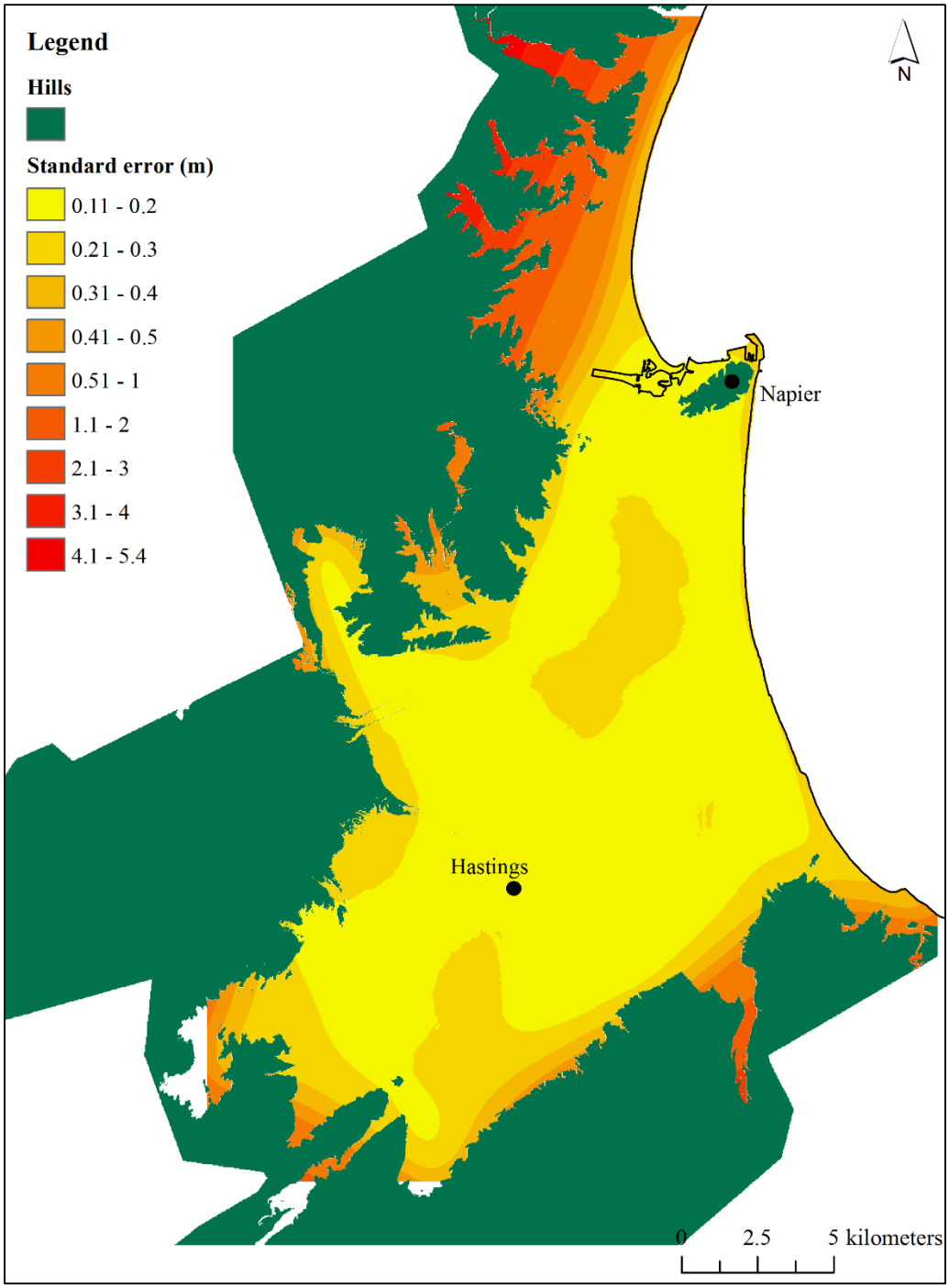

Figure C.10: Prediction standard error map for the Heretaunga Plains

3. Present-day Depth-to-Water Table Map

3.1 *Construction* of the Map

The depth-to-water table map is obtained by the subtraction of the water elevation map (Figure C.8) from the ground elevation DEM. Figure C.11 represents the depth to water table map using present-day ground elevations.

3.2 Validation of present-day Depth-to-Water Map

To validate the depth-to-water map developed above and thus validate the water elevation map from which it was derived, surface water was the main feature to check. Surface water (e.g. lakes, swamps, rivers and streams) is delineated by the dark blue color ("above ground" label) in Figure C.11. Figure C.12 shows locations where the predicted surface water matches the actual surface water. The instances close to the west boundary of the model are not of interest for this study and thus are not further discussed. There are 2 instances to the west of Hastings which are not discerned on the underlying imagery in Figure C.12 . This might be the result of recent reclamations or model errors. More generally, shallow groundwater table (bin "0.1-1m" in Figure C.11) is observed in Awatoto (a strip running parallel to the coastline south of Napier), the former Ahuriri lagoon, Napier suburbs and Hastings. Table C.3 justifies these observations and confirms that these instances match the actual conditions. For future work, a more robust validation approach is recommended such as measurements of groundwater levels at different locations across the area of study.

Table C.3: Justification of shallow GW predicted in some locations

Location	Justification of shallow GW	Reference
Awatoto	Location - Proximity to the sea	By inspection
Ahuriri Lagoon	Swampy area due to the uplifted lagoon	Marshall (1933), Callaghan (1933), Henderson (1933)
Napier suburbs	Former swamps	Telegraph Daily (1981)
Hastings	Former swamp	Telegraph Daily (1981)

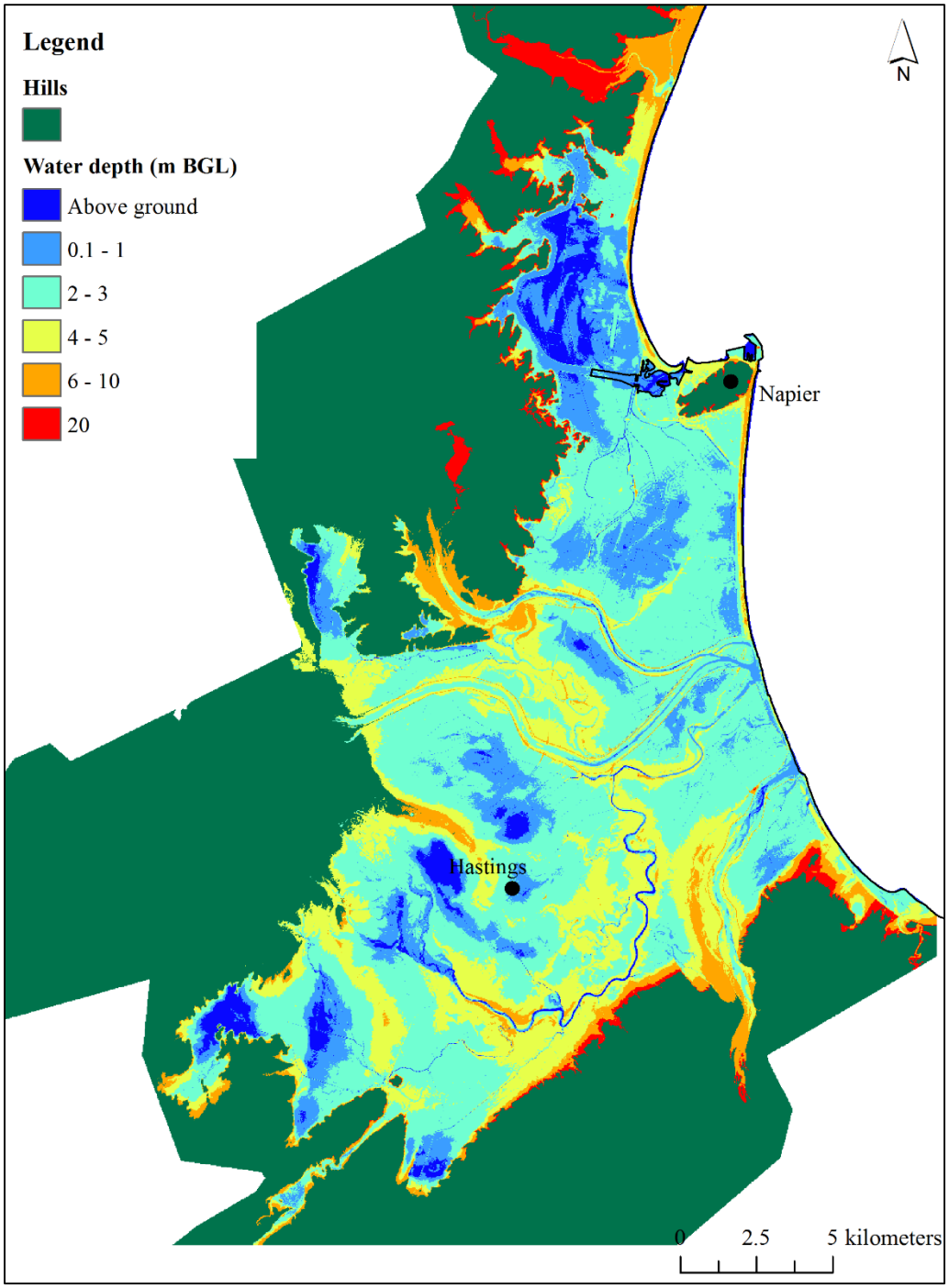

Figure C.11: Depth to water table map for the Heretaunga Plains

Figure C.12: Validation of surface water as predicted by the contemporary depth-to-water map

4. Pre-earthquake Groundwater Model

4.1 Pre-earthquake Ground Elevations

The 1931 event induced tectonic movement which resulted in an uplift of the ground around Napier and subsidence around Hastings. This change in elevation is documented in Hull (1990) (see Section 2.3.4). To obtain the ground elevation prior to to the 1931 earthquake, this change (Figure C.13) is subtracted from the current ground elevations to reverse the tectonic movement due to the earthquake and reproduce pre-earthquake ground elevations (Figure C.14).

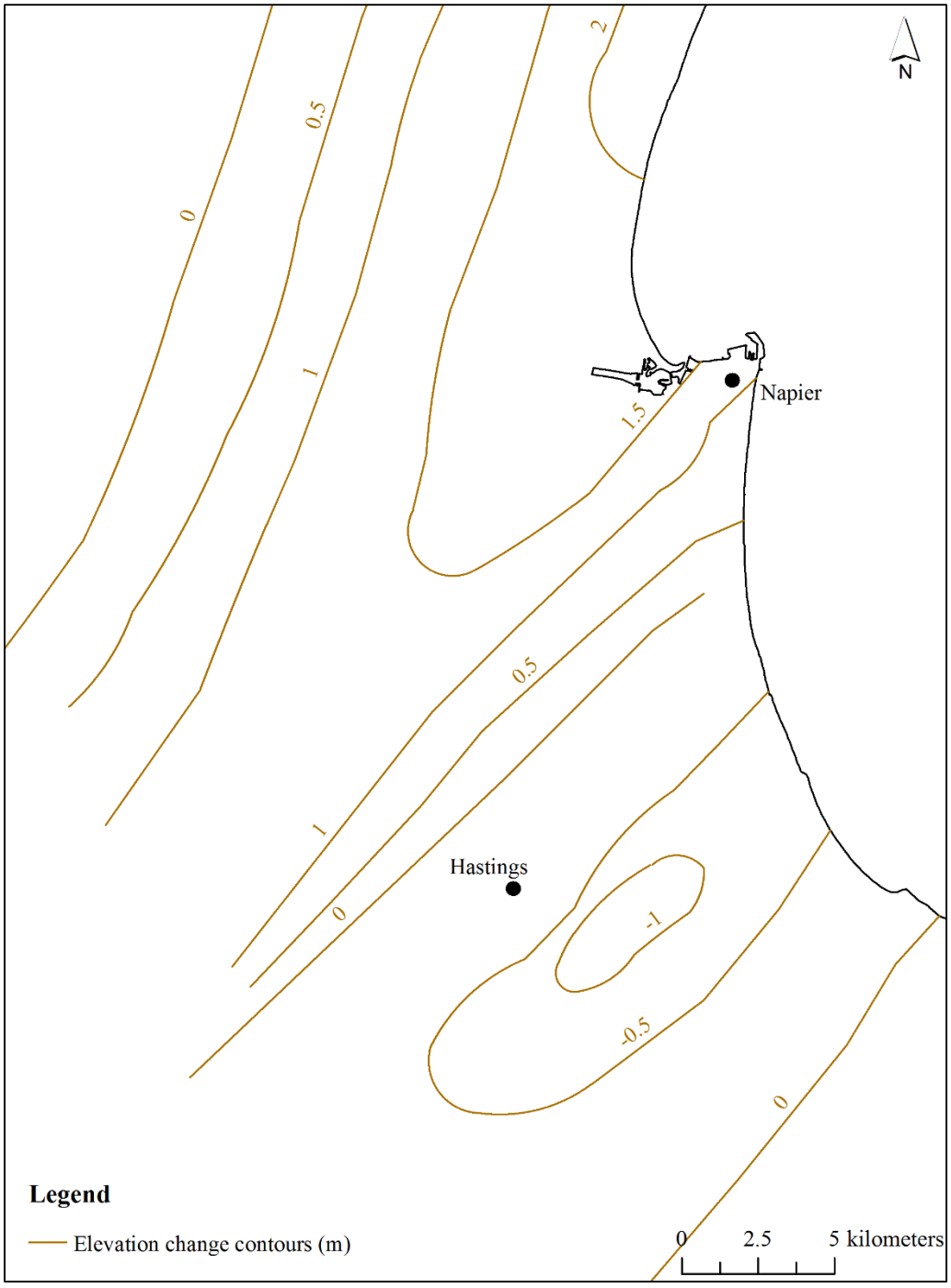

Figure C.13: Changes in elevation the area of study *(reproduced from Hull 1990)*

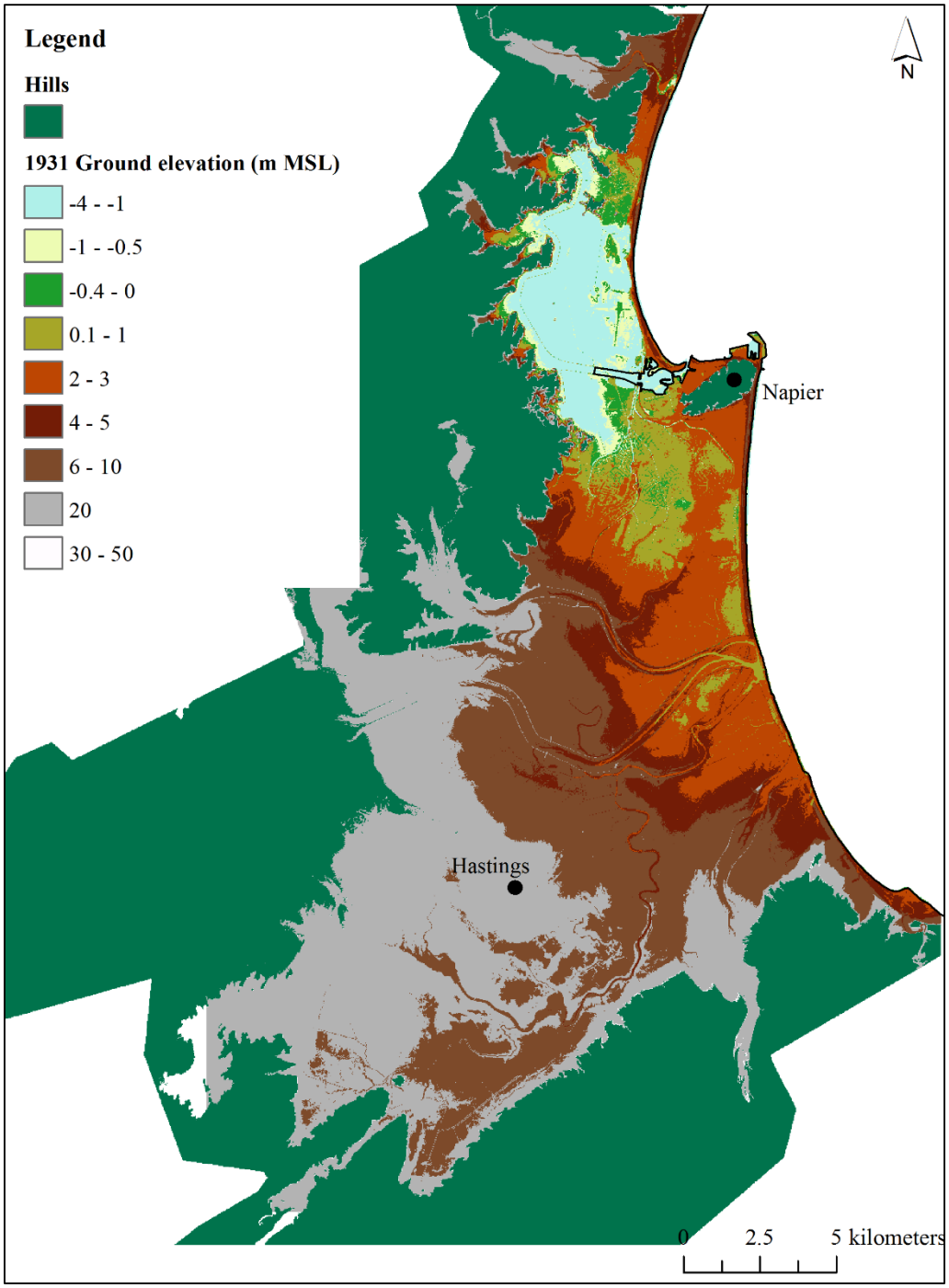

Figure C.14: Pre-1931 estimated ground elevation for the Heretaunga Plains

4.2 Pre-earthquake Water Elevation

As a result of the seismic waves and the change in ground elevations due to tectonic movement, it is important to consider the effect of groundwater responses on the groundwater table elevation. Groundwater level offsets were documented in more recent earthquakes, for example the 2010 M_w7.1 Darfield earthquake, the 2011 M_w6.2 Christchurch earthquake (Gulley et al. 2013) and the 2011 M_w5.8 Mineral, Virginia earthquake (Roeloffs et al. 2015). Hydrological responses to earthquakes comprise groundwater responses in wells, increased spring or river flows and the occurrence of new springs. Monitored wells show a sharp increase or decrease in water level and this change in level can be permanent. Gulley et al. (2013) observed that deeper wells showed lower post-seismic water level (negative offset) and shallower wells showed higher post-seismic water level (positive). Water levels dropped 0.47 m and rose 0.15 m after the 2011 Mineral, Virginia earthquake. This vertical movement of the water, which was only noticeable by instrumental measurements, was largely proportional to ground motions, regardless of epicentral distance. It is also a function of different aquifer properties and hydrogeological settings (Roeloffs et al. 2015). In the absence of information on groundwater responses after the 1931 earthquake, the concepts mentioned above cannot be inferred. Thus, the groundwater table elevation pre and post-earthquake is assumed to be unchanged. Therefore, the water elevation map developed in Figure C.8 is considered to represent estimates of the groundwater table elevation at the time of the earthquake.

4.3 Pre-earthquake Depth-to-Water Map

Based on information from the 2 previous sub-sections, the pre-earthquake depth-to-water map is obtained by taking the difference between the pre-earthquake estimated ground elevations and the water table elevation map (Figure C.15).

4.4 Validation of Pre-earthquake Depth-to-Water Map

Similarly to the validation of the present-day depth-to-water map, surface water features are used to validate the pre-earthquake depth-to-water map. Surface water before the earthquake is deduced from a famous map of Napier at 1865 (Department of Survey and Land Information, Wellington, New Zealand) and accounts on land reclamation in Napier (Annabell 2012). The map of Napier 1865 shows that Napier Hill was almost an island surrounded by the sea and occasionally linked to the main land by strips of gravels. Major reclamations were done in Napier from 1860s to 1931 in an effort to expand the town. Of interest to this work is the Ahuriri Port reclaimed between 1860s and 1870s and Napier South reclaimed from 1900 to 1908. Greater Napier suburbs were reclaimed in the late 1920s to 1960s (Annabell 2012). This information assists in the validation of the pre-earthquake depth-to-water map. Points A and B on Figure C.15 represent pre-earthquake surface water. Point A shows the former Ahuriri Lagoon and Point B shows the greater Napier suburbs which were not reclaimed at the time of the earthquake. On the other hand, points C and D show Napier South and the Ahuriri Port, respectively which were reclaimed at the time of the

earthquake. Therefore, it can be concluded that the developed pre-earthquake depth-to-water map reasonably estimates the actual groundwater depths in Napier at the time of the earthquake.
There is no information on surface water or the development of Hastings, thus the model cannot be validated there.

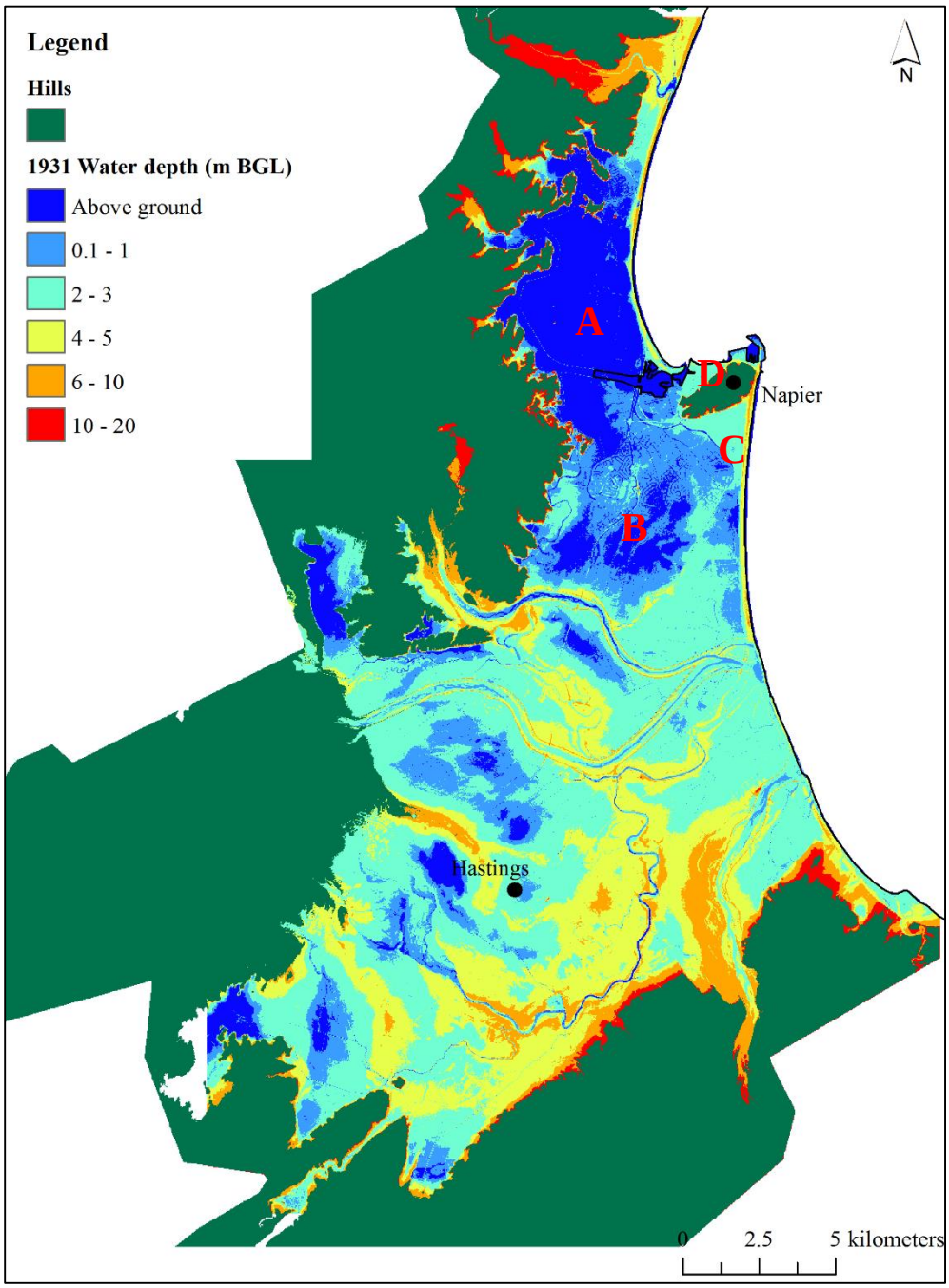

Figure C.15: Pre-earthquake estimated groundwater depths for the Heretaunga Plains

5. References

Annabell, J. B. (2012). “Planning Napier 1850-1968.” Massey University, Manawatu, New Zealand.

Daily Telegraph. (1981). *Hawke’s Bay “Before” and “After”: the Great Earthquake of 1931, an Historical Record*. Daily Telegraph Co Ltd, Napier, New Zealand.

Elleithy, D., Hassan, A., Hagras, M., and Riad, P. (2015). “Best Applicable Geostatistical Model for Interpolating Groundwater-Levels in El-Obour City, Egypt.” *Sustainable Development*, 1, 435–446.

Esri. (2016). “ArcMap online tutorial.” ESRI.

Hassan, I., Lawal, I. M., Mohammed, A., and Abubakar, S. (2016). “Analysis of Geostatistical and Deterministic Techniques in the Spatial Variation of Groundwater Depth in the North-western part of Bangladesh.” *American Journal of Engineering Research (AJER)*, 5(3), 29–34.

Hussain, M., Bari, S., Tarif, M., Rahman, T., and Hoque, M. (2016). “Temporal and spatial variation of groundwater level in Mymensingh district , Bangladesh.” *International Journal of Hydrology Science and Technology*, 6(2), 188–197.

Marko, K., Al-Amri, N. S., and Elfeki, A. M. M. (2014). “Geostatistical analysis using GIS for mapping groundwater quality: case study in the recharge area of Wadi Usfan, western Saudi Arabia.” *Arabian Journal of Geosciences*, 7(12), 5239–5252.

APPENDIX D: LIQUEFACTION TRIGGERING ASSESSMENT

Supplemental material to the liquefaction triggering assessment is presented in Appendix D. Included is the parametric study done for the variations in PGA and inclusion/exclusion of short CPTs for Napier and Hastings.

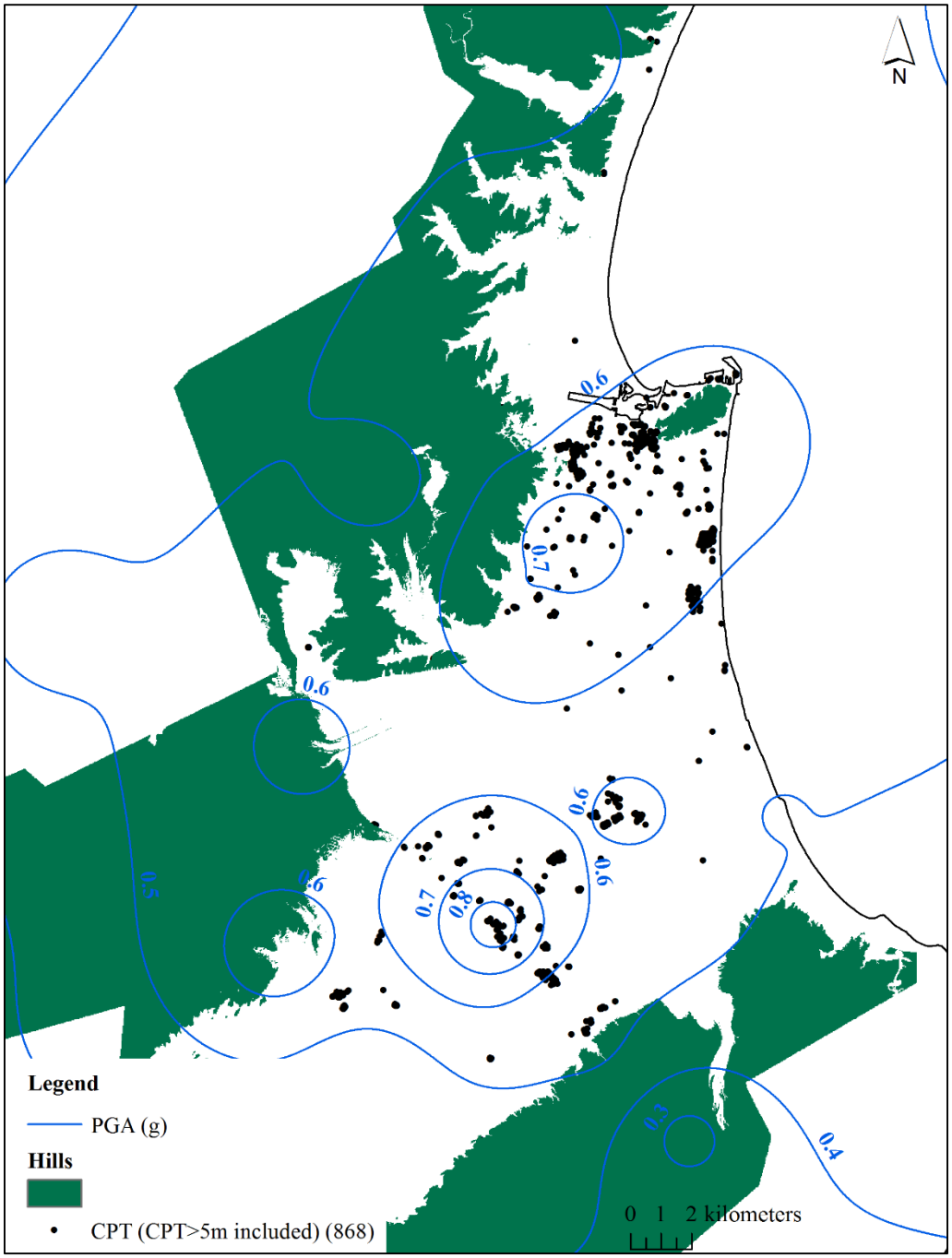

Figure D.1: Spatial distribution of CPT with depth greater than 5m

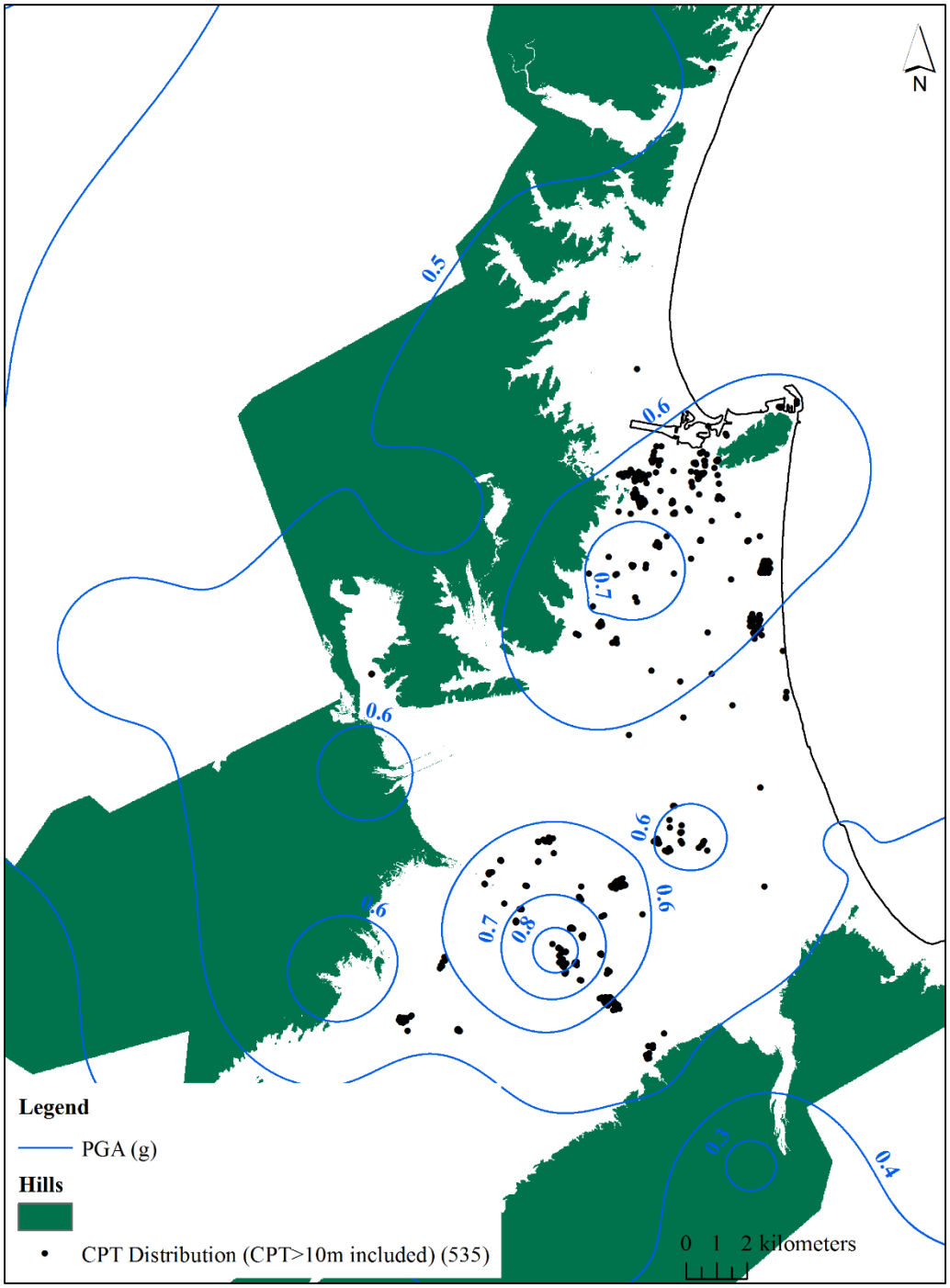

Figure D.2: : Spatial distribution of CPT with depth greater than 10m

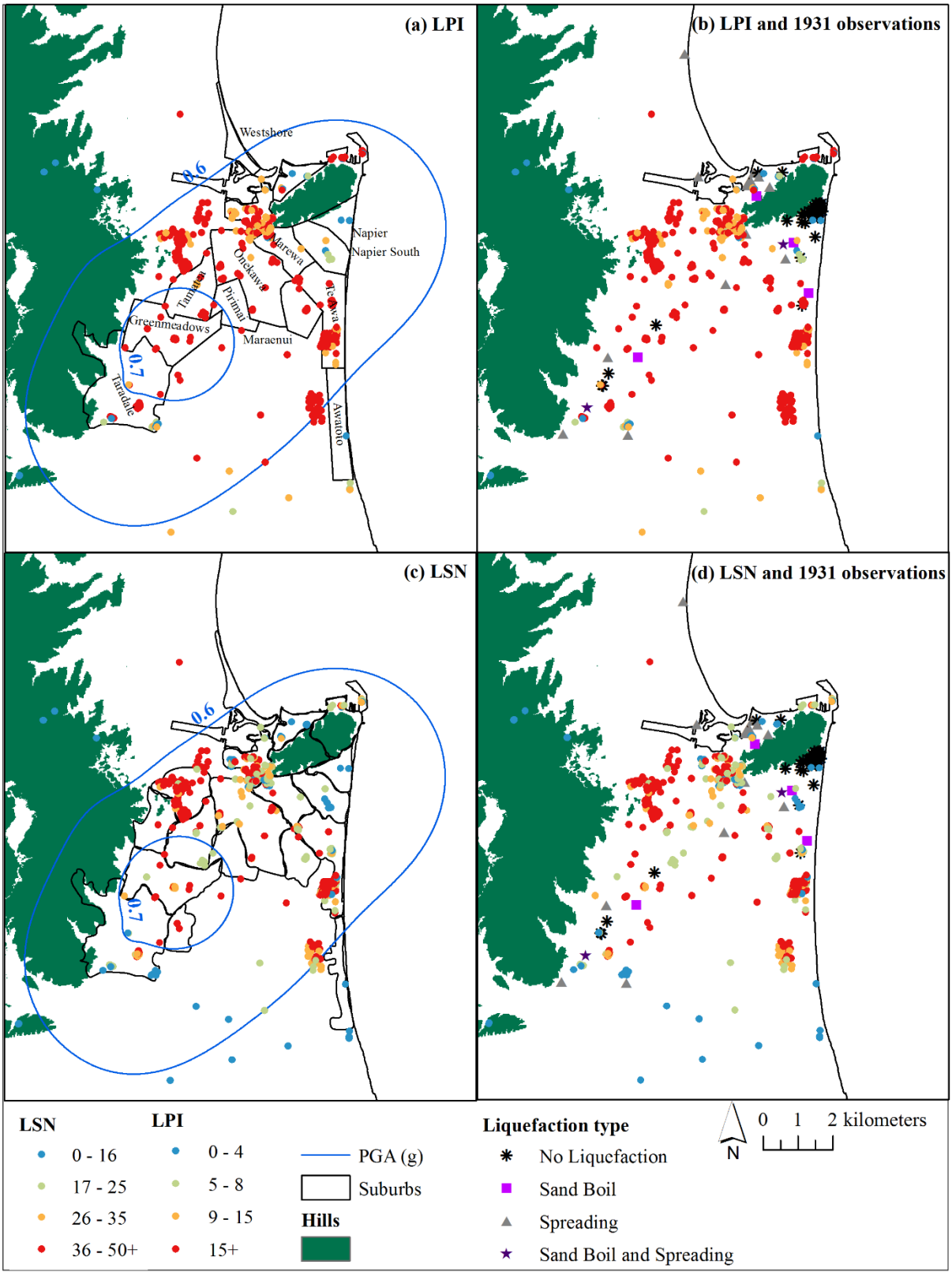

Figure D.3: Computed liquefaction severity indices for Napier- Case 2 (a) LPI, (b) LPI overlaid with 1931 observations, (c) LSN, (d) LSN overlaid with 1931 observations

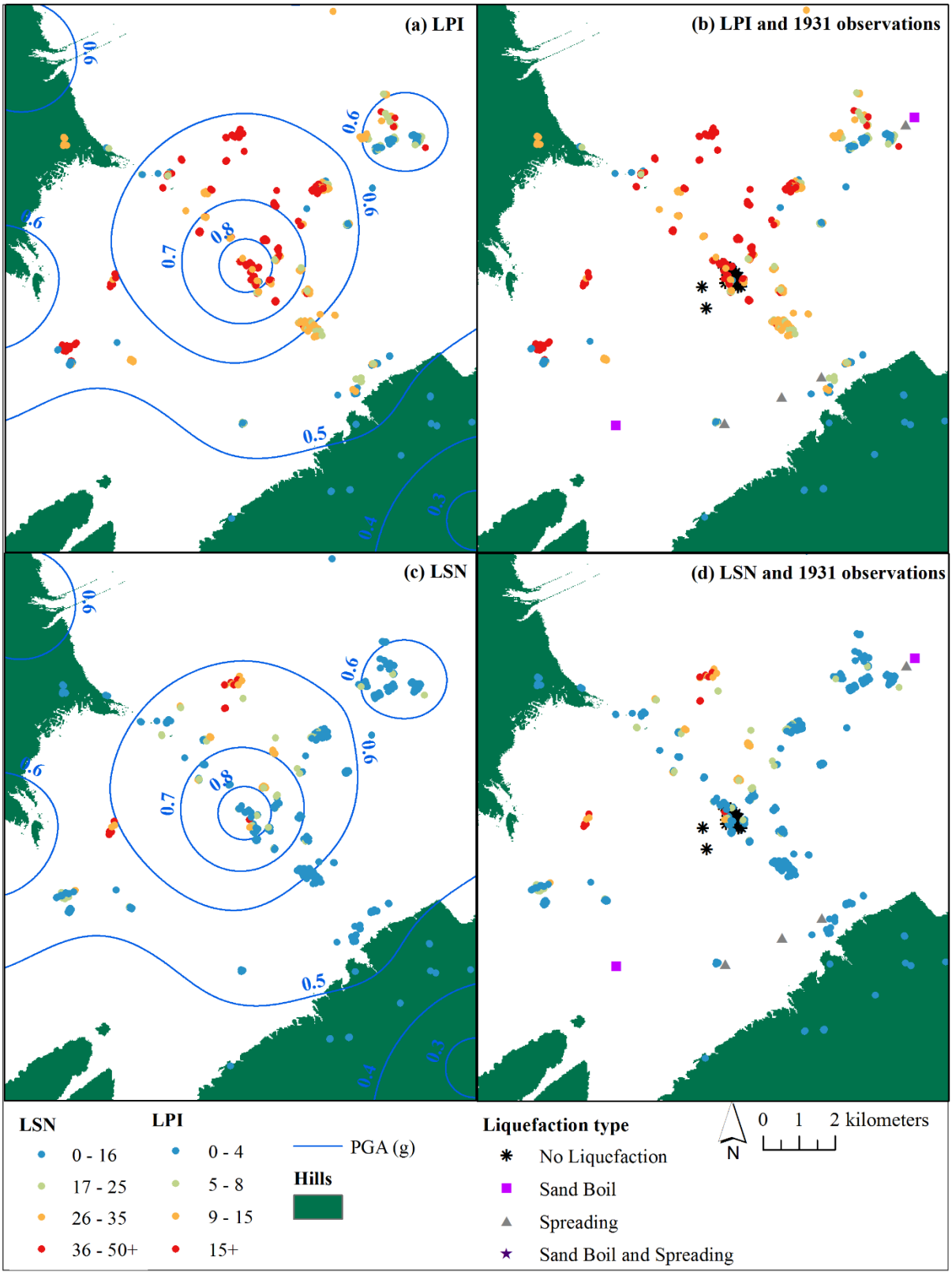

Figure D.4: Computed liquefaction severity indices for Hastings- Case 2 (a) LPI, (b) LPI overlaid with 1931 observations, (c) LSN, (d) LSN overlaid with 1931 observations

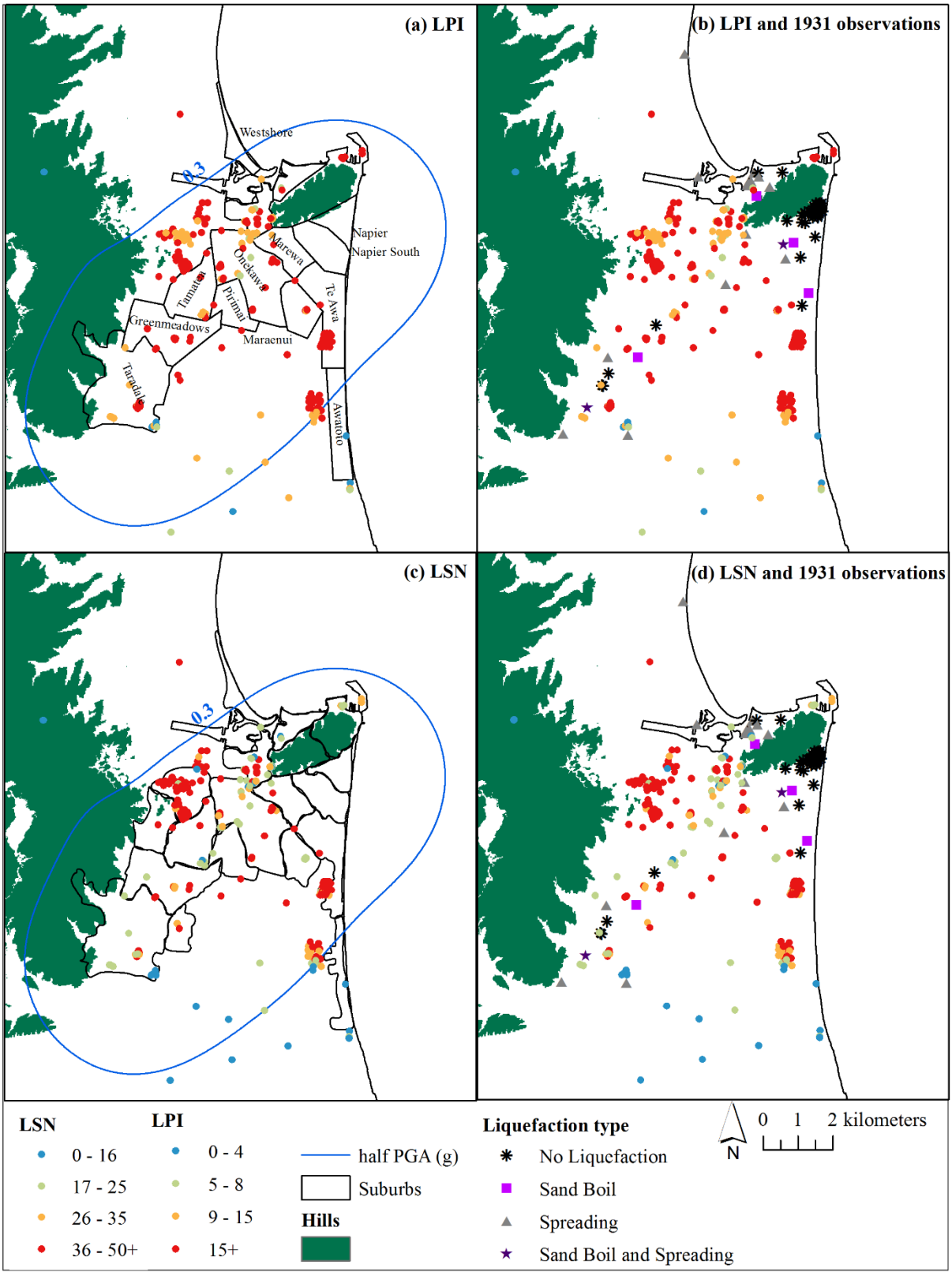

Figure D.5: Computed liquefaction severity indices for Napier- Case 3 (a) LPI, (b) LPI overlaid with 1931 observations, (c) LSN, (d) LSN overlaid with 1931 observations

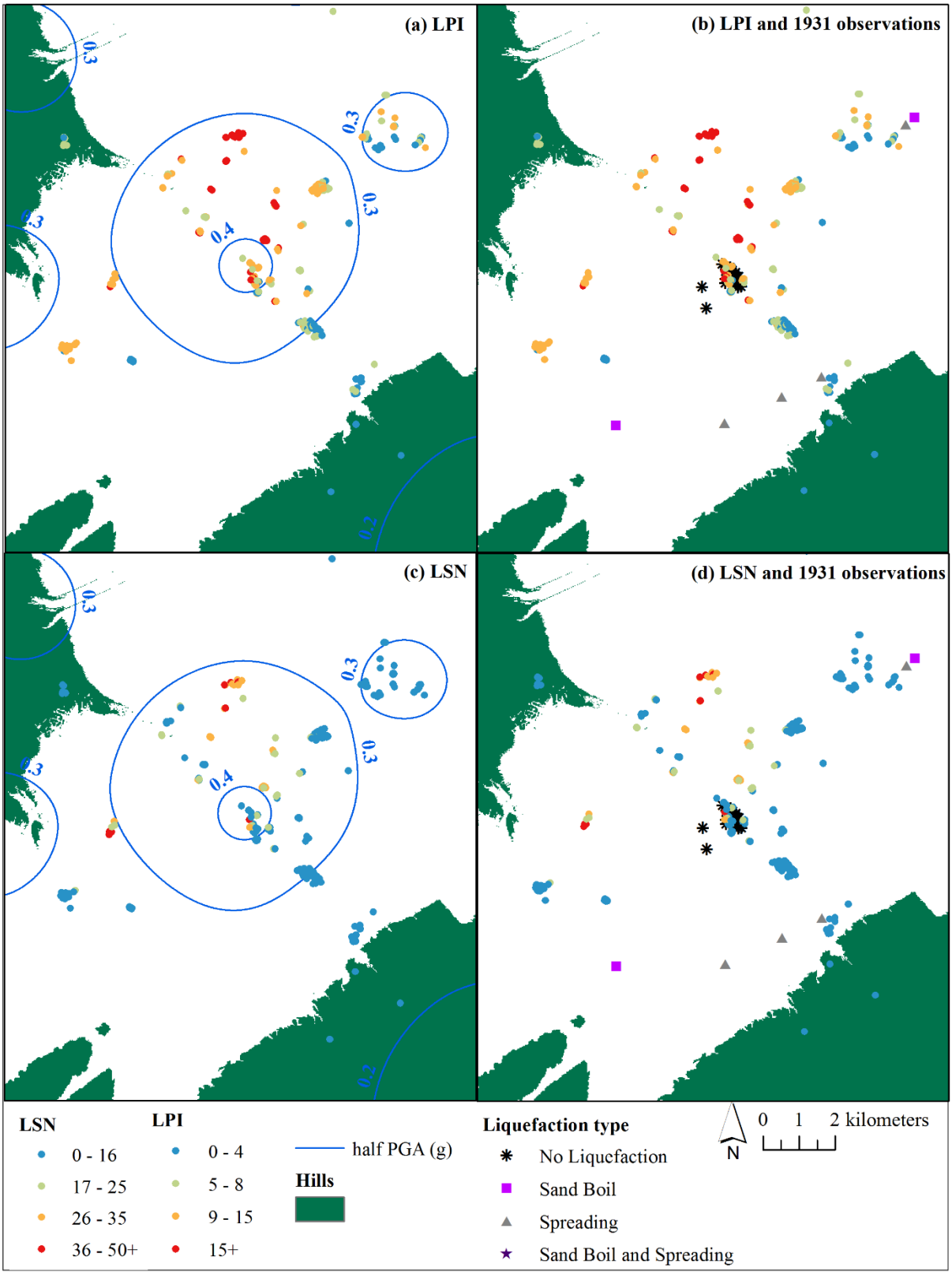

Figure D.6: Computed liquefaction severity indices for Hastings- Case 3 (a) LPI, (b) LPI overlaid with 1931 observations, (c) LSN, (d) LSN overlaid with 1931 observations

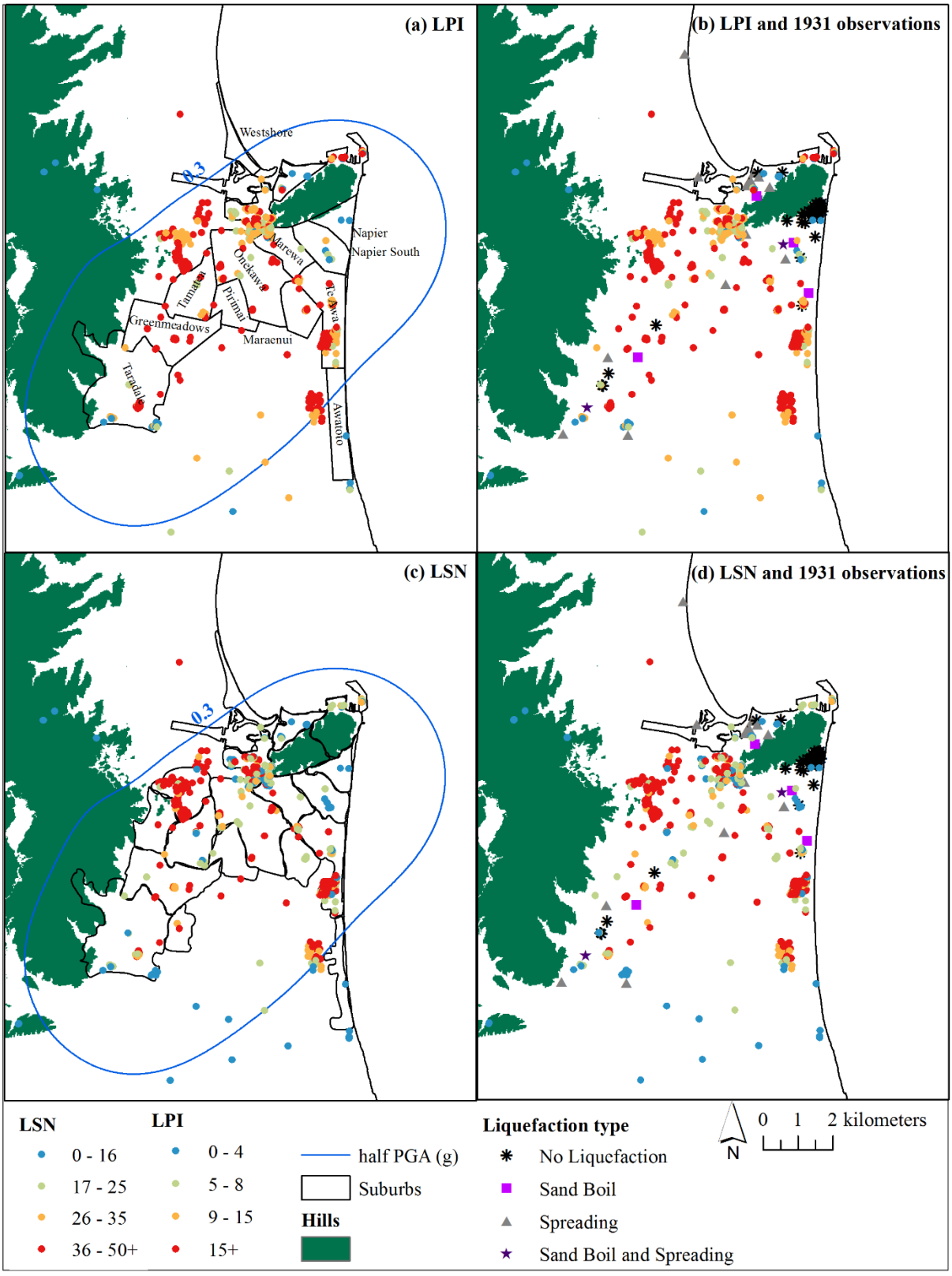

Figure D.7: Computed liquefaction severity indices for Napier- Case 4 (a) LPI, (b) LPI overlaid with 1931 observations, (c) LSN, (d) LSN overlaid with 1931 observations

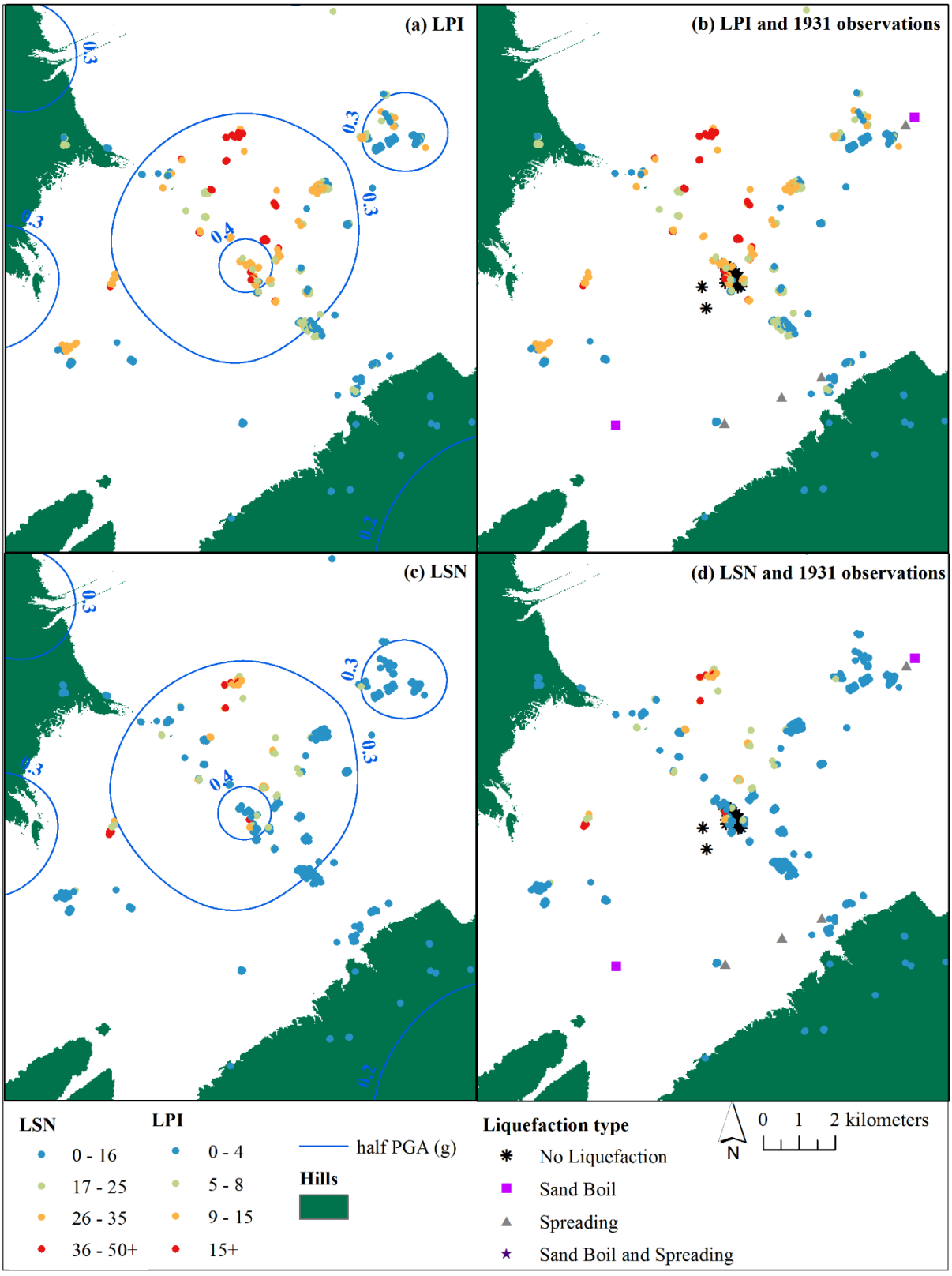

Figure D.8: Computed liquefaction severity indices for Hastings- Case 4 (a) LPI, (b) LPI overlaid with 1931 observations, (c) LSN, (d) LSN overlaid with 1931 observations